Preliminary Design of a Smart Powered Dolly for an A-double High Capacity Vehicle

R.M.C.M. Wouters

D&C 2016.081

Master's thesis

Declaration concerning the TU/e Code of Scientific Conduct
for the Master's thesis

I have read the TU/e Code of Scientific Conduct[i].

I hereby declare that my Master's thesis has been carried out in accordance with the rules of the TU/e Code of Scientific Conduct
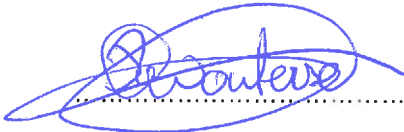
<u>Date</u>

17-10-2016
....

<u>Name</u>

R.M.C.M. Wouters
....

<u>ID-number</u>

0777384
....

<u>Signature</u>

....

Submit the signed declaration to the student administration of your department.

January 15 2016

Acknowledgements

First of all, I would like to express my sincere gratitude to my supervisors dr. ir. Igo Besselink and MSc. K. Kural for their support during my research. Secondly, I would like to thank prof. dr. H. Nijmeijer for his useful input during the monthly meetings.

A special mention goes to the members of the famous AES lab. We had a lot of fun during the lunch breaks and helped each other when needed. Next, I would like to thank my mother, sister and close friends for their support.

Last but not least, I would like to thank my grandmother, who has always been there for me and made me who I am today. Unfortunately, she died during my research. Therefore, I would like to thank her one last time by dedicating this thesis to her.

Abstract

Due to the predicted freight transport increase more and more commercial vehicles are required. A solution to meet the increasing demand for commercial vehicles is the usage of longer vehicle combinations. The European commercial vehicle legislation states that commercial vehicles, which are used for cross-border traffic, should weigh at most 44 t and the maximum length is limited to 16.5 m. A High Capacity Vehicle (HCV) is a vehicle which exceeds these limits and is only allowed to be operated within specific countries. Although these HCVs show some significant reduction in the CO_2 emissions and costs, more beneficial HCV configurations can be derived. Such a concept of a future HCV is an A-double HCV, which is a vehicle combination consisting of a tractor with two semi-trailers connected via a dolly.

The manoeuvrability and high speed stability of the HCVs decrease in comparison with standard commercial vehicles, due to the increased mass and length of the HCVs. In this report two smart dolly designs have been proposed to improve the manoeuvrability and high speed stability of the A-double HCV. Furthermore, the dollies are equipped with an electric powertrain to assist the tractor's engine in high power demanding scenarios. The performance of the smart dolly is evaluated by means of the Performance Based Standards, that state goals and objectives for commercials vehicles and describe ways to test them.

The 4x2 dolly design is two-wheel driven via a single electric motor that propels the rear wheels. Due to this configuration, only the front wheels of the 4x2 dolly can be steered, which limits the steering performance. The 4x4 dolly is four-wheel driven by in-wheel motors, which makes it possible to steer all four wheels. Since the vertical axle force limits should not be violated, the front and rear axle of the 4x2 dolly are placed at a distance of 1.40 m from the CoG of the dolly and the fifth wheel is placed 0.97 m in front of the rear axle. For the 4x4 dolly the distance between the CoG and both axles is limited to 1.39 m and the fifth wheel is placed at the centre between the two axles.

The steering system of the 4x2 dolly is a system in which the drawbar can rotate with respect to the dolly chassis and the wheels are steered with a constant gain between this drawbar rotation angle. With this steering system the low speed swept paths in a 90 degree turn and the Dutch HCV 360 degree turn are reduced by 9% and 16% in comparison with a non-steered standard dolly in an A-double HCV. The 4x4 dolly uses a path following steering system that follows the trajectory of the tractor's fifth wheel. The 4x4 dolly equipped A-double reduces the 90 degree and the EU 360 degree turn swept paths with 25% and 39%, in comparison with a non-steered standard dolly equipped A-double.

For highway driving scenarios on a flat road a standard 4x2 tractor with single semi-trailer has enough drivetrain power reserve to haul the dolly and second semi-trailer. However, should the dolly and second semi-trailer not limit the performance of the tractor semi-trailer combination, the dollies should be equipped with an electric driveline with a total motor power of 307 kW. Accordingly, the maximum requested torque at each wheel equals 25.9 kNm and 12.62 kNm, for the for the 4x2 dolly and 4x4 dolly design respectively.

Overall, it can be stated that the 4x4 smart dolly is the best design and can already match the tractor semi-trailer manoeuvrability performance when used in an A-double HCV configuration. The high speed stability performance of this A-double HCV equipped with the 4x4 dolly is still worse than the tractor semi-trailer combination, so further research is required to improve the high speed stability of the 4x4 dolly A-double HCV.

Nomenclature

Abbreviations

CoG	Centre of Gravity
CVL	Commercial Vehicle Library
DLTR	Dynamic Load Transfer Ratio
DoM	Difference of Maxima
GVW	Gross Vehicle Weight
HCV	High Capacity Vehicle
HoD	Hybrid-on-Demand
ICE	Internal Combustion Engine
MoD	Maxima of Difference
PBS	Performance Based Standards
VRT	Virtual Reality Toolbox

Symbols

Symbol	Unit	Definition
A	[-]	Amplitude
a	[m]	Longitudinal distance from CoG to front axle
A_f	[m^2]	Frontal Area of the vehicle
a_x	[m/s^2]	Longitudinal acceleration
a_y	[m/s^2]	Lateral acceleration
b	[m]	Longitudinal distance from CoG to rear axle
C	[-]	Instantaneous turn centre
c	[m]	Longitudinal distance from fifth wheel coupling to rear axle
c_d	[-]	Air drag coefficient
$c_{F\alpha}$	[N/rad]	Cornering stiffness
c_r	[-]	Roll resistance coefficient of the tyres
D	[-]	Yaw damping ratio
d	[m]	Longitudinal distance from king pin to CoG of the trailer
d_{axle}	[m]	Longitudinal distance between the axles of a tandem axle set
e	[m]	Longitudinal distance from CoG of the trailer to centre axle
F_s	[N]	Tyre shear force
F_x	[N]	Longitudinal (tyre) force
F_y	[N]	Lateral (tyre) force
F_z	[N]	Vertical (tyre) force
g	[m/s^2]	Gravitational constant
I	[kgm^2]	Inertia
k	[-]	Gain
l	[m]	length
M	[Nm]	Moment
m	[kg]	Mass
P	[W]	Power
r	[m]	Radius
R	[-]	Ratio
s	[m]	Track width
T	[Nm]	Torque
V_x	[m/s]	longitudinal velocity
V_{sy}	[m/s]	Lateral sliding velocity of the tyre
w	[m]	Width
x	[m]	Offset drawbar mouting point from front axle
z	[-]	Dimensionless deceleration

Symbols

Symbol	Unit	Definition
α	[rad]	Tyre side slip angle
β	[rad]	Vehicle side slip angle
γ	[-]	Overall transmision ratio
δ	[rad]	Steer angle
η	[-]	Efficiency
θ	[rad]	Articulation angle between adjacent vehicles
μ	[-]	Friction coefficient between tyre and road
ρ_a	[Pa]	Ambient pressure
τ	[s]	Time delay
Φ	[rad]	Roll angle
ϕ	[rad]	Road inclination angle
ψ	[rad]	Yaw angle
ω	[rad/s]	Angular wheel velocity

Subscripts

$chas$	Chassis
co	Coupling overhang semi-trailer
con	Connection point of the drawbar at the dolly's chassis
$crit$	Critical dimension
D	Desired
d	Dolly
db	Drawbar
$DLTR$	Dynamic Load Transfer Ratio
dm	Displacement moment
ff	Tractor fifth wheel to dolly fifth wheel
fo	Front overhang semi-trailer
FP	Follow point
fw	Dolly's fifth wheel to pin coupling
$HSFP$	High speed follow point
$HSLP$	High speed lead point
kp	King pin trailer
$link$	Link dolly steering
LP	Lead point
ltm	Load transfer moment
n	Tyre id
om	Overturning moment
pin	Pin coupling
RA	Rearward Amplification
ro	Rear overhang semi-trailer
rcu	Roll coupled units
sa	Steer axle of the tractor
$shift$	Offset between the low speed lead point and high speed lead point
sl	Support legs of semi-trailer
t	semi-trailer
tot	Total
$trac$	Tractor
v	Vehicle total

Contents

Chapter 1

Introduction

1.1 Motivation and background

For ages people have been trading goods all over the world. Due to the technological innovations over time, the carriages and vessels of the old days have been replaced with complex and high efficient ships, trains, commercial vehicles and planes. According to the most recent statistics from [11], trucks transport 75.4% of the total European inland freight, trains transport 18.0 % of the freight and ships transport the remainder of 6.6%, excluding the freight transported by planes. Even though the energy efficiency of road transport may be lower than the other two categories, transport via road has one important advantage: trucks can transport goods to even the most remote places as long as there is a road. Ships and trains, however, require a waterway or expensive railroad infrastructure and can, therefore, only reach a limited number of destinations. This already explains the high share of commercial vehicles in the total freight transport.

It is predicted in [10] that the freight transport increases by 50% between 2000 and 2020. This indicates that more commercial vehicles are required for the freight transport via road. The increasing growth of freight transport, stricter emission legislations, scarcity of oil and available space on the roads all introduce major challenges on the design of future commercial vehicles. These challenges can be solved by either designing the vehicle itself to be more clean and efficient and/or to combine multiple vehicles into one. This report focuses on the last solution.

European legislation on commercial vehicles mainly focuses on weight and dimensions. For cross-border traffic within Europe three configurations are currently allowed, which are shown in Fig. 1.1a. Legal limitations on these vehicles are stated in directives 96/53/EC [7] and 97/27/EC [8]. Vehicle configuration L1 has a total allowed length of 16.5 m and weight of 40 t. When configuration L1 is used for intermodal transport, the maximum gross vehicle weight (GVW) of this vehicle increases to 44 t. The maximum length and GVW of vehicle configurations L2 and L3 is 18.5 m and 40 t respectively. Combining multiple vehicles into one results in longer and possibly heavier vehicle combinations, which exceed these limits and are known as High Capacity Vehicles (HCV). In other literature HCVs are also known as: Eco-Combis, road trains, Long Combination Vehicles (LCV), Long Heavy Good Vehicles (LHGV) and Longer Heavier Vehicles (LHV). HCVs are only allowed to be operated within the borders of a European country, since the HCVs do not meet the European legislations for cross-border transport. HCVs with maximum length of 25.25 m and mass of 60 t are already allowed in Sweden, Finland and the Netherlands [18], [38]. Denmark, Belgium and several federal states in Germany, however, are in a test phase that will be finished by the end of 2016 for the first two countries [18], [54]. Spain recently started a test phase with HCVs by April 2016 [53].

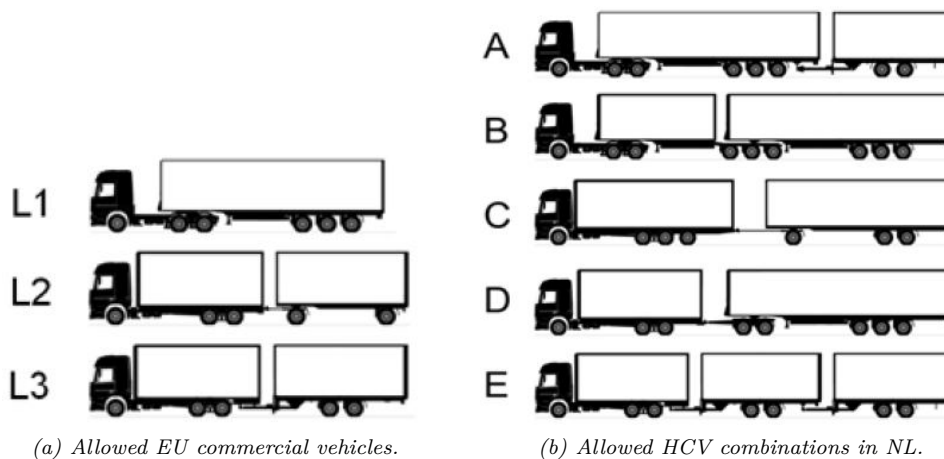(a) Allowed EU commercial vehicles.   (b) Allowed HCV combinations in NL.

Figure 1.1: Vehicle configurations allowed for international transport within the EU and Dutch HCVs [27].

According to [40] and [18], HCVs have many advantages. These studies show a CO_2 emission reduction between 24 and 38% and a cost reduction between 30 and 50%, when standard vehicles are replaced by HCVs with the same loading units. Furthermore, fewer vehicles are required to haul the same amount of goods, which is beneficial for the congestions on motorways and reduces the number of required drivers. Disadvantages of a HCV are a decrease in safety, manoeuvrability and high-speed stability. The safety may be reduced, since due to the increased mass there is a larger impact in case of a crash in comparison with a standard commercial vehicle. The increased length of the HCVs decreases the manoeuvrability, since more space is needed to manoeuvre. This last disadvantage can be reduced by implementing steered axles.

The next step in the HCV approach is to create even longer vehicles that have a better modularity with the standard commercial vehicles in Fig. 1.1a than the current allowed HCVs. As indicated by [18], 86% of the long-haul segment consists of tractor semi-trailer combinations. It can, therefore, be concluded that the semi-trailer is the most used transport unit for freight transportation via road. Therefore, the most obvious configuration for a future HCV is a combination of a tractor and two semi-trailers interconnected by a dolly, which is shown in Fig. 1.2. This configuration is also known as an A-double, A-train or double road train.
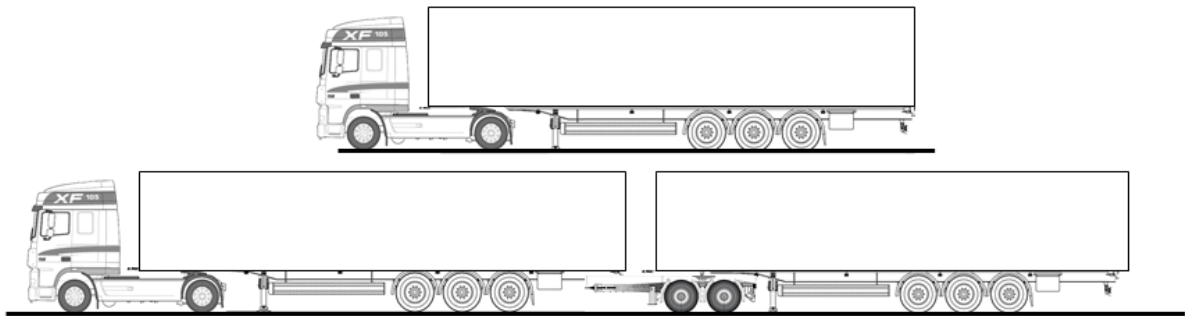

Figure 1.2: Standard tractor semi-trailer combination (top) and A-double HCV (bottom).

1.2 Existing projects and literature survey

The A-double HCV is already allowed on the public roads in Mexico and Canada and is restricted to 39.08/38.33 m and 66.5/62.5 t, respectively [62]. In Australia, A-double HCVs are known as double road trains and have a maximum length of 36.5 m and GVW of 85.5 t [37]. In the EU there are some projects to evaluate A-double HCVs. In a recent study of an A-double road train in Finland [21], the vehicle has a maximum GVW of 90 t and a total length of 34 m . In a second project the A-double has a length of 31.5 m [20]. Important to mention is that all these A-doubles have three articulation points and exceed the current dimension and GVW limits for HCVs in every European country.

The Dutch HCV legislation states that these vehicles only can be operated on designated roads [40]. This implies that at a certain moment, the vehicle needs to be decoupled and the trailer units need to be hauled separately. The main advantage of an A-double HCV in comparison with the other HCVs, is that it uses two standard semi-trailers. These semi-trailers can also be hauled separately by the same motor vehicle. However, for e.g the A- and D-configuration in Fig. 1.1b a different type of hauling unit, either truck or tractor, is required to haul the second (semi-)trailer on these roads. The A-double can haul both semi-trailers by itself, always hauling the maximum allowed loading length, either in HCV or tractor semi-trailer configuration. Also note, that with this configuration standard semi-trailers can be used whereas e.g. a B-double configuration uses a special link trailer, which is bad for the total cost of the vehicle. Furthermore, the A-double when equipped with two 45 ft. (13.7 m) containers, shows a potential reduction of the CO_2 emission of 24.5% and total cost of ownership reduction of 36.5%, according to [18].

In Europe commercial vehicles and HCVs are categorized based on the weight and dimensions. However, another approach is to categorize the vehicles based on their performance, as is being done in Australia. Performance Based Standards, or PBS, state goals and objectives that should be achieved by the vehicles [35]. These standards are divided in two fields, which are infrastructure and safety. The first field evaluates the performance in terms of infrastructure damage and the second field in terms of: stability, dynamic performance, powertrain performance and manoeuvrability. Modelling of the A-double configuration in [18] shows a decrease in the manoeuvrability and powertrain performance. This has to do with the higher weight and increased length of the vehicle. Increasing the size of the engine of the tractor and switching from a two-wheel driven (4x2) to a 4-wheel driven (6x4) tractor should result in enough tractive power to haul both semi-trailers in most scenarios. However, such tractors are more expensive and have increased driveline losses due to the second driven axle. Nevertheless, most of the A-double configurations currently in operation make use of 6x4 tractors. Also note, that the total tractive force that can be transferred to the road is a function of the vertical force on the driven axles. To ensure that enough tractive force is available in demanding conditions, e.g. startability and driving uphill, 25% of the total mass of the vehicle should be borne by the driven axles, as stated in [7].

A recent study of a 6x4 A-double HCV in [1] states that it is simply impossible to achieve the 25 % GVW distribution on the driven axles when the vehicle is evenly loaded. Another approach to meet this requirement and to be able to use a 4x2 tractor, is to equip the dolly with its own propulsion system that can assist the tractor when needed [56]. The Transformers project, which is collaboration between different truck and trailer manufacturers, suppliers and research institutes, supports this view with their Hybrid-on-Demand (HoD) driveline [55]. The idea of the HoD-driveline is to equip the (semi-)trailer with electric motors/generators that can harvest energy during braking, store this in batteries and assist the tractor's combustion engine when propulsion is needed. The potential fuel reduction can be as high as 8 %.

The poor manoeuvrability and high speed stability performance of the A-double combination can be improved with a dedicated steering system on the dolly of the A-double configuration. Trailer manufacturer Krone has designed a steerable dolly for the D-configuration HCV, which is steered via a mechanical linkage between the drawbar and front wheels of the dolly [13]. The Australian company Trackaxle Ltd. claims that their dolly, equipped with a similar steering system, reduces the tyre wear and improves both the rearward amplification and yaw damping in comparison with a non-steered dolly [51]. Patents on such a mechanically steered dolly date back to 1963 [43]. Another recent project on steerable dolly axis is performed in [61]. In this report the steering system for the dolly has been designed and tested on a radio controlled scale truck.

When the dolly is equipped with a powertrain and steering system, it can be used for autonomous operation to e.g. dock or pick up semi-trailers. The study by Kabos [22] shows the design and implementation of an auto-docking system on a DAF tractor semi-trailer combination. Chalmers University has recently published a movie of the design of an active dolly for the Duo2-project, which uses the same ideas as described above [34]. The proposed dolly design has active steering, propulsion for hill assist and eventually may be able to dock semi-trailers autonomously.

1.3 Problem statement and contributions

The A-double HCV appears to be very promising for fuel cost and emission reduction. However, several design challenges have to be tackled for this vehicle configuration. It is chosen to build up the A-double HCV with existing modules to reduce the investment costs. This means that for this project two standard, closed semi-trailers and a single axle driven tractor are used, which are coupled via a newly designed dolly. The aim of this thesis is to make a feasible design of such a smart dolly that can both assist the tractor in hauling the semi-trailers and ensures an acceptable manoeuvrability and stability. Furthermore, the autonomous operation of the dolly, with a coupled semi-trailer, should be taken into account when designing the dolly.

To solve the reduction in the manoeuvrability and stability of a conventional A-double HCV, the dolly is equipped with a steering system. Furthermore, to prevent over-dimensioning of the tractor powertrain for worst case scenarios, the dolly is equipped with its own propulsion system to assist the tractor when needed. By doing so, it is possible to use a standard 4x2 tractor, which has less driveline losses and is

cheaper than a 6x4 tractor. By using electric motors for the driveline of the dolly, the complete combination can be seen as a through-the-road hybrid. With such a driveline, the vehicle is able to harvest energy via regenerative braking. With both steering and propulsion applied to the dolly, it can also be used for autonomous driving around the warehouse or container terminal.

The aim of this thesis project is to make a preliminary design of this smart dolly and do a performance analysis of this smart dolly when coupled in an A-double HCV configuration. The smart dolly, in the context of an A-double configuration, should be able to:

1. Reduce the fuel consumption and CO_2 emissions per ton payload.

2. Provide enough tractive power for hill-assist, startability and acceleration requirements of the vehicle combination.

3. Improve the manoeuvrability and high-speed stability in comparison with a standard non-steered dolly by means of a dedicated steering system.

Research questions that need to be answered to achieve these goals are:
- What are the main dimensions of this smart dolly, while satisfying most of the dimension and weight requirements regarding international transport in the EU?

- How should the dolly be steered to obtain an acceptable manoeuvrability and high-speed stability?

- What should be the performance of the electric driveline in terms of output power and torque to ensure sufficient powertrain assist for the tractor and driving autonomously?

- What is the manoeuvrability and stability performance of this smart A-double HCV, using Performance Based Standards?

Since the smart powered dolly is designed from scratch, the following points will not be researched in this project:
- Strength calculations on the dolly chassis and components

- Cost and transport efficiency calculations, including cost of ownership

- Detailed powertrain component and suspension design

- Detailed safety assessment

- Hybrid drivetrain control strategy development

- Autonomous driving application of the dolly

1.4   Vehicle requirements

Requirements on the design of the smart dolly and the A-double HCV are divided in three groups: Dimensions and loads, Driveline and steering and Practical. The main requirements are listed below.

Dimensions and loads

1. Axle loads as stated in the EU 96/53/EC directive should be met.

2. Dimension limits for the individual components, e.g. tractor and semi-trailers, as stated in EU 96/53/EC should not be exceeded.

3. The dolly should fit in the space as defined by the tractor and semi-trailer dimensions.

4. The total vehicle length should be in the range of 30-34 meters, while minimizing distance between semi-trailers to improve aerodynamic efficiency.

5. The gross combination weight should be below 88 tonnes, which is the equivalent of two tractor semi-trailer combinations for intermodal transport.

6. The drawbar coupling should not be located more than 1.5 meter under the first semi-trailer.

7. Any standard curtain side, box or container semi-trailer that meets the EU 96/53/EC directive can be coupled via the smart dolly in an A-double configuration with minimal modifications required to the semi-trailer. The large volume/low coupling and extendable semi-trailers are neglected.

Driveline and steering of dolly

8. The dolly should have a steering system to improve the cornering performance and high speed stability of the A-double HCV in comparison with a non-steered dolly equipped A-double.

9. The dolly itself should have a turning radius equal or smaller than a regular tractor to be able to pick up any parked semi-trailer dropped off by a tractor.

10. The dolly should be able to assist the tractor via its own propulsion system in high power demanding driving situations, e.g. driving up-hill, startability and accelerations.

11. When the dolly is not coupled in an A-double configuration, it should be able to drive autonomously for small ranges, while hauling a semi-trailer.

12. The dolly should be equipped with a battery powered electric driveline, making the complete HCV combination a hybrid vehicle.

13. The batteries of the dolly should be rechargeable via regenerative braking, via the combustion engine while driving or charged with the electricity from the grid.

Practical

14. The drawbar should be retractable to avoid unnecessary large turning radii/swept paths while driving autonomously and to reduce the space between semi-trailers for semi-trailers with different pin coupling locations.

15. The dolly itself or fifth wheel should be height adjustable to haul semi-trailers with different king pin heights.

16. The dolly should be equipped with a 24V system for the electric components and supplying power to the semi-trailer.

17. The dolly should be equipped with a pneumatic system for application of the semi-trailer brakes.

For the smart A-double configuration two designs are proposed. The first configuration is two-wheel-driven, making it a 4x2 dolly. By doing so, the rear wheels can be driven by a single motor that drives the wheels via a driveshaft and differential. This configuration is less complex than the other design and thus cheaper. However, only the front wheels can be steered in this dolly design. The second configuration is a 4x4 in-wheel motor driven dolly. The wheels of this dolly design are propelled by in-wheel motors, which makes it possible to steer all the wheels. This configuration may be more expensive, but has better steering performance than the 4x2 design. Furthermore, since in this design both axles are driven, the allowed vertical axle forces are higher and it is easier to meet the 25% gross vehicle weight distribution on the driven axles. At the end of this report, the four configurations are compared and conclusions are made with respect to the performance achieved by the various configurations.

The performances of the smart dolly equipped A-double configurations are compared with both the performance of a tractor semi-trailer combination and a baseline A-double. The baseline A-double consists of a MAN TGX 4x2 BLS tractor, two Krone SDC 27 eL45' Box Liner semi-trailers and uses a non-steered, non-driven Krone (ZZB 18 eL) dolly [32], [12]. To make a fair comparison, the A-doubles with smart dollies and tractor semi-trailer combination use the same tractor and 45 ft. container semi-trailer as the baseline vehicle.

1.5   Organization of the report

Chapter 2 explains the Performance Based Standards approach to evaluate the vehicle's performance. At the end of this chapter the used simulation model is explained. In Chapter 3 the legislations are explained in detail and the available space for the dolly is determined in a geometry study. Finally, two different dolly geometry designs are developed. Chapter 4 deals with the selection of the best steering system for both dolly configurations and their implementation in the simulation model. In Chapter 5 the driveline performance requirements are derived and the driveline controller is explained. The results of the comparison between the various vehicles are presented in Chapter 6. The conclusions and recommendations can be found in Chapter 7.

Chapter 2
Performance Based Standards

In the European countries High Capacity Vehicles are categorised based on their dimensions and weights. However, HCVs can also be categorized based on their performance. In New Zealand, Canada and Australia this approach is used and vehicles are categorized using Performance Based Standards (PBS). The PBS approach states performance requirements that should be achieved by vehicles in order to get access to a certain road class. Furthermore, the PBS describes the methods to test the performance requirements.

The Australian PBS evaluates the vehicle in two main fields, which are infrastructure and safety. The first field assesses the performance of vehicles with respect to infrastructure damage and the second field assesses the safety in terms of stability, dynamic performance, powertrain performance and manoeuvrability. The performance level that is achieved by the vehicle corresponds to a certain road class. For Australian HCVs it does, therefore, not matter how the vehicle is configured, how long or how heavy it is, but only the performance of the vehicle matters [35], [18]. Boundary values to categorize vehicles into road class levels are not available in Europe. It is not useful to use the Australian road class boundary values for the European HCVs, since the European road infrastructure differs from the Australian infrastructure [18]. Therefore, it is chosen to perform the same tests as being described in the Australian PBS requirements, but compare the performance with a normal tractor semi-trailer configuration, instead of categorization using (Australian) road class levels.

This thesis mainly focusses on the preliminary steering system design of the smart dolly, so only the PBS manoeuvres that evaluate the steering performance of the vehicle are used. The manoeuvrability and stability of the vehicle is evaluated by means of nine different performance criteria that are tested with three different manoeuvres. Note that two of these criteria do not originate from the Australian PBS, but are added for the European legislation. These are the swept path tests in a 360 degree turn, as also explained in the EMS book of requirements [18]. The three manoeuvres include a:

- 90 degree turn
- 360 degree turn with different radii
- Single sine steer input, also known as a lane change manoeuvre

With these three manoeuvres, it is possible to calculate the performance criteria that are listed below. These performance criteria originate from [35] and [18] and are explained in the next sections.

1. Frontal swing
2. Tail swing
3. Low speed swept path
4. EU circle swept path
5. NL HCV circle swept path
6. Static roll-over threshold
7. Rearward amplification
8. Yaw damping
9. High speed off-tracking.

These performance values are calculated for four configurations, which are the: tractor with single semi-trailer, A-double HCV with non-steered dolly and the A-double HCV configurations with the 4x2 and the 4x4 dolly. Each configuration is evaluated for three loading conditions and the worst performance value is used in the performance assessment of the vehicle. The three loading conditions are:

1. Fully loaded 45 ft. containers
2. Empty 45 ft. containers on top of the semi-trailer chassis
3. Semi-trailer chassis without containers

The performance criteria are used to evaluate the behaviour of the vehicle during a certain manoeuvre. These values can be obtained via real-life tests or adequate modelling of the vehicle. The last approach is used in this research, since no prototype of the smart dolly is available yet. For the modelling of the A-double, the TU/e commercial vehicle library available in MATLAB/Simulink is used. More information about this model can be found at the end of this chapter.

2.1 The 90 degree turn

The first manoeuvre that is explained in detail is the 90 degree turn. With this manoeuvre three performance criteria can be determined, which are the frontal swing, tail swing and low speed swept path. In the 90 degree turn manoeuvre, the outer tyre of the tractor's steer axle follows a prescribed 90 degree turn with a 12.5 m radius. The vehicle speed during this manoeuvre equals 5 km/h.

Frontal swing

The first performance criterion that can be determined with this manoeuvre is the frontal swing of a vehicle. The frontal swing of a vehicle occurs due to the overhang of the cabin/bumper with respect to the first axle of the tractor and the front overhang of the semi-trailer. The front overhang of the semi-trailer is defined as the distance between the kingpin and front of the semi-trailer. The frontal swing performance is evaluated by means of three performance values. The first one is the Frontal Swing Swept Path Width and evaluates the frontal swing of the tractor. The second and third values are defined as the Maxima of Difference (MoD) and Difference of Maxima (DoM) and evaluate the frontal swing of the semi-trailer with respect to the tractor.

Due to the front overhang of the cabin, the path of the vertical projection of the outermost point on the cabin follows a path that exceeds the prescribed path of the outside tyre on the front axle, see Fig. 2.1. The performance value of the Frontal Swing Swept Path Width is the maximum radial distance between the outer- and innermost path, which is shown in Fig. 2.1. Smaller values for this performance standard are desired to limit the required space for cornering.
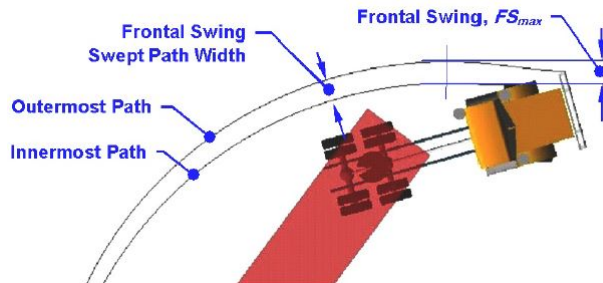

Figure 2.1: Definition of frontal swing for a low speed 90 degree turn [35].

Furthermore, when an articulated vehicle is cornering, the outermost point of the semi-trailer may exceed the trajectory followed by the outside tyre of the tractor's first axle or the trajectory followed by the outermost point of the cabin. This is caused by the overhang from kingpin to the front of the semi-trailer. This situation is shown in Fig. 2.2. The performance values that describe this behaviour are the *MoD* and *DoM*. The first performance value, *MoD* is defined as the Maximum of Difference and evaluates the frontal swing between adjacent vehicles in the configuration. This parameter describes the maximum lateral distance that the semitrailer needs while cornering, as shown in Fig. 2.2b. The second parameter, *DoM*, is known as the Difference of Maxima. This parameter describes the distance between the maximum lateral displacements of the tractor and semi-trailer. For clarification Fig. 2.2b can be consulted. The *DoM* and *MoD* evaluate the frontal swing of the semi-trailers and are measured at the exit side of the turn, perpendicular to the exit path, just as is the case for the tail swing and high-speed off-tracking. The purpose of all three frontal swing performance criteria is to reduce the safety risk by limiting the required road space while cornering.

(a) Cabin and semi-trailer trajectories.
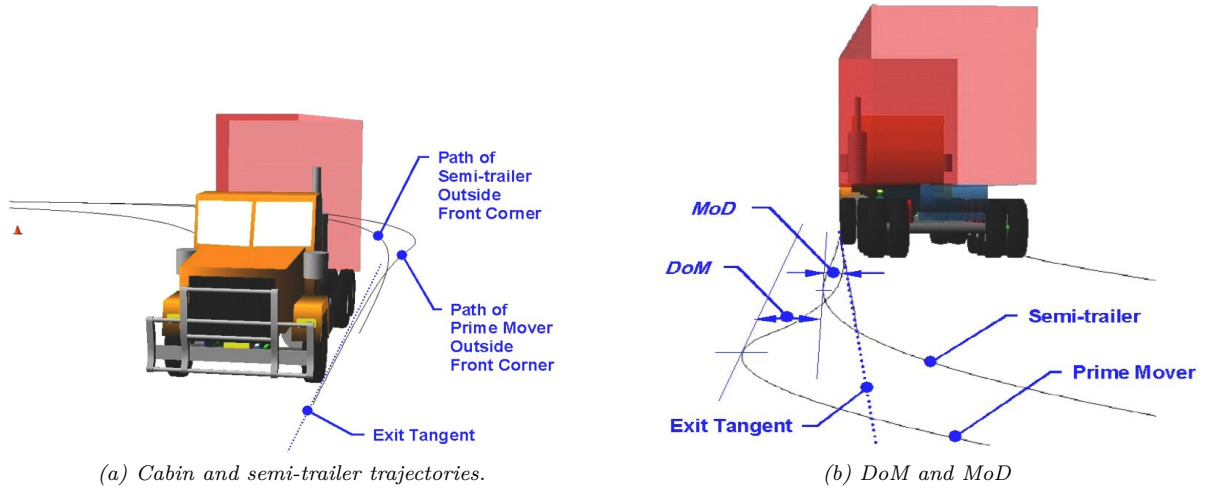
(b) DoM and MoD

Figure 2.2: Trajectories of the outermost points of the tractor and semi-trailer for the 90 degree turn [35].

Tail swing

The second performance criterion that can be determined with the 90 degree turn manoeuvre is the tail swing. The tail swing of a vehicle is defined as the maximum outward lateral displacement of the rearmost point of the vehicle. This performance value is mainly determined by the rear overhang of the last semi-trailer, which is defined as the distance between the rearmost axle of the semi-trailer and the outermost point at this semi-trailer. The tail swing is the maximum lateral distance between the trajectory of the most outer point of the semi-trailer and the entry path tangent of this point, as shown in Fig. 2.3. The greater this value, the worse the performance. This performance criterion is evaluated to reduce the safety risk by limiting the required road space.
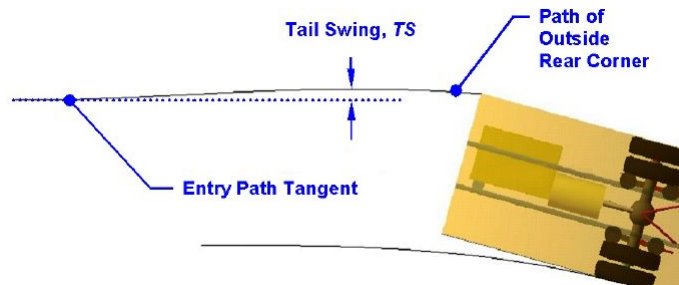

Figure 2.3: Definition of tail swing for a low speed 90 degree turn [35].

Low speed swept path

The last performance criterion that can be determined with the 90 degree turn is the swept path. When an articulated vehicle makes a low-speed turn at an intersection or roundabout, the trailing vehicles in the configuration follow a path that is inside the path of the tractor's front axle. This is an undesired effect, because the vehicle may require more road space than is available and may collide with the road infrastructure or vehicles in neighbouring lanes. From Fig. 2.4 it follows that the swept path is defined as the maximum radial distance between the outermost path and innermost path of the vehicle. The outermost path is defined by the outermost point at the tractor's cabin/bumper. The innermost path is defined by the innermost wheel of the last axle group in the vehicle configuration. For a three-axle semi-trailer this corresponds to the inner wheel of the centre axle. The vehicle performance in a low speed 90 degree turn manoeuvre primarily depends on the wheelbase, number of articulations and steerability of axles [18].
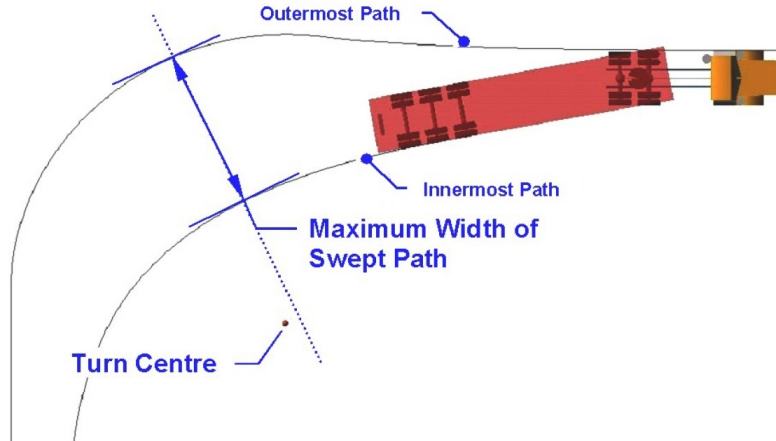
Figure 2.4: Definition of swept path for a low speed 90 degree turn [35].

2.2 The 360 degree turn

The second manoeuvre that is used in the PBS approach is a 360 degree turn. For this test, the outside wheel of the front axle follows a predefined circular path with a constant radius. This manoeuvre is used for the low speed manoeuvrability and high speed stability PBS criteria. For the low speed manoeuvrability criteria, the 360 degree turn manoeuvre is used to determine the circle swept paths. For the high speed stability assessment, the 360 degree turn is used for to determine the static roll-over threshold. The high speed stability 360 degree turn has an increased radius in comparison with the low speed manoeuvrability 360 degree turn.

High Capacity Vehicles are currently not allowed for cross-border traffic, so country specific legislations hold for the circular swept path performance. The country specific legislations regarding the low speed 360 degree turn swept path are shown in Table 2.1. European international traffic regulations state: "Any motor vehicle or vehicle combination which is in motion must be able to turn within a swept circle having an outer radius of 12.50 m and an inner radius of 5.30 m" [7]. This results in a maximum swept path of 7.20 m. The EU circle swept path is shown in Fig. 2.5. The Dutch swept path legislation for HCVs is less critical, since a larger swept path is allowed for HCV vehicles. The Dutch HCV legislation states that the vehicle should be able to turn within the area of two circles having radii of 14.50 m and 6.50 m [38]. This results in a maximum swept path of 8 m. The Swedish HCV swept path legislation is also added to Table 2.1, which has an inner and outer radius of 2.0 m and 12.5 m respectively [1].

Table 2.1: Country specific legislation regarding the 360 degree turn swept path of commercial and HCV vehicles [38], [7], [1].

		EU cross-border	Dutch HCV	Sweden HCV
r_{outer}	[m]	12.5	14.5	12.5
r_{inner}	[m]	5.30	6.50	2.00
swept path	[m]	7.20	8.00	10.5

Circle swept path

The first two performance criteria that can be determined with this manoeuvre are the NL HCV and EU circle swept paths. For these performance values, the outermost wheel of the front axle follows the predefined circular path with outer radii as listed in Table 2.1. The vehicle speed is set to 5 km/h. This standard is added to the Australian PBS by [18], since there are many roundabouts in the European infrastructure. The swept path is calculated as the radial distance between the outermost trajectory of the cabin and innermost wheel of the last semi-trailer [18]. For this calculation, the positions of the innermost axle of the last trailing vehicle and the positions of the outermost point of the cabin need to be sensed.
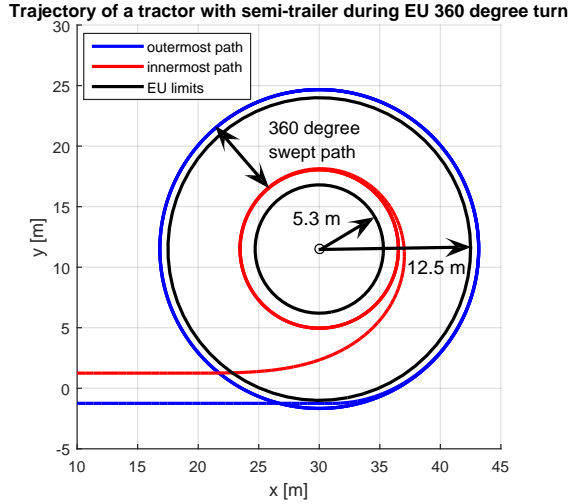
Figure 2.5: Trajectories of the inner- and outermost path for the EU 360 degree turn [7].

Static roll-over threshold

Vehicles encounter lateral accelerations when cornering. These accelerations induce a change in the vertical forces on the left and right tyres of the vehicle. In a HCV multiple vehicle units are coupled to each other, such that changes in the vertical tyre forces can be transferred via the couplings. Too high lateral accelerations, which can occur at high longitudinal velocities and small turning radii, may induce a too large roll angle, causing the vehicle to roll-over. The third performance criterion for the 360 degree turn manoeuvre is the static roll-over threshold. This criterion is used to assess the safety risk of a possible vehicle roll-over during high lateral accelerations. More information on the roll behaviour of a commercial vehicle can be found in Appendix A.

During the static roll-over manoeuvre the vehicle must be steered such that the centre of the tractor's steer axle follows a circular path with a 100 m radius. The velocity is gradually increased with 0.396 m/s^2, until roll-over occurs. Roll-over instability is achieved when the lateral acceleration of the vehicle decreases for increasing roll angle. This means that the point of roll instability is achieved when the vertical forces on all the tyres along one side of the vehicle are equal to zero, excluding the tyres on the lightly loaded side of a steer axle with soft springs [35]. The tyres at the side that looses contact with the ground can no longer generate lateral forces, so the resulting lateral acceleration of the vehicle decreases for increasing roll angle. This indicates that the vehicle starts to roll-over.

With the Dynamic Load Transfer Ratio (DLTR) it can be determined when the wheels loose contact with the ground [19]. This value describes the vertical tyre force distribution between the left and right side of a vehicle at a given time instance and can be calculated with:

$$R_{DLTR} = \frac{\sum_{n=1}^{N}(-1)^n F_{zn}}{\sum_{n=1}^{N} F_{zn}} \tag{2.1}$$

In this equation, N represents the total number of wheels of the vehicle unit and F_{zn} represents the vertical tyre force of the nth wheel. In (2.1) the vertical tyre forces on the left side of the vehicle, which have odd numbers, are subtracted from the tyre forces at the right side of the vehicle to calculate the DLTR. This means that the DLTR equals zero when the vehicle is evenly loaded and stands still. However, when the wheels at one side of the vehicle looses contact with the ground during a cornering manoeuvre, the absolute value of the DLTR equals one.

The static roll-over threshold is defined as the lateral acceleration divided by the gravitational constant at which roll-over instability occurs. Roll-over instability is achieved when the DLTR of a roll coupled unit equals one. Note that for roll coupled vehicle units, the resultant lateral acceleration needs to be used to determine the lateral acceleration at which roll-over occurs. Roll coupled units are the entire set of units that are coupled with only fifth wheel couplings [35]. For the A-double this means that the rearmost roll coupled units are the dolly and second semi-trailer, since the dolly's drawbar can rotate freely with respect to the first semi-trailer. For roll coupled units, any roll moment originating from the

rear unit is directly transferred to the other roll coupled unit(s). The resulting lateral acceleration $a_{y,rcu}$ of the roll coupled units can be calculated with:

$$a_{y,rcu} = \frac{\sum_{n=1}^{N} m_n h_n a_{yn}}{\sum_{n=1}^{N} m_n h_n} \tag{2.2}$$

The parameter m_n represents the sprung mass of the vehicle unit, h_n represents the CoG height of the sprung mass and a_{yn} represents the lateral acceleration at the CoG of the sprung mass. The subscript n represents the nth vehicle in the roll coupled units. The total number of roll coupled vehicle units is represented by N [35].

From the above it can be concluded that the static roll-over threshold of a vehicle is defined as: the maximum resultant lateral acceleration of the roll-coupled units at which the absolute DLTR value of all vehicles is smaller than one.

2.3 Single sine steer input

The single sine manoeuvre is added to the PBS to evaluate the dynamic roll-over performance. The steer input for this manoeuvre is defined by ISO 14791:2000(E) and the velocity equals 88 km/h [35]. This manoeuvre is known as a single sine steer input, which resembles an obstacle avoidance/lane change manoeuvre at high velocity. The vehicle should achieve a maximum lateral acceleration at the front steer axle of no less than 0.15g and the steer input should have a steer frequency of 0.40 Hz [35]. This means that for each vehicle configuration, the amplitude of the single sine steer input needs to be tuned to meet the 0.15g acceleration requirement. The single sine manoeuvre is used to evaluate the: rearward amplification, yaw damping and high speed off-tracking performance criteria.

Rearward amplification
The first criterion that can be determined with the single sine manoeuvre is the rearward amplification of a vehicle. This criterion is introduced to evaluate the roll-over risk of the last vehicle in the configuration during an avoidance manoeuvre. During the single sine manoeuvre, the trailing vehicles encounter higher lateral acceleration than the hauling unit, due to the yaw- and/or roll moment transfer along the vehicle.

Rearward amplification is defined as the ratio between the maximum absolute lateral acceleration of the last roll-coupled vehicle units and the lateral acceleration of the steer axle. Rearward amplification reduces with: fewer articulation points, roll coupling, increased drawbar lengths, larger trailer wheelbases, tyres with higher cornering stiffness and shorter distances between the couplings and the CoG of the hauling unit [18]. The rearward amplification R_{RA} of a HCV can be calculated with:

$$R_{RA} = \frac{max(|a_{y,rcu}|)}{max(|a_{y,sa}|)} \tag{2.3}$$

The parameter $a_{y,rcu}$ represents the resulting lateral acceleration of the last roll coupled unit, which can be calculated with (2.2). The parameter $a_{y,sa}$ represents the lateral acceleration at the steer axle of the tractor. Small values for the rearward amplification are desired, since this reduces the roll-over risk of the rearmost vehicle units during the single sine manoeuvre [35].

Yaw damping
The tyres at a vehicle need to generate lateral tyre forces to initiate a turn. At high velocities the yaw orientation of the rearmost vehicles may show oscillatory behaviour, since it takes some time to generate sufficient lateral tyre forces. At increasing velocities, the oscillations may take longer to settle down and could lead to roll-over of the vehicle. The second performance criterion that is evaluated with the single sine test manoeuvre is the yaw damping. This criterion: "assesses the safety risk by requiring acceptable attenuation of any sway oscillations" [35]. The yaw damping coefficient can be determined with the time history of the: articulation angle, articulation angle velocity or the yaw rate of the last vehicle unit. A typical representation of the yaw rate during a single sine manoeuvre is shown in Fig. 2.6. Seven amplitudes are shown in Fig. 2.6, which are used in the calculation of the yaw damping coefficient.
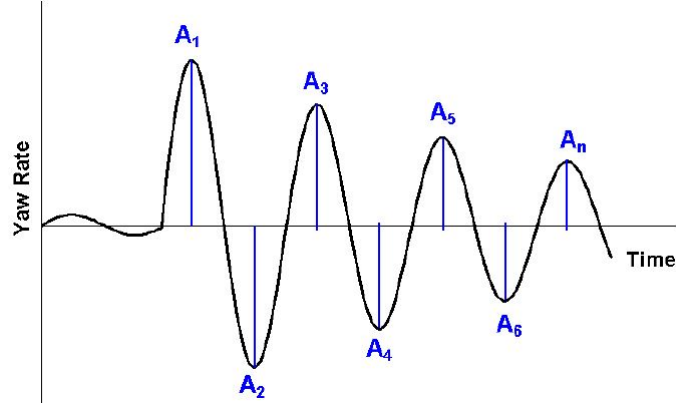
Figure 2.6: Yaw rate of an articulated vehicle during the single sine manoeuvre [35].

The yaw rate amplitude ratio $\overline{A}$ is required to calculate the yaw damping coefficient D. Depending on the number of amplitudes, the yaw rate amplitude ratio is defined as the ratio between consecutive amplitudes or between consecutive amplitudes having the same sign. The value of $\overline{A}$ can be calculated with:

$$\overline{A}_1 = \frac{1}{n-2}\left(\frac{A_1}{A_3} + \frac{A_2}{A_4} + ... + \frac{A_{(n-2)}}{A_n}\right) \tag{2.4}$$

or

$$\overline{A}_2 = \frac{1}{n-1}\left(\frac{A_1}{A_2} + \frac{A_2}{A_3} + ... + \frac{A_{(n-1)}}{A_n}\right) \tag{2.5}$$

The parameter n represents the amplitude peak number at which the yaw rate magnitude is equal to or smaller than 5% of the first amplitude, since then it is assumed that the sway oscillations are settled down. The amplitude ratio $\overline{A}$ is calculated with (2.5) when the value of n is less than six. When n is equal to or greater than six, the amplitude ratio is calculated with (2.4) [35].

Depending on the amplitude number n at which the absolute maximum is reduced to 5% of the first maximum, the yaw damping coefficient D can be calculated with:

$$D_1 = \frac{\ln(\overline{A}_1)}{\sqrt{(2\pi)^2 + [\ln(\overline{A}_1)]^2}} \tag{2.6}$$

or

$$D_2 = \frac{\ln(\overline{A}_2)}{\sqrt{\pi^2 + [\ln(\overline{A}_2)]^2}} \tag{2.7}$$

The yaw damping coefficient is calculated with (2.6) when n is equal to or greater than six. For all other cases, (2.7) is used [35].

Fewer articulation points and increased distances between kingpin and axle groups are beneficial for the yaw damping. The yaw damping can also be improved by adequate air suspension design and increased roll-centre height. These last two solutions counteract the roll behaviour of the vehicles [18].

High speed off-tracking

The last performance criterion that is evaluated with the single sine manoeuvre is the high speed off-tracking. This standard is used to: "assess the sway of the rearmost semi-trailer during a single sine manoeuvre at high velocity " [35]. During severe lane change manoeuvres at high velocities, the trajectory of the rearmost trailer exceeds the path of the hauling unit, as can be seen in Fig. 2.7. The off-tracking performance is the maximum lateral distance between the path followed by the centre of the rearmost axle of the last semi-trailer and the exit path tangent of the centre of the tractor's steer axle. High off-tracking values indicate that the rearmost trailer sways more, which may cause collisions with objects in neighbouring lanes.
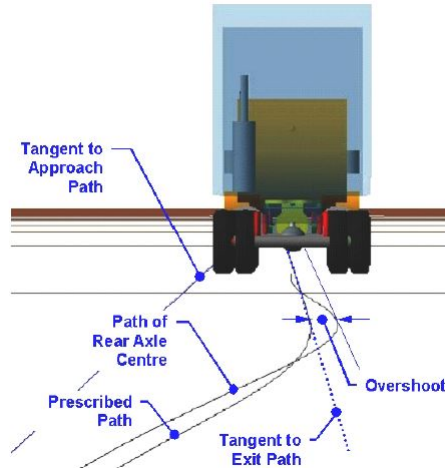
Figure 2.7: High-speed off-tracking of a commercial vehicle [35].

2.4 TU/e Commercial Vehicle Library

The PBS criteria can be evaluated via real life testing or via simulation models. For this research a multibody vehicle model is used, because there are no physical prototypes of the smart dolly yet. In a multibody model the dynamic behaviour of a system is modelled by means of interconnected bodies, which are able to rotate and translate under the presence of a force or torque. The connections between these bodies can be modelled as kinematic constraints like joints or force elements like e.g. springs and dampers. The TU/e Commercial Vehicle Library (CVL) model is used in this research, which is based on the SimMechanics multibody toolbox of MATLAB. The TU/e CVL is a generic commercial vehicle library with different components and vehicles [28].

SimMechanics is a multibody simulation environment in which 3D mechanical systems can be modelled by blocks that represent: bodies, joints, constraints, force elements and sensors. Bodies in this model are connected via user defined joints. Kinematics, forces and torques at- and between the bodies can be obtained via sensors and applied to the bodies via actuators. The SimMechanics toolbox formulates and solves the equations of motion for each body, such that kinematics and dynamics of the bodies can be retrieved.

Five different sections can be distinguished within the TU/e CVL, these are:

- Vehicles, e.g. trucks, tractors
- Trailers, e.g. drawbar trailers, dollies, centre-axle trailers, semi-trailers
- Assemblies, e.g. cabins, loading units, axles,...
- Components, e.g. tyres, brake system,...
- Utilities, e.g. filters, sensors

The user can build vehicles in a modular way by using the blocks available in the five sections above. Trailers can be coupled to motor vehicles and components and assemblies can be added to each vehicle or trailer. The library represents an average vehicle and avoids manufacturer dependent details. If desired, the models can be customized by the user [28]. The TU/e CVL is validated in [28] and it is stated that the TU/e CVL represents the real-life behaviour of a HCV well.

Two important MATLAB Toolboxes that are used by this library are the TNO-Delft Tyre model and the Virtual Reality Toolbox (VRT). The first toolbox describes the tyre forces and moments of each tyre by means of Pacejka's Magic Formula. Three different types of tyres are included, which are the tyres of a: steered axle, driven axle and trailer axle. The second toolbox is the Virtual Reality Toolbox, which can be used for 3D simulations of the vehicle. By using basic shapes, like cylinders and cubes a 3D representation of the vehicle can be generated. The 3D representation of the A-double HCV, as generated by the VRT, is shown in Fig. 2.8.
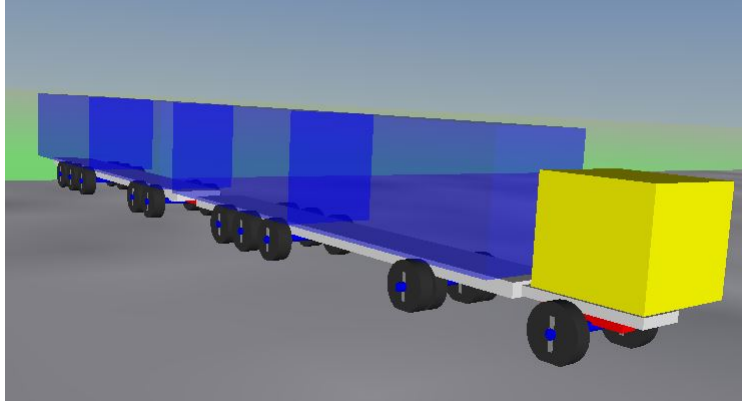
Figure 2.8: Virtual reality representation of the A-double HCV.

The positions of all vehicle units, couplings and assemblies needs to be defined by the user. For simplicity reasons each vehicle has its own local coordinate system. The used coordinate system corresponds to the ISO sign convention, as shown in Fig. 2.9. This coordinate system has its origin at the contact point between a vertical line through the centre of the tractor's/truck's steer axle and the ground. The longitudinal component is directed to the front of the vehicle, the lateral component is directed to the left of the vehicle and the vertical component is directed upwards. The trailer coordinate system starts at the centre of the coupling point. In Fig. 2.9 the local coordinate system of the semi-trailer starts at $-x_{ref}$, and z_{ref} with respect to the steer axle. The positions of the assemblies of a particular vehicle or trailer are defined by the distances with respect to the origin of the local coordinate system. More information on the TU/e CVL can be found in [28] and [19].
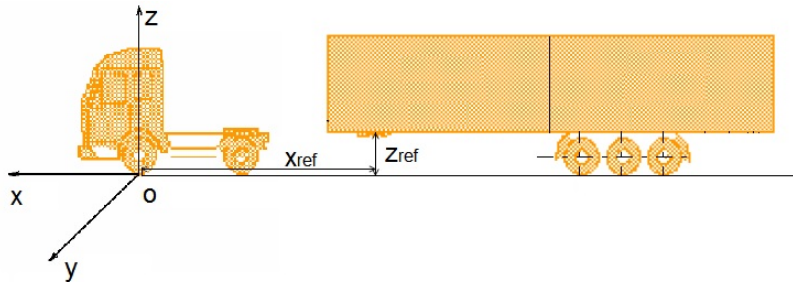

Figure 2.9: Coordinate system of a tractor semi-trailer combination in the TU/e Commercial Vehicle Library [19].

Input for the models include a predefined path and initial velocity. This input originates from the PBS criteria explained earlier. After the simulation, the data is stored and can be used for further processing. Post processing scripts are available to retrieve the performance values for the nine PBS criteria. Similar to the research in [18], the post processing scripts analyse the data and calculate the relevant performance value for each PBS criterion. Note that these scripts depend on e.g. the number of: trailers, axles and vehicle mass, so the scripts are adapted for the A-double HCV.

2.5 Summary

To evaluate the steering performance of the A-double HCV, a Performance Based Standards approach is used. The PBS state goals and objectives that should be achieved by the vehicles and describes the methods to test them. The manoeuvrability and high speed stability are evaluated by means of three manoeuvres and nine criteria. The three manoeuvres include a 90 degree turn, 360 degree turn and a single sine steer input. With these three manoeuvres it is possible to determine the: frontal swing, tail swing, low speed swept path, EU circle swept path, NL HCV circle swept path, static roll-over threshold, rearward amplification, yaw damping and high speed off-tracking. Main aim of these tests is to evaluate the required road space during these manoeuvres and evaluate the roll-over tendency of the vehicle.

The performance values of the individual criterion can be determined by means of real life testing or adequate modelling of the HCV. The last approach is used in this project, because there is no real-life prototype of the smart dolly yet. The TU/e Commercial Vehicle Library is used, which is based on the SimMechanics multibody toolbox of MATLAB. With this library it is possible to build multi-body models of (A-double) HCVs and test the performance of this vehicle during certain manoeuvres.

The input of the multi-body model simulations is defined by the path and velocity of the different PBS test manoeuvres. The simulation results are processed afterwards to calculate the performance value of each PBS criterion. A detailed comparison of the performance criteria of four different vehicles is provided at the end of this report.

Chapter 3
Commercial vehicle legislation and geometry study

In this chapter the EU commercial vehicle legislation is explained in detail. Commercial vehicles driving cross-border on European roads should meet certain dimension, weight and safety legislation, as stated in Directives 96/53/EC [7] and 97/27/EC [8]. The legislation on dimensions is used to ensure safe operation of the vehicle within the infrastructure and the weight legislation is introduced to limit the road wear and damage to bridges. Adaptations of these rules for national transport can be made by the individual countries. High Capacity Vehicles are vehicles which exceed these gross vehicle weights and/or dimensions and are currently not allowed for cross-border traffic in the EU. Therefore, country specific HCV legislation holds. This chapter starts with the weight legislation, followed by the dimensions legislation and semi-trailer dimensions. The available space for the dolly is determined next and the optimal locations for the axles and fifth wheel coupling at the dolly are determined at the end of this chapter.

3.1 Legislation

In this part of the report the legislation that holds for the commercial vehicles is explained. First the allowed vehicle configurations for EU cross-border traffic and the Dutch HCV vehicles are explained in detail. Next, the weight and dimension limits are explained.

Vehicle configurations

The commercial vehicles that are currently allowed on European roads are configured by using different vehicle units. The vehicle units that are currently allowed for cross-border traffic can be divided into two main groups and are shown in Fig. 3.1. These groups are the motor vehicles and the towed vehicles. It should be clear that a towed vehicle cannot drive on its own and needs to be connected to a motor vehicle.

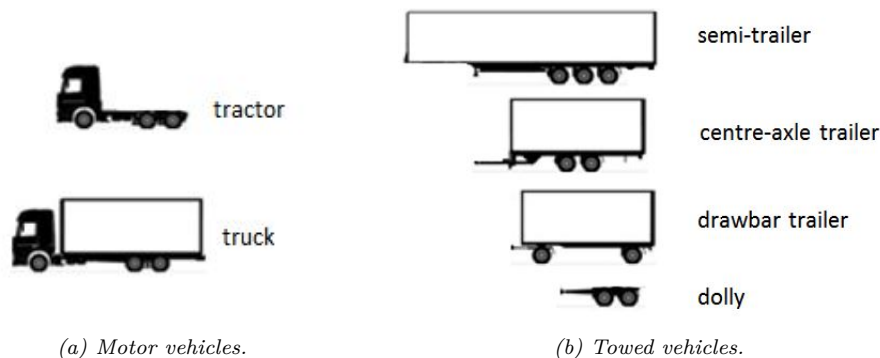(a) Motor vehicles.   (b) Towed vehicles.

Figure 3.1: Available vehicle units for road transport [27].

The motor vehicle unit is either a tractor or a truck. A tractor is coupled to a semi-trailer by means of a fifth wheel coupling. This fifth wheel coupling has two degrees of freedom, since it can rotate with respect to the vertical and lateral axes of the vehicle. The corresponding semi-trailer has a king pin, that is coupled to this fifth wheel. The truck, however, can transport goods on its own and can also be coupled to a trailer. This trailer can either be a centre-axle trailer or drawbar trailer. The difference between these two is that at a drawbar trailer, the axles are placed at the front and rear of the trailer and the first axle can rotate with respect to the vertical axis of the trailer. The centre-axle trailer has the axles mounted close to each other at approximately the centre of the trailer. Both the centre-axle trailer and drawbar trailer are coupled via a pin coupling to a truck, which has three degrees of freedom. These degrees of freedom include rotations with respect to the longitudinal, lateral and vertical axis of the coupling. The last towed vehicle is a dolly. The dolly can be used to couple a semi-trailer to a motor vehicle by means of a pin coupling.

Combining these vehicle units, results in the vehicle configurations as shown in Fig. 3.2. The current allowed HCV configurations on the Dutch roads are shown in Fig. 3.2b. The A-configuration consists of a tractor, standard semi-trailer and centre-axle trailer. The B-configuration (or B-double) consists of tractor with two semi-trailers of which the first one is equipped with a fifth wheel coupling, also known as a link trailer. The C-configuration consists of a large truck with a large drawbar trailer and the D-configuration consists of a truck with a semi-trailer connected via a dolly. The last configuration is known as the E-configuration and combines a truck with two centre-axle trailers. The HCVs that are shown in Fig. 3.2b are not allowed for international traffic, but are only allowed to be operated in specific countries.

(a) Allowed EU commercial vehicles.   (b) Allowed HCV combinations in NL.
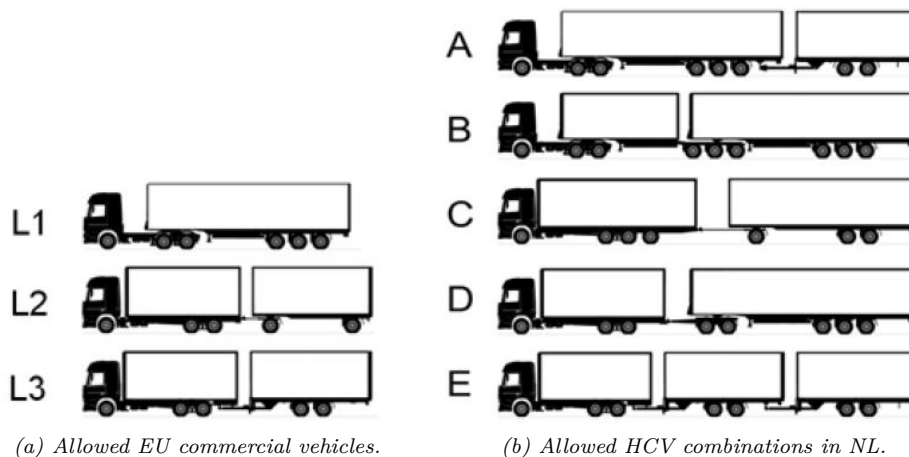
Figure 3.2: Vehicle configurations allowed for international transport within the EU and Dutch HCVs [27].

The Dutch HCV legislations states that these vehicles are only allowed on designated routes, which implies that at a certain point, for example in dense city-areas, the vehicles should be decoupled and hauled separately [40]. With the standard towed vehicle units in Fig. 3.2a, the best case scenario is that 3 full trucks (e.g. two 'L1' vehicles and one 'L2' or 'L3' vehicle) can be replaced by two HCVs due to the length restriction of the Dutch HCVs configurations. In the hub-spoke logistics concept, vehicles are split at a certain point to supply different 'spokes' in a city. With the currently allowed configurations, this already implies that more beneficial configurations can be designed that are better suited for the hub-spoke logistics concept. Furthermore, remark that the current allowed HCVs require special trailers or combine different towed vehicles. A study performed in [18], shows that 86% of the currently used vehicle configurations is a tractor with semi-trailer. To keep the investments costs for the HCV as low as possible, it is logical to configure a HCV that only uses a tractor and multiple semi-trailers. The A-double HCV is an example of such a concept, which is better for the hub-spoke logistic concept and uses two semi-trailers. Note, however, the A-double violates the current Dutch HCV legislation [38].

Weight legislation
The aim of the weight legislation of commercial vehicles is to limit the road wear and damage to bridges. This legislation can be divided in axle weight and gross vehicle weight. The axle weight (or vertical axle force) limit is a function of the space between the axles and whether this axle is driven or not. The maximum gross vehicle weight of a standard tractor semi-trailer combination is limited to 40 t (44 t for intermodal transport). Dutch HCV regulations state that the complete configuration has a maximum weight of 60 t, while meeting the axle weight limits of normal commercial vehicles that are shown in Fig. 3.2a [40], [38]. The maximum allowed gross vehicle weights, axle weights of them and other requirements are listed in 96/53/EC [7]. The relevant legislation for the A-double is listed below. This A-double legislation originates from the EU directive [7], if not stated otherwise.

Gross vehicle weight

- Two-axle motor vehicle with three-axle semi-trailer: 40 tonnes
- Two-axle motor vehicle with three-axle semi-trailer carrying, in intermodal transport operations, one or more containers or swap bodies, up to a total maximum length of 45 feet: 42 tonnes
- Three-axle motor vehicle with three-axle semi-trailer carrying, in intermodal transport operations, one or more containers or swap bodies, up to a total maximum length of 45 feet: 44 tonnes
- Two-axle motor vehicles other than buses: 18 tonnes*
- Dutch HCV with a maximum loading length of 25.25 m [38]: 60 tonnes

* plus 1 tonne when an alternative fuelled motor is used in the propulsion (e.g. electric motor).

The wheelbase of an axle set determines the maximum allowed vertical force on each axle. A set of two axles is called a tandem axle set when the distance between the centres of the axles d_{axle} is less than 1.8 m. If the distance between them exceeds this value, the axles are treated as individual axles.

Axle weight single axles on motor vehicles

- Single non-driving axle 10 tonnes
- Driving axle 11.5 tonnes

Axle weight tandem axles on motor vehicles.
The sum of the axle loads per tandem axle must not exceed, if the distance d_{axle} between the axles is:

- less than 1 m ($d_{axle} <1,0$) 11.5 tonnes
- 1.0 m or greater, but less than 1.3 m ($1.0 \leq d_{axle} < 1.3$): 16 tonnes
- 1.3 m or greater, but less than 1.8 m ($1.3 \leq d_{axle} < 1.8$): 18 tonnes

Axle weight tri-axles on trailers
The sum of the axle loads per tri-axle must not exceed, if the distance d_{axle} between the axles is:

- 1.3 m or less ($d_{axle} <1,3$) 16 tonnes
- over 1.3 m and up to 1.4 m ($1.3 \leq d_{axle} < 1.4$): 21 tonnes

Another important requirement is:

- The weight borne by the driven axle(s) of a vehicle or vehicle combination must not be less than 25 % of the total laden weight of the vehicle or vehicle combination, when used in international traffic.

Concluding from the above and under the assumption that the smart dolly is categorized as a motor vehicle, the dolly has a maximum weight of 18 t. The axle weight limit depends on the distance between the axles of the dolly. For a distance between 1.3 m and 1.8 m, the maximum allowed sum of the axle weights is 18 t. However, when the distance between the axles is greater than 1.8 m, the individual axle weight is 10 or 11.5 t for a non-driving and driving axle, respectively. This already implies that a larger wheelbase is beneficial for the axle weight legislation. It is assumed that the maximum allowed gross vehicle weight equals 88 tonnes, which corresponds to two, three-axle motor vehicles coupled to a 45 ft. container semi-trailer.

Dolly weight assumption
An assumption on the smart dolly's mass is required to calculate the vertical axle forces and to perform PBS simulations. Although there is no strict GVW limit for the A-double HCV yet, the dolly needs to be as light as possible to increase the payload of the A-double. The weight of the smart dolly increases in comparison with a standard dolly, because of the presence of the powertrain and steer system. The powertrain weight of the smart dolly depends on the number of electric motor(s) that are used and the battery size. No detailed powertrain design is developed in this research, so an assumption of the smart dolly's powertrain weight is made based on the available information.

The standard Krone ZZB 18 eL dolly, that is used by the baseline A-double, weighs 2.7 t [12]. However, the steered Krone ZZB 18 eLZ dolly weighs 3.4 t, resulting in a mass increase of 0.7 t caused by the steering system [12]. The weight of the steered dolly from Fliegl, however, equals 2.5 t [58]. Based on these

numbers, it can be concluded that the mass of dolly steering systems differ a lot. Therefore, it is assumed that the steering system increases the mass of the non-steered dolly with 0.5 t. For now, it is further assumed that the dolly uses the same motors as an electric bus. ZF's Electric Portal Axle AVE 130 bus axle has two build in asynchronous motor and the mass of this bus axle, including the weight of the: suspension arms, rods, air springs and shock absorbers, is 1.2 t [63]. Directive 96/53/EC allows an additional GVW of 1 t for motor vehicle other than busses that use alternative fuels like e.g. electric motors [7]. Therefore, it assumed that the additional mass increase for the smart dolly's electric powertrain equals 1 t.

Based on these numbers, it is assumed that the smart dollies are 1.5 t heavier than the non-steered and non-driven Krone ZZB 18 eL dolly. This results in a total mass of 4.2 t for the smart dolly designs. Comparing this with the mass of the MAN TGX 4x2 tractor, the dolly weighs 2.8 t less than the tractor. Since the dolly does not have a heavy cabin, ICE and body parts, this is a reasonable number.

Dimensions and Geometry legislation
The dimension and geometry legislation is used to ensure safe operation of the vehicle while cornering or manoeuvring. This legislation not only states limits on the total length of the vehicle, but also on the length of individual components and the couplings. All the maximum and minimum dimensions of the trucks are shown in Table 3.1 and Fig. 3.3. This Table also includes the Dutch HCV dimension legislation. The Dutch HCV legislation states that the complete configuration should have at most two turning points and a maximum length of 25.25 m [38]. It is obvious that A-double HCV violates these two limits.

Another important dimension limit is the clearance between the rear protective device and the ground of the semi-trailer as stated in EU Directive 70/221/EEC [9]. This clearance limits the pitch movement of the dolly's drawbar. A pitch movement is defined as a rotation with respect to the lateral axis of the vehicle that e.g. occurs on inclined roads. Note, however, the rear protective device is not required for the first semi-trailer in the A-double configuration. This means that a retractable underride protection and bumper can be used on the first semi-trailer. Krone already delivers trailers with such systems [14]. When the bumpers are fully retractable, the chassis height of the semi-trailer becomes the limiting factor for the maximum drawbar height. Research should show if it is required to use a removable/retractable bumper and rear protection device on the first semi-trailer.
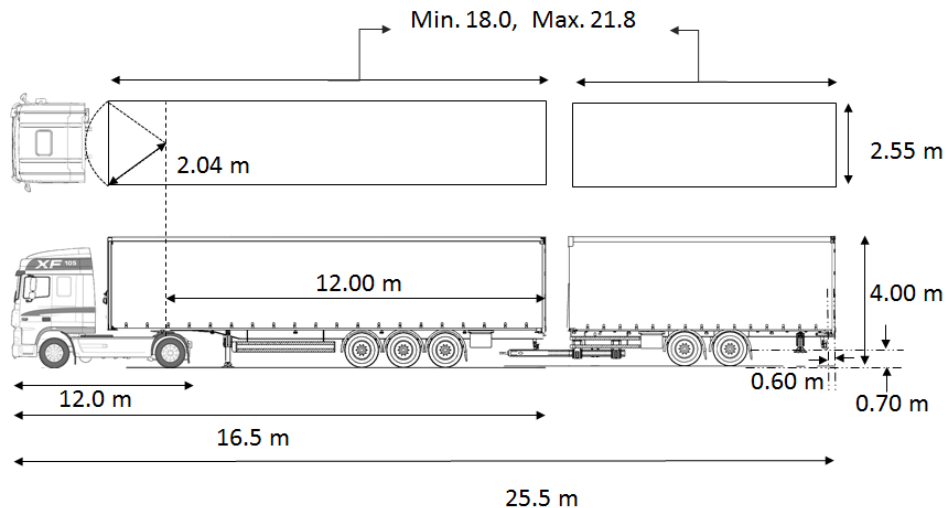

Figure 3.3: Maximum dimensions for tractor with semi-trailer in EU cross-border traffic and Dutch HCV [38], [9], [7].

Table 3.1: Legislation regarding dimensions of tractor, semi-trailer and Dutch HCVs.

Dimension	Value		Source
Max. length motor vehicle	12.00	m	[7]
Max. length articulated vehicle	16.50	m	[7]
Max. width vehicle	2.55	m	[7]
Max. distance from kingpin to rear semi-trailer	12.00	m	[7]
Max. height	4.00	m	[7]
Max. distance kingpin to any point in front of the semi-trailer	2.04	m	[7]
Min. distance between the rear axle of motor vehicle and the front axle of towed unit	3.00	m	[7]*
Min. total inner loading length of Dutch HCV	18.00	m	[38]
Max. total inner loading length of Dutch HCV	21.8	m	[38]
Max. length Dutch HCV combination	25.3	m	[38]
Max. ground clearance rear protection device	0.70	m	[9]
Max. distance between rear of trailer and front of protection device	0.60	m	[9]

* Directive 97/27/EC states that a semi-trailer coupled to a dolly should be considered as a drawbar trailer, so this requirement also needs to be taken into account when configuring the A-double HCV.

Since the smart dolly is equipped with a steering system and powertrain, it is possible to use the smart dolly for autonomous operation. Based on this, it is assumed that the smart dolly will be categorized as a motor vehicle in the EU directives. Combined with Table 3.1 it is concluded that the maximum dolly length equals 12.00 m. Furthermore, the width of the dolly is limited to 2.55 meter and the distance between the rearmost axle of the tractor and the first dolly axle should be greater than 3.00 meter. It is assumed that the MAN 4x2 tractor and 45 ft. container semi-trailer meet the dimension legislation shown in Table 3.1.

Semi-trailer dimensions

The aim of this project is to combine a standard tractor semi-trailer combination with a second semi-trailer via a specially designed dolly. This implies that the dolly should fit within the space available between two standard semi-trailers. With standard semi-trailers only three-axle closed semi-trailers are evaluated, excluding: lightweight, extendable and/or mega-volume semi-trailers. A closed semi-trailer can be a: box-, curtain- or container semi-trailer. Trailer dimensions are not all limited by legislation, so the individual semi-trailer dimensions partially determine the space that is available between the semi-trailers in the A-double configuration. Therefore, semi-trailer tech sheets of different manufactures are consulted to ensure that the dolly fits between both semi-trailers.

The height of the dolly is limited by the coupling height of the semi-trailer. This is represented by h_{kp}. The front drawbar height of the dolly is limited by the semi-trailer chassis thickness, represented by h_{chass}. The resulting height that can be used by the drawbar in front of the dolly is defined as the difference between h_{kp} and h_{chass}. The total length of the semi-trailer is represented by $l_{tot,t}$ and the wheelbase of the semi-trailer by l_t. The wheelbase of a semi-trailer is defined as the distance between the king pin and the centre axle of the tri-axle set. To determine the maximum distance between the rear of the vehicle and the pin coupling location, the lengths l_{ro} and l_{co} are required. The rear overhang of the semi-trailer, measured from the rear of the last axle to the rear of the trailer is represented by l_{ro} and limits the coupling overhang l_{co}. The distance between the support legs and king pin of the semi-trailer is represented by l_{sl}. The front overhang of the semi-trailer is represented by l_{fo}. The semi-trailer dimensions listed above are shown in Fig.3.4.

Semi-trailer tech sheets of several large trailer manufacturers like: Kässbohrer, Fliegl, Krone and van-Hool are consulted and the dimensions of these semi-trailers are listed in Appendix B. The most critical dimensions are listed in Table. 3.2. These critical dimensions are the minimum or maximum found values of a certain semi-trailer parameter.
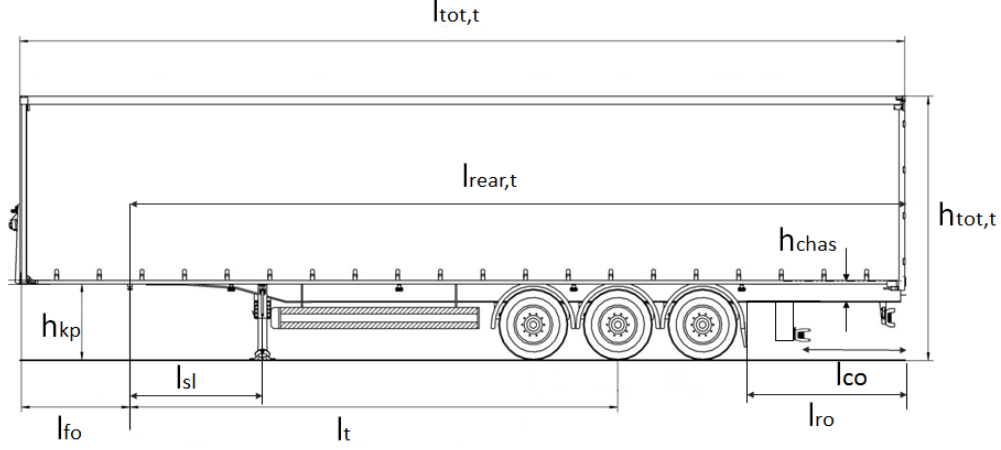
Figure 3.4: Semi-trailer dimensions [44].

Table 3.2: Worst case dimensions for a standard closed semi-trailer.

Parameter	Value	
Min. king pin height/coupling height (h_{kp})	1.05	m
Min. distance king pin to support legs (l_{sl})	2.32	m
Max. distance king pin to front of trailer (l_{fo})	2.00	m
Min. rear overhang (l_{ro})	1.28*	m
Max. thickness chassis rear (h_{chass})	0.40	m
Pin coupling overhang (l_{co})	1.50/0.76**	m

* Smallest found value. This rear overhang does not allow a pin coupling overhang of 1.50 m

** Only these two values have been found, but they differ a lot.

The pin coupling overhang l_{co} determines the required drawbar length of the dolly. However, the pin coupling overhang is limited by the available space at the rear of the semi-trailer, determined by the rear-overhang l_{ro}. The rear-overhang is typically measured from the centre of the last axle of the semi-trailer to the rear of the semi-trailer. The tyre radius is added to the rear overhang l_{ro} obtained from the tech sheets, to determine the maximum value of l_{co}. The semi-trailers in Appendix B have different rear overhangs l_{ro}, which allow different maximum pin coupling overhangs l_{co}. Remark that the space between the semi-trailers may increase for different pin coupling overhangs. The only way to reduce this space is to either make the drawbar length variable or fix the location of the pin coupling position of all semi-trailers via legislation.

3.2 Geometry study

This section deals with the geometrical design of the dolly. The geometry design of the dolly is limited by several aspects. First of all, the dolly should fit within the space available between the two semi-trailers. Secondly, the dolly should not violate the EU dimension legislation of a motor vehicle. Thirdly, the space between both semi-trailers should be as small as possible to minimize the additional air drag. Lastly, the vertical axle forces should not exceed the axle weight limits as stated in the EU directives. The locations of the axles and fifth wheel at the dolly determine the vertical axle forces, so the axles and fifth wheel positions should be chosen correctly. The organisation of this section is as follows: the available space for the dolly is derived first. With these dimensions, the maximum wheelbase can be determined. The vertical tyre force equations are derived in the second part. The axle and fifth wheel positions are chosen in the third part, using the vertical tyre force equations and maximum achievable wheelbase.

Available space

In this section the dimensions and available space for the wheelbase of the smart dolly are determined. Note that the dimensions of the semi-trailers and the EU legislation limit most of the dolly dimensions. However, some additional space is required for the dolly while cornering to avoid collisions between the dolly and the semi-trailers. For evaluation of the movements of the dolly while cornering, it is assumed that a fixed, non-rotating drawbar is used, which is shown in Fig. 3.5a. There are special designs with drawbars that can rotate with respect to the chassis of the dolly, see Fig. 3.5b, or shovel-like articulated dollies, but these are not considered in this geometry study.
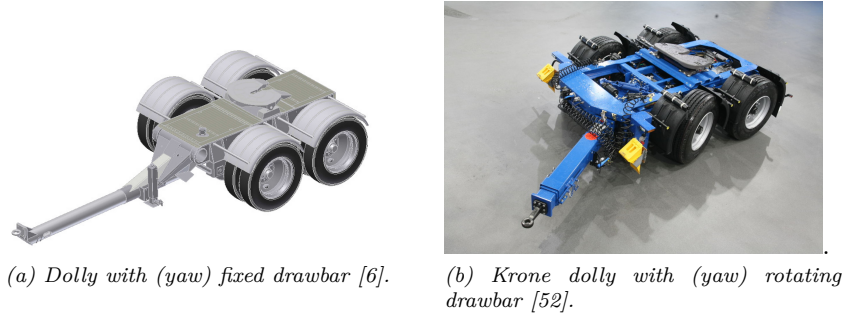

(a) Dolly with (yaw) fixed drawbar [6].

(b) Krone dolly with (yaw) rotating drawbar [52].

Figure 3.5: Different dolly drawbar configurations.

The non-steered dolly in an A-double HCV configuration has two articulation points which are located below the first semi-trailer at the pin coupling and at the fifth wheel coupling of the dolly. Collisions while cornering can occur at three places and are denoted by the numbers 1, 2 and 3 in Fig. 3.6. These collisions can occur between the front and rear of the bumper/underride protection of the first semi-trailer and the dolly (1), between the dolly and the support legs of the second semi-trailer (2) and between the two semi-trailers (3).
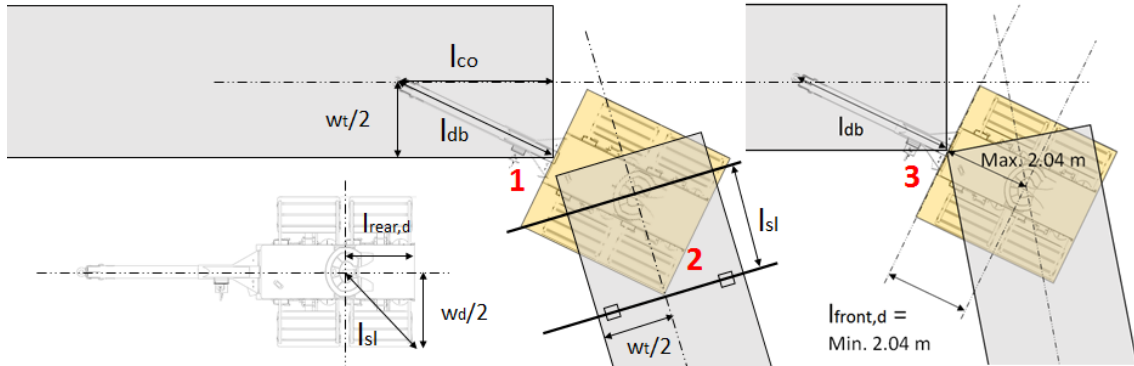

Figure 3.6: Worst case orientation of the A-double configuration regarding space, while cornering.

The worst case scenario for the first collision in Fig. 3.6 is when the bumper is located directly at the rear of the first semi-trailer. The full coupling height h_{kp} can only be used by the dolly from a certain distance to the pin coupling of the dolly's drawbar, because of the rear underride protection/bumper of the lead semi-trailer. This distance is defined as the drawbar length l_{db}. The drawbar length is determined by the pin coupling overhang l_{co} and the width (w_t) of the first semi-trailer. Using Pythagoras, the drawbar length is calculated with:

$$l_{db} = \sqrt{l_{co}^2 + (w_t/2)^2} \tag{3.1}$$

The two found values for the pin coupling overhang l_{co} are listed in Table 3.2 and equal 1.5 and 0.76 m. From (3.1) it can be concluded that the drawbar length increases for increasing drawbar coupling overhangs. However, the required space measured from the rear of the first semi-trailer to the front of the dolly l_{db}-l_{co} reduces for increasing l_{co}. It is, therefore, chosen to use the pin coupling overhang of 1.5 m, since this results in the smallest distance between the two semi-trailers. Note that a pin coupling overhang of 1.50 m is not feasible for the semi-trailer with the smallest rear overhang of 1.28 m. The pin

coupling overhang of this semi-trailer, therefore, equals 1.28 meter, which increases the space between the rear of the first semi-trailer and the dolly. When the leading semi-trailer has a rear overhang smaller than 1.5 m, the additional space between the semi-trailers is taken for granted.

The critical dimension to avoid the second collision in Fig. 3.6 is defined as $l_{rear,d}$ and is the critical distance from fifth wheel to the rear of the dolly. This distance is limited by the longitudinal distance between the king pin and support legs of the trailer l_{sl} and the width w_d of the dolly. By using Pythagoras, the following equation is obtained:

$$l_{rear,d} = \sqrt{l_{sl}^2 - (w_d/2)^2} \tag{3.2}$$

Small values for l_{sl} are undesired, because this reduces the available space and hence; wheelbase of the dolly. It is assumed that the dolly width equals 2.55 m and the worst case value for l_{sl} is 2.32 m, as shown in Table 3.2.

The third collision that is shown in Fig. 3.6 occurs between the two semi-trailers. The worst case scenario is determined by the EU directive legislation that states that the distance between kingpin and any point in front of the trailer should not exceed 2.04 meter, see Table 3.1. The distance between the fifth wheel centre and front of the dolly's chassis is represented by $l_{front,d}$. The distance $l_{front,d}$ should be equal to 2.04 m to ensure that every semi-trailer can be hauled, without hitting the first semi-trailer.

The dimensions from Chapter 3.1 and the critical distances of the dolly while cornering are used to calculate the available space for the dolly. A C-shaped region below the first and second semi-trailer is obtained, as shown in Fig. 3.7. The dimensions of this region are shown in Table 3.3. With a pin coupling overhang of 1.5 m, MAN TGX 4x2 tractor and two Krone 45 ft. container semi-trailers, the overall length of the vehicle equals 31.01 m. The maximum dolly chassis length is limited by $l_{front,d}$ and $l_{rear,d}$ and equals 3.98 m. The maximum wheelbase is limited by the chassis length and the tyre radius. It is assumed that the dolly is equipped with the same tyres as fitted on the steered tractor axles, which are 315/80 R22.5 tyres. These tyres have a radius of 0.55 m and require the wheelbase of the dolly to be larger than 1.10 m and smaller than 2.88 m.

Note, in Fig. 3.7 and Table 3.3 the maximum clearance between the rear bumper/underride protection equals 0.7 m. All the evaluated semi-trailer blueprints in Appendix B show bumper heights lower than the bottom of the rear-chassis. However, no values on the relative positions of the bumpers are found, so the maximum clearance of 0.7 m is used for the drawbar height h_{middle}. Due to this, the front height of the C-shaped region is actually lower than the height in the middle, which obviously is contradicting. The bumper and/or underride protection of the first semi-trailer can be made retractable if more space is required.
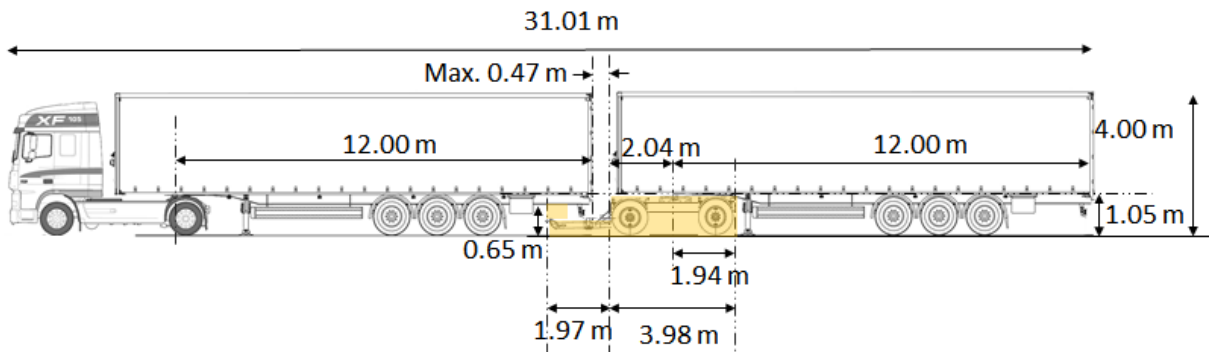

Figure 3.7: Available space for the smart dolly, coupled in an A-double configuration.

Parameter	Length [m]	Determined by:
Front height (h_{front})	max. 0.65	chassis thickness h_{chass} and coupling height h_{kp}
Middle height (h_{middle})	max. 0.70[1]	legislation bumper/underride protection
Rear height ($h_{rear,d}$)	max. 1.05[2]	coupling height trailer h_{kp}
Critical distance drawbar (l_{db})	min. 1.97	pin coupling overhang l_{co} and dolly width w_d
Critical distance support legs ($l_{rear,d}$)	max. 1.94	support legs location l_{sl} and dolly width w_d
Width of dolly (w_d)	max. 2.55	legislation
Critical distance first trailer ($l_{front,d}$)	min. 2.04	legislation
Required space behind semi-trailer for yaw rotation at pin coupling	max. 0.47[3]	pin coupling overhang l_{co} and drawbar length l_{db}
Distance between the rear axle of motor vehicle and first axle dolly	min. 3.00	legislation
Total length dolly ($l_{tot,d}$)	min. 5.95	$l_{front,d}$, $l_{rear,d}$ and l_{db}
Total vehicle length ($l_{tot,v}$)	31.01	$l_{front,d}$, $l_{rear,t}$, $l_{tot,t}$, and $l_{tot,L1}$[4]

1) No specific dimensions and locations of the rear bumper can be found. In reality, this value will be smaller than h_{front}.
2) This coupling height does not allow usage of standard, steered 315/80 R22.5 tyres.
3) For pin coupling overhang of 1.5 m. For the worst case pin coupling overhang l_{co} of 1.28 m, the value equals 0.69 m.
4) Maximum vehicle length of a tractor with single semi-trailer for EU cross-border traffic.

Vertical tyre forces

The maximum allowed wheelbase of the dolly should not exceed 3.98 m minus two times the radius of the tyres, as determined in the previous section. This results in a maximum wheelbase of 2.88 m. The vertical tyre forces are partly determined by the wheelbase and location of the fifth wheel coupling at the dolly. A design study is required to evaluate the best design considering the vertical axle forces. On the one hand, the aim of this geometry study is to ensure that the vertical axle forces stay within the limits set by the EU directives. On the other hand the geometry study should ensure that the wheels do not loose contact with the ground during severe accelerations/decelerations. For now, it is assumed that the dolly is capable of hauling the second semi-trailer on its own, indicating that there are no forces transmitted via the drawbar. The tractor may have a power reserve in some scenarios, but this is neglected for now. Three sets of vertical axle force equations are derived, considering: the static vertical forces, the vertical forces during startability on an inclined road and the vertical forces during braking.
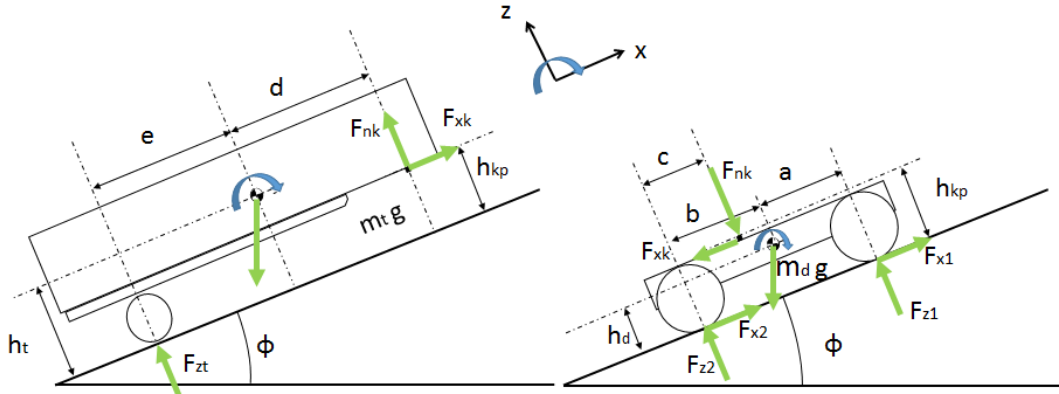

Figure 3.8: Free body diagram of a dolly semi-trailer combination.

The free body diagram shown in Fig. 3.8 is used for the calculation of the vertical tyre forces. In this figure, the dolly and second semi-trailer are decoupled from the A-double, since it is assumed that there are no forces transferred via the drawbar. The dolly and semi-trailer are placed on an inclined road and there is no lateral acceleration. Furthermore, the three trailer axles are lumped into one equivalent axle and roll movements are not taken into account. With Newton's second law, six equations are derived.

For the dolly this results in:

$$m_d \cdot a_x = F_{x2} + F_{x1} - F_{xk} - m_d g sin\phi \tag{3.3}$$

$$F_{z2} + F_{z1} - F_{nk} - m_d g cos\phi = 0 \tag{3.4}$$

$$F_{z2} \cdot b - F_{z1} \cdot a - F_{nk}(b-c) - F_{xk}(h_{kp} - h_d) - (F_{x1} + F_{x2})h_d = 0 \tag{3.5}$$

For the trailer, the following equations hold:

$$m_t \cdot a_x = F_{xk} - m_t g sin(\phi) \tag{3.6}$$

$$F_{zt} + F_{nk} - m_t g cos(\phi) = 0 \tag{3.7}$$

$$F_{zt} \cdot e - F_{nk} \cdot d - F_{xk}(h_t - h_{kp}) = 0 \tag{3.8}$$

The parameters F_{zi} and F_{xi} represent the vertical and longitudinal forces at the axles of the vehicle. The index $i = 1$ corresponds to the first dolly axle and the index $i = 2$ corresponds to second dolly axle. The index $i = 3$ corresponds to the semi-trailer axle. The forces F_{nk} and F_{xk} represent the normal and longitudinal force at the fifth wheel coupling. The parameters h_t, h_d and h_{kp} represent the CoG height of the trailer, CoG height of the dolly and the height of the fifth wheel coupling, respectively. The inclination angle of the road is represented by the parameter ϕ. The distances between the front and rear axle of the dolly to the CoG are represented by the parameters a and b. The sum of a and b is defined as the wheelbase l_d. For the semi-trailer, the wheelbase l_t is defined as the sum of the distances between the king pin and CoG d and the centre axle and CoG e. The mass of the dolly is represented by m_d and that of the trailer by m_t. The gravitational constant in these equations is represented by g. The distance between the rear axle of the dolly and the fifth wheel coupling is represented by the parameter c.

After substitution and rearranging, the following equations for the vertical tyre forces are found:

$$F_{z1} = \frac{1}{l_d}\left(g cos(\phi)(bm_d + \frac{m_t e}{l_t}c) + (a_x + g sin(\phi))\left(\frac{m_t}{l_t}(h_{kp} - h_t)c - h_{kp}m_t - h_d m_d\right)\right) \tag{3.9}$$

$$F_{z2} = \frac{1}{l_d}\left(g cos(\phi)(am_d + \frac{m_t e}{l_t}(l_d - c)) + (a_x + g sin(\phi))\left(\frac{m_t}{l_t}(h_{kp} - h_t)(l_d - c) + h_{kp}m_t + h_d m_d\right)\right) \tag{3.10}$$

$$F_{zt} = \frac{m_t}{l_t}(d g cos(\phi) + (a_x + g sin(\phi))(h_t - h_{kp}) \tag{3.11}$$

A detailed derivation can be found in Appendix C.1.

Remark that these three equations consists of two parts. The first part only depends on the CoG locations, wheelbase, mass of the vehicle and inclination angle. This part of the vertical axle force is defined as the static axle load. The second part depends on the longitudinal acceleration a_x of the vehicle and is known as the dynamic load transfer. The dynamic load transfer part of each vehicle is represented by ΔF_{zi} and can be calculated with:

$$\Delta F_{z1} = \frac{1}{l_d}a_x\left(\frac{m_t}{l_t}(h_{kp} - h_t)c - h_{kp}m_t - h_d m_d\right) \tag{3.12}$$

$$\Delta F_{z2} = \frac{1}{l_d}a_x\left(\frac{m_t}{l_t}(h_{kp} - h_t)(l_d - c) + h_{kp}m_t + h_d m_d\right) \tag{3.13}$$

$$\Delta F_{zt} = \frac{m_t}{l_t}a_x(h_t - h_{kp}) \tag{3.14}$$

Depending on the sign of the longitudinal acceleration, the dynamic load transfer increases or decreases the vertical force on the front or rear axle during nonzero accelerations . During severe braking or acceleration, an axle may loose contact with the road due to this dynamic load transfer.

Vertical tyre forces while accelerating

For the startability of the A-double HCV, the aim is to ensure that the front wheels do not loose contact with the road for maximum acceleration. The acceleration performance of a vehicle is limited by either the maximum force that can be transferred to the road or the maximum tractive force, which is limited by the engine torque or power. For now, it is assumed that the tyre friction is the limiting factor.

A rolling tyre can be seen as: "a friction element which generates a shear force F_s, due to a relative sliding velocity V_s with respect to the ground" [3],. This shear force is limited by the vertical force acting on the rolling tyre:

$$F_s \leq \mu F_z \tag{3.15}$$

In (3.15) the vertical tyre force is represented by F_z and the friction coefficient between the road and the tyres is represented by μ. The friction coefficient is determined by the road conditions and the tyre characteristics of a vehicle. On a dry, clean road the friction coefficient of a truck tyre is ranging from 0.6 to 0.8 [3]. The shear force F_s of a tyre, represents the combined longitudinal and lateral tyre forces of a single tyre, as shown in Fig. 3.9. The lateral and longitudinal tyre forces are represented by F_y and F_x, respectively. The friction circle in Fig. 3.9 limits the maximum combined tyre force and originates from (3.15). Assuming that the lateral tyre forces are negligible during the startability test, the relation shown in (3.15) reduces to:

$$F_{xi} = \mu F_{zi} \tag{3.16}$$

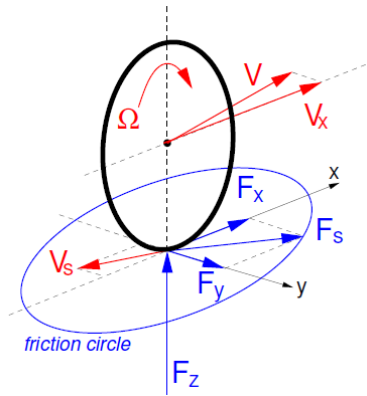This equation is used to calculate the maximum achievable longitudinal friction force F_x for tyre i.

Figure 3.9: Forces acting on a rolling tyre and friction ellipse.

The most severe scenario for the startability of a truck is: achieving maximum acceleration on a maximum slope. As stated in [8], "Motor vehicles towing a trailer and laden to their technically permissible maximum laden mass of the combination, must be capable of starting five times within five minutes at an up-hill gradient of at least 12%". During high accelerations on an inclined road, the wheels at the front axles may loose contact with the ground. This has two causes. Firstly, the presence of a non-zero inclination angle ϕ reduces the vertical force on the front axle. Secondly, the dynamic load transfer that is represented by (3.12) decreases the vertical force on the front tyres even more. Assuming that the engine and dolly's electric motor(s) deliver enough power and torque, the maximum acceleration of the vehicle is limited by the tyres, as defined by (3.16). This means that the maximum achievable acceleration is determined by the friction coefficient μ between the tyres and road and the vertical force on the driving axle. Combining (3.16) with (3.9) and (3.10), results in the maximum achievable acceleration:

$$a_{x,max} = \frac{1}{m_{tot}} \left(\mu(F_{z2} + F_{z1}) - (m_{tot}) g sin(\phi) \right) \tag{3.17}$$

From (3.17) it follows that the maximum acceleration depends on the vertical force F_{zi} on the driven tyres. For the 4x4 dolly; (3.17) combined with (3.9) and (3.10) results in:

$$a_x = \frac{g cos(\phi)(\mu \frac{m_t}{l_t} e + \mu m_d) - g sin(\phi)(m_{tot} + \mu \frac{m_t}{l_t}(h_t - h_{kp}))}{m_{tot} + \mu \frac{m_t}{l_t}(h_t - h_{kp})} \tag{3.18}$$

In the 4x2 dolly dolly design only the rear wheels are driven, so μF_{z1} cancels (3.16). This results in the following equation:

$$a_x = \frac{\frac{\mu}{l_d}(gcos(\phi)(m_d a + \frac{m_t e}{l_t}(l_d - c))) + gsin(\phi)(\frac{\mu}{l_d}(\frac{m_t}{l_t}(h_{kp} - h_t)(l_d - c) + h_{kp}m_t + h_d m_d) - m_{tot})}{m_{tot} - \frac{\mu}{l_d}(\frac{m_t}{l_t}(h_{kp} - h_t)(l_d - c) + h_{kp}m_t + h_d m_d)} \quad (3.19)$$

A new parameter is introduced in these equations, which is m_{tot}. This parameter corresponds to the total vehicle mass, which equals the sum of the dolly mass and semi-trailer mass when coupled. The maximum achievable accelerations by the 4x4 and 4x2 dolly in (3.18) and (3.19) are used in (3.9) and (3.10) to evaluate if the vertical tyre forces remain positive on both axles. The aim is to reduce the dynamic load transfer that occurs during acceleration. If a trailer is attached to the dolly, the maximum tractive force that can be transferred by the wheels in (3.18) and (3.19) increases in comparison with a decoupled dolly. This is caused by the increase of the vertical force on the driven axle(s) by the additional vertical king pin force. However, the trailer adds almost 37 tonnes in case of a 45 ft. semi-trailer to the total vehicle mass, which reduces the acceleration performance. The dynamic load transfer parts from (3.9) and (3.10), need to be as small as possible to ensure that none of the wheels loose contact with the ground.

Vertical tyre forces while braking
Braking is another scenario where the vertical tyre forces play a role. The free body diagram shown in Fig. 3.8 changes slightly for this driving scenario. First of all, the trailer axle can now also generate a longitudinal force. Secondly, some parameters are introduced to evaluate the braking performance. Assuming that each axle brakes its own load, the following equation holds:

$$\frac{F_{xt}}{F_{zt}} = \frac{F_{x1}}{F_{z1}} = \frac{F_{x2}}{F_{z2}} = k \quad (3.20)$$

Note that in this equation k corresponds to the road friction coefficient μ [4]. Ideally, if all tyres have equal friction coefficients, the following equation holds:

$$\frac{F_{xt} + F_{x1} + F_{x2}}{F_{zt} + F_{z1} + F_{z2}} = \frac{m_{tot}a_x}{m_{tot}g} = z \quad (3.21)$$

In this equation z is the dimensionless deceleration, which is the deceleration in m/s^2 divided by the gravitational constant. By means of substitution and rearranging, the following vertical axle forces are obtained:

$$F_{z2} = \frac{1}{l_d}\left(m_d g(a - kh_d) + (l_d - c - kh_{kp})m_t g \frac{e + kh_t}{l_t + kh_{kp}}\right) \quad (3.22)$$

$$F_{z1} = \frac{1}{l_d}\left(m_d g(b + kh_d) + (c + kh_{kp})m_t g \frac{e + kh_t}{l_t + kh_{kp}}\right) \quad (3.23)$$

$$F_{zt} = m_t g \frac{d - k(h_t - h_{kp})}{l_t + kh_{kp}} \quad (3.24)$$

The detailed derivation of these equations is shown in Appendix C.2.

Requirements to be met by the geometry design
To ensure safe operation of the A-double on the public roads, the coupled smart dolly with semi-trailer should meet certain requirements. These requirements are:

1. The wheelbase should be within 1.10 and 2.88 m, taking into account the 315/80 R22.5 tyre radii, due to the geometry constraints listed in Table 3.7.

2. Static axle weights on a flat road surface should be within the legal EU limits.

    (a) Front axle weight should be within 10 t for the un-driven 4x2 design or 11.5 t when driven in the 4x4 design.

    (b) Rear axle weight should be within 11.5 t for both dolly designs.

3. As stated in [7], the axle weight on the driven axle(s) should not be less than 25% of the total vehicle weight.

4. Minimize dynamic load transfer during maximum acceleration/deceleration to maintain the highest possible vertical force on the front- and rear axle of the dolly.

5. Fifth wheel coupling should be placed such that the dolly does not hit the support legs of the second semi-trailer and the semi-trailers do not hit each other, see Fig. 3.6.

6. Preferably, vertical dolly axle forces should be equally distributed to generate enough and equal lateral and longitudinal tyre forces.

The fifth wheel position and axle locations should be chosen correctly to meet these requirements. Note that Requirement 6 is not a strict requirement. A weight distribution on the front axle lower than 50%, which is normal for a standard tractor, also ensures enough vertical force on the front axle for steering during maximum acceleration. From Requirements 2, 3 and 6 it follows that the 4x2 dolly has a disadvantage in comparison with the 4x4 dolly. The maximum allowed vertical front axle force is smaller for the 4x2 dolly, since this axle is not driven in the 4x2 dolly design. However, the dolly should still meet the preferred 50-50 load distribution among the axles, while having a 25% GVW load distribution on the rear axle. For the 4x4 dolly, however, higher vertical axle forces are allowed since both axles are driven. For the 4x4 dolly it is, therefore, easier to come up with a design that meets the six requirements above. In the next section the equations and requirements are combined to determine the optimal designs for both dollies.

3.3 Dolly geometrical design

The aim of the geometry study is to derive the dolly design that fits the six requirements from the previous section best. Assuming a fixed mass for both dolly configurations and fixed semi-trailer parameters, only three parameters can be varied in order to determine the best geometrical design of the dolly. The first two parameters are a and b, which are the distances between the CoG and front- and rear axle respectively. The sum of a and b is defined as the wheelbase l_d of the dolly. The third parameter that can be adapted is c. This parameter represents the distance between the centre of the rear axle and the centre of the dolly's fifth wheel. The parameters listed in Table 3.4 are used to determine the best design for the dolly. The trailer CoG location in Table 3.4 is retrieved from the TU/e CVL Simulink model, by simulation of a fully loaded tractor semi-trailer combination at static conditions.

Table 3.4: Dolly and semi-trailer parameters used for the static axle force calculations [4], [12].

Parameter			Value
Gravitational constant	g	$[m/s^2]$	9.81
Semi-trailer wheelbase	l_t	$[m]$	7.48
Semi-trailer CoG height	h_t	$[m]$	2.31
Dolly CoG height	h_d	$[m]$	0.60
Coupling height	h_{kp}	$[m]$	1.05
Mass of dolly	m_d	$[kg]$	4200
Mass of fully loaded semi-trailer	m_t	$[kg]$	37000
Distance from king pin to semi-trailer CoG	d	$[m]$	4.81
Distance from semi-trailer centre axle to semi-trailer CoG	e	$[m]$	2.67
Friction coefficient of tyres	μ	$[-]$	0.8

The combined design of the parameters a, b and c is limited by: the available space for the dolly, the position of the fifth wheel and the six requirements listed above. From Fig. 3.10 it follows that the distance from fifth wheel to the rear of the dolly should not exceed 1.94 m. This value corresponds to the $l_{rear,d}$ value in Table 3.3. To ensure that the front of the second semi-trailer does not hit the rear of the first semi-trailer, the distance between the front of the dolly and the centre of the fifth wheel should not exceed 2.04 m. This is determined by the parameter $l_{front,d}$ in Table 3.3. Too large values for $l_{front,d}$ are undesired, since this increase the space between both semi-trailers and the air drag accordingly. Summarizing, $l_{front,d}$ and $l_{rear,d}$ need to meet the following requirements:

$$l_{front,d} = r_{wheel} + a + (b - c) \geq 2.04 \tag{3.25}$$

$$l_{rear,d} = r_{wheel} + c \leq 1.94 \tag{3.26}$$

The parameters a and b represent the axle positions with respect to the dolly's CoG. The parameter c represents the fifth wheel offset in front of the rear axle and r_{wheel} represents the wheel radius.
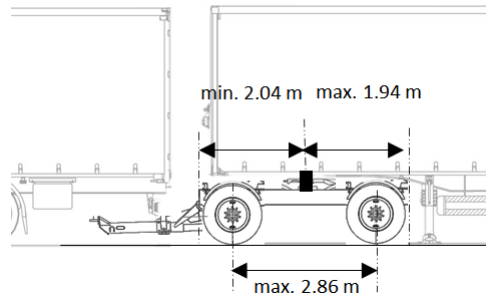

Figure 3.10: Geometrical limits on the dolly's fifth wheel position.

From Requirement 4 in combination with (3.12) and (3.13) it follows that a large wheelbase l_d reduces the dynamic load transfer. However, too large values for a and b conflict with Requirements 2 and 3 and violate the limits shown in (3.26) and (3.25). The influence of the parameters a and b on the vertical axle forces is shown in Fig. 3.11. In these plots the fifth wheel coupling is at a fixed distance from the rear of the dolly, for varying a and b. From this figure it can be concluded that an increase of a for fixed b and c, reduces the vertical force on the front axle, but increases the one on the rear axle. An opposite relation holds for a change in b for fixed a and c.
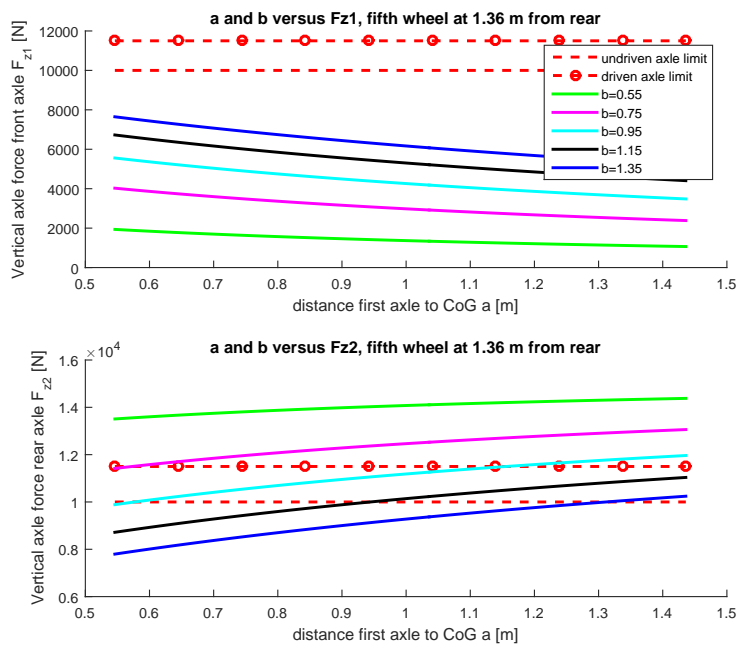

Figure 3.11: Dolly axle positions versus vertical axle force for fixed fifth wheel offset from the rear of the dolly.

The influence of a change in the fifth wheel position c on the vertical axle forces is shown in Fig. 3.12. Increasing c for a fixed a and b, increases the vertical forces on the front axle and reduces the vertical forces on the rear axle. Therefore, small fifth wheel offsets c are desired for the 4x2 dolly design to meet 25% gross vehicle weight distribution on the driven axle. However, too small values may result in violation of the axle load limits.
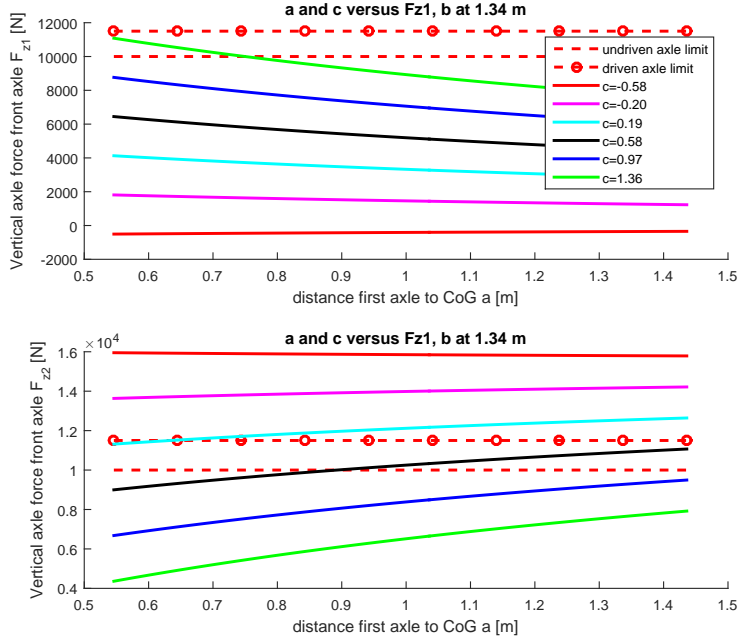
Figure 3.12: Dolly front axle and fifth wheel positions versus vertical axle force for fixed rear axle position.

4x2 dolly design

Due to the trade-off of various requirements, it is chosen that c equals 0.97 m for the 4x2 dolly design. The chosen values for a and b equal 1.40 m, which are limited by the vertical axle force on the rear axle. Together, this set of parameter results in the best GVW distribution on the driven axle for the largest possible wheelbase. This geometry ensures that all the requirements are met for the decoupled autonomous dolly. When a trailer is coupled, the best force distribution between front and rear axle is achieved, while meeting the vertical axle force limits. In coupled operation, the GVW distribution on the driven axle equals 26.1%.

4x4 dolly design

The 4x4 dolly is four-wheel driven, so the 25% limit does not result in conflicting design requirements. For this setup the maximum allowed wheelbase is chosen and the fifth wheel coupling is placed exactly at the centre between both axles. This results in a value of 1.39 m for the three design parameters a, b and c. This value is limited by $l_{rear,d}$, which is the maximum available space from fifth wheel to the support legs of the second semi-trailer. The chosen geometry design of the 4x4 dolly ensures an equal force distribution among the axles and ensures the lowest possible dynamic load transfer.

3.4 Dynamic and static axle weight comparison

In this section the vertical axle forces of the dolly are compared with the MAN TGX tractor semi-trailer combination, for both the static and dynamic conditions. The static vertical axle weights for all vehicles are obtained from the TU/e CVL, whereas the dynamic performance is calculated with the equations derived in (3.9), (3.10), (3.18) and (3.19). The used tractor and semi-trailer parameters are listed in Table 3.4 and Table 3.5. For the dynamic calculations it is assumed that the dolly and last semi-trailer do not influence the dynamics of the leading tractor semi-trailer combination in the A-double configuration. By doing so, it is assumed that the dolly does not transmit any force via the drawbar, indicating that the dolly and second semi-trailer can be evaluated separately.

Parameter			Value
Wheelbase	$l_{d,trac}$	$[m]$	3.90
Distance front axle to CoG	a	$[m]$	1.09
Distance rear axle to CoG	b	$[m]$	2.81
Tractor CoG height	h_{trac}	$[m]$	0.90
Mass of tractor	m_{trac}	$[kg]$	6955
Weight on front axle when unloaded	m_1	$[kg]$	5005
Weight on rear axle when unloaded	m_2	$[kg]$	1950
Distance from fifth wheel to rear axle	c	$[m]$	0.60
Friction coefficient of tyres	μ	$[-]$	0.80

Static axle forces

For the static axle force comparison, the vehicle is standing still on a flat road. The vertical axle forces of the tractor, 4x2 dolly and 4x4 dolly are listed in the Table 3.6. A distinction is made between two operating conditions, which are operation with and without semi-trailer. The vertical axle forces of the coupled vehicles are retrieved from simulation with the TU/e CVL in Simulink, whereas the vertical axle forces of the decoupled vehicles are calculated with (3.9) and (3.10). In the last column of Table 3.6, the percentage of the GVW on the driven axle(s) is listed. It is assumed that the dolly does not transfer forces via the drawbar to the first semi-trailer. Therefore, the GVW of the dolly semi-trailer combination equals the sum of the dolly and second semi-trailer mass.

From Table 3.6 it follows that during operation without semi-trailer, the vertical axle forces on the front wheels of both dollies are smaller than the vertical axle force of the tractor. This can be explained by the absence of a cabin and engine in the smart dolly designs. The heavy cabin and engine are mounted close to the front axle on a tractor, which increases the vertical axle force on the tractor's front axle. For coupled operation, the 4x4 dolly has the best design, since a 50-50 vertical force distribution can be achieved. Furthermore, the vertical axle forces stay well within the axle weight limits. Both rear axles of the 4x2 dolly and tractor, however, are close to the axle weight limit of 11.5 tonnes, see Table 3.6. For the 50-50 vertical force distribution among the axles, the 4x2 dolly has a worse distribution at the front axle in comparison with the tractor, because of the absence of the cabin and ICE. It follows from Table 3.6 that the 4x4 dolly is the best design. The vertical axle forces of the 4x4 dolly stay well within the limits of 11.5 tonnes and the GVW distribution on the driven axles can reach values up to 37.94 %.

Remark that the GVW percentage on the driven axle of the coupled 4x2 dolly in Table 3.6 is smaller than the calculated 26.06% in Chapter 3.3. The calculation in Chapter 3.3 uses the semi-trailer CoG position listed in 3.4. However, in the final A-double simulation models, the CoG of the semi-trailer is shifted more towards the rear. This causes a difference in the vertical axle force distribution between the front and rear axle of the dolly. The EU directive states that the GVW distribution on the driven axles should be equal to or greater than 25%. It can be concluded from Table 3.6 that the 4x2 dolly violates this limit with 1.2%. The GVW of a 4x2 dolly equipped A-double equals 85.2 t. Including the vertical axle force on the tractor's driven axle, results in a 24.9 % GVW distribution on all driven axles of the 4x2 dolly equipped A-double. Therefore, it can be concluded that the chosen geometric design of the 4x2 dolly is still able to meet the EU axle weight legislation.

Table 3.6: Static axle weights and GVW distribution on the driven axle(s) for standard MAN TGX 4x2 BLS tractor and 4x2- and 4x4 dolly without semi-trailer and with fully loaded semi-trailer.

	a [m]	**b** [m]	**c** [m]	F_{z1} [kN]	F_{z2} [kN]	GVW percentage on driven axle(s)
4x2 dolly without trailer	1.40	1.40	0.97	20.6	20.6	50.0%
4x2 dolly with trailer	1.40	1.40	0.97	58.3	96.7	23.8%
4x4 dolly without trailer	1.39	1.39	1.39	20.6	20.6	100%
4x4 dolly with trailer	1.39	1.39	1.39	76.7	76.8	37.9%
4x2 tractor without trailer	1.09	2.81	0.60	49.1	19.1	28.0%
4x2 tractor with trailer	1.09	2.81	0.60	69.3	111.4	25.8%

Dynamic load transfer

The dynamic load transfer is evaluated for two driving scenarios. These driving scenarios are startability on a flat road and 12% grade road. The vertical axle forces during these driving scenarios are shown in Table 3.7 and are calculated with (3.9), (3.10), (3.18) and (3.19). One remark on this approach is that during severe longitudinal accelerations, the available engine power or torque also needs to be taken into account. For now, interests only lies in the vertical forces, so the tyre friction is assumed to be the limiting factor. The aim of these tests is to maintain the highest possible vertical axle force(s) on the steered axle(s), to ensure that the vehicle is still able to steer.

The dynamic load transfer on the front axle ΔF_{z1} is calculated with (3.12). High dynamic load transfer values are undesired, since the front wheels can lift during startability tests. From Table 3.7 it can be concluded that the dolly can achieve higher maximum accelerations than the tractor. This is caused by the fact that the dolly weighs 2.8 t less than the tractor. The total vehicle mass m_{tot} in (3.18) and (3.19) reduces for the dollies, which results in a higher maximum acceleration.

From Table 3.7 it can be concluded that the dollies encounter more load transfer than the tractor. This is caused by the relatively short wheelbase and higher achievable acceleration of the dollies. The wheelbase of the 4x2 dolly is 1.10 m shorter than the tractor's wheelbase. When used in (3.12), this results in more load transfer on the front axle. The vertical force distributions among the axles of the vehicles on a 12 % inclined road are shown in Table 3.7. From these values it can be concluded that the 4x2 dolly has the worst force distribution on the front axle during startability on an inclined road. With a force distribution of 21.2 %, the 4x4 dolly almost matches the 4x2 tractor semi-trailer force distribution of 22.6%. Therefore, it can be concluded that the 4x4 dolly is the best dolly design regarding dynamic load transfer.

From Table 3.7 it follows that the 4x4 dolly is the best design with respect to the dynamic load transfer. The static vertical axle force distribution between the front and rear axle of the 4x4 dolly is better than the force distribution of the 4x2 dolly. This results in larger vertical forces on the front axle during startability on inclined roads.

Table 3.7: Vertical axle forces during maximum acceleration at 0% and 12% inclined road for standard MAN TGX 4x2 BLS tractor and 4x2- and 4x4 dolly coupled with a fully loaded semi-trailer.

	max a_x (0%)$[m/s^2]$	ΔF_{z1} (0%)[kN]	max a_x (12%)$[m/s^2]$	ΔF_{z1} (12%) [kN]	F_{z1}/F_{z2} percentage (12%)
4x2 dolly with trailer	2.58	-43.9	1.40	-43.5	14.0 %
4x4 dolly with trailer	2.96	-53.1	1.77	-52.7	21.2%
4x2 tractor with trailer	2.32	-29.0	1.13	-28.8	22.6%

3.5   Summary

In this chapter, both the European and Dutch HCV legislation have been explained in detail. The commercial vehicle legislation states limits on the weight and dimensions of the vehicle. To determine the geometrical design of the dolly, the available space for the dolly has been determined. This available space is limited by the legislations, semi-trailer dimensions and required space for cornering. Taking into account the tyre radius of standard steering tyre of a commercial vehicle, the wheelbase should be within 1.10 and 2.88 m.

To ensure that the axle weight limits are not exceeded and ensure safe operation of the vehicle, vertical axle force equations have been derived. These equations show that the choice of the axle- and fifth wheel coupling positions influence the axle weights. The main requirements on the wheelbase of the dolly is that the dolly wheels should not loose contact with the ground during severe braking or acceleration when driving autonomously and axle load limits should not be violated when coupled with a semi-trailer.

From the above it can be concluded that the 4x2 dolly has axle offsets to the CoG of 1.40 m and a fifth wheel offset to the rear axle of 0.97 m. The 4x4 dolly has axle offsets and a fifth wheel offset of 1.39 m. Both designs ensure a 50-50 vertical weight distribution among the axles of the dolly when decoupled and meet the axle load limits in coupled operation. Only the 4x4 dolly is able to still meet the 50-50 weight distribution in coupled operation.

Chapter 4
Steering system design

In this chapter the performance of different dolly steering systems are evaluated in the context of an A-double HCV. Note, that a distinction is made for the steering systems designs of the 4x2 dolly and 4x4 dolly. The 4x2 dolly will be propelled by a single motor connected to a driveshaft and differential that transfers the power to the rear wheels. This configuration only allows the front wheels to be steered. In the 4x4 dolly design it is possible to steer all four wheels, since this dolly uses in-wheel motors. Important assumptions for this chapter are that the single track vehicle model describes the behaviour of the vehicle well enough and steady state cornering can be considered.

When a vehicle is cornering, it rotates around the instantaneous centre C of the corner, as shown in Fig. 4.2. For steady state cornering the radius between the wheel to this instantaneous centre will not change. Furthermore, during steady state cornering the vehicle has zero acceleration in the longitudinal and yaw directions and the steer angles of the wheels are kept constant.

In a single track model, the tyres on the left and right side are lumped into a single equivalent tyre that is located at the centre of the vehicle. The required steer angles are calculated for this equivalent tyre. For a single track model, no distinction is made between the left and right steer angles, so both wheels are steered with the same angle.

When cornering, the tyres need to generate a lateral force towards the instantaneous centre of the turn. As [3] explains, the lateral force generated by a tyre depends on the longitudinal velocity and lateral sliding velocity of that wheel. This relation is also shown in Fig 4.1. The angle between the longitudinal velocity V_x and lateral sliding velocity V_{sy} is defined as the side slip angle α. This side slip angle α can be calculated with:

$$tan(\alpha) = -\frac{V_{sy}}{V_x} \tag{4.1}$$

The lateral tyre force that can be generated depends on the magnitude of the side slip angle α. For small side slip angles, the lateral tyre force can be approximated with:

$$F_y = C_{f\alpha}\alpha \approx C_{f\alpha} \cdot -\frac{V_{sy}}{V_x} \tag{4.2}$$

The cornering stiffness $C_{F\alpha}$ is determined by the tyre characteristics. It follows from (4.2) that the generated lateral tyre forces increase for increasing side slip angles and constant cornering stiffness.
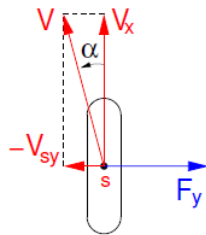

Figure 4.1: Lateral tyre force while cornering [3].

Five side slip angles can be obtained from the single track model of a tractor semi-trailer combination in Fig. 4.2. The side slip angle at the front and rear tyre of the tractor are defined as α_1 and α_2. The tyre side slip angles of the three semi-trailer tyres are defined as $\alpha_{n,t}$, with $n=1$ for the first wheel, $n=2$ for the second wheel and $n=3$ for the last wheel. For low longitudinal velocities during steady state cornering, it can be assumed that the lateral acceleration is small. For this driving condition, it can be assumed that the tyre side slip angles of the tractor and the centre axle of the semi-trailer are small too. With this assumption, the tractor's axles and the centre axle of the semi-trailer are oriented perpendicular to the instantaneous centre of the turn, see Fig. 4.2. For non-steered semi-trailer axles, the other two semi-trailer axles always have non-zero tyre side slip angles. This is also shown in Fig. 4.2..
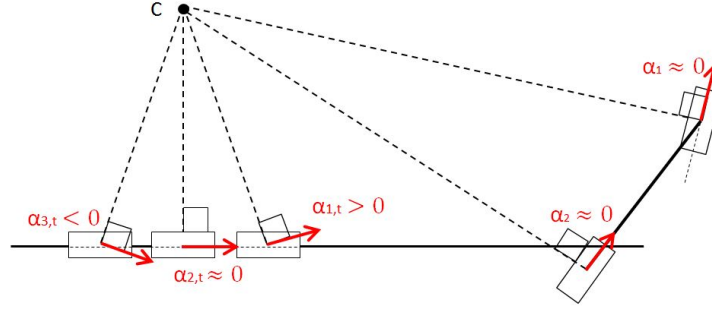
Figure 4.2: Low speed steady state cornering assumption on the tyre side slip angles of a tractor semi-trailer with non-steered semi-trailer axles.

A standard dolly is in most cases connected to the truck via a drawbar that is fixed to the dolly's chassis. For now, a standard dolly is considered to be non-steered, although there are some dollies available with a steering system [26]. As explained in Chapter 2, an articulated commercial vehicle encounters large swept path widths caused by the wheelbase of the semi-trailer. The swept path of the second semi-trailer can be reduced when the dolly is equipped with single or multiple steered axles. In Fig 4.3 a standard non-steered dolly and semi-trailer are shown during steady state cornering with low longitudinal velocity. From Fig. 4.3 it follows that:

$$r_{crit} = \sqrt{r_{kp,D}^2 - l_t^2} - w_t/2 \tag{4.3}$$

In this equation, r_{crit} is the distance from the innermost tire of the semi-trailer to the instantaneous centre of the turn. This parameter is the critical factor for the swept path. The parameter $r_{kp,D}$ is the desired radius from C to the king pin at the trailer. This radius equals the radius from C to the centre of the dolly's fifth wheel. The wheelbase of the trailer is represented by the parameter l_t and the width of the semi-trailer is represented by w_t. The last parameter that is used in Fig. 4.3 is the radius of the pin coupling below the first semi-trailer to the instantaneous centre C, as represented by r_{pin}.
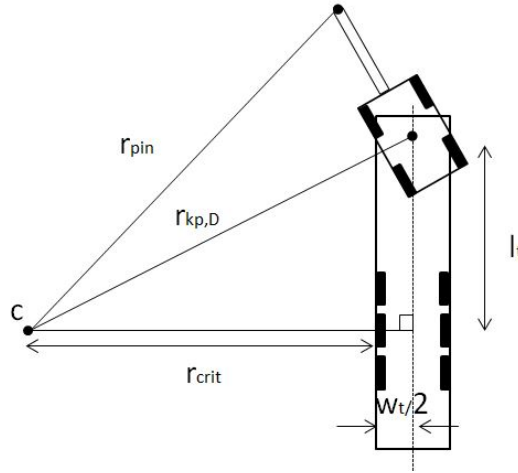

Figure 4.3: Kinematics of a dolly semi-trailer combination during steady state cornering.

The swept path of the second semi-trailer improves for increasing r_{crit}. From (4.3) it follows that only the desired king pin radius $r_{kp,D}$ can be changed. The wheelbase l_t and semi-trailer width w_t are determined by the semi-trailer geometry and cannot be changed. The tractor and first semi-trailer trajectory on the steady state circle is unaffected by the dolly, when it is assumed that the drawbar of the dolly does not transfer forces to the pin coupling. This means that the radius of the pin coupling r_{pin} does not change when driving with a single semi-trailer or in the A-double configuration. The steering systems that are evaluated in this chapter, therefore, use this pin coupling radius r_{pin} as a starting point. This pin coupling radius is determined for both the EU and Dutch HCV 360 degree turns, by using of the TU/e CVL. By designing the steering geometry, the desired king pin radius $r_{kp,D}$ can be increased, such that the critical radius r_{crit} increases and the swept path reduces.

4.1 Design of the 4x2 dolly

Drawbar steering

The first steering system that is evaluated for the 4x2 dolly is a drawbar steering system. This steering system originates from the drawbar trailer. In such a system, the first axle of the trailer/dolly is rigidly connected to the drawbar. The combined drawbar and first axle can rotate with respect to the vertical axis of the trailer, see Fig. 4.4. When implemented on a dolly, the axle and drawbar can rotate with respect to the vertical axis of the pin coupling and the vertical axis of the front axle connection point at the dolly. A steering angle at the wheels is induced as soon as the drawbar is rotated. Note, the drawbar rotation point can be located at an arbitrary position on the dolly chassis. In Fig. 4.5, this offset of the connection point is defined by the parameter x. The 4x2 dolly is propelled by a single motor via a driveshaft and differential, so the maximum value of x is set to 1.00 m in front of the rear axle. This should ensure that there is enough space available for the driveline.
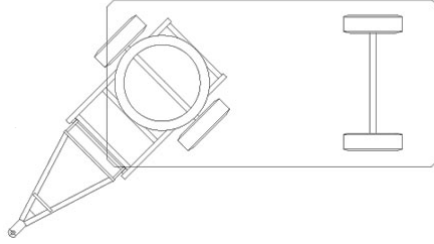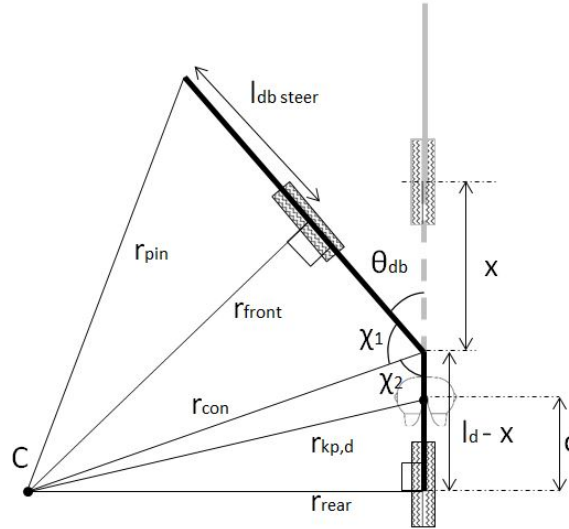

Figure 4.4: Drawbar steering system [47].

Figure 4.5: Steady state cornering with drawbar steering.

With Pythagoras' theorem, the relations below can be obtained:

$$l_{db,steer} = l_{db} + r_{wheel} \tag{4.4}$$

$$r_{front} = \sqrt{r_{pin}^2 - l_{dbsteer}^2} \tag{4.5}$$

$$r_{con} = \sqrt{r_{front}^2 + x^2} \tag{4.6}$$

$$r_{rear} = \sqrt{r_{con}^2 - (l_d - x)^2} \tag{4.7}$$

$$r_{kp,D} = \sqrt{r_{pin}^2 - (l_{db} + r_{wheel})^2 + 2l_d x - l_d^2 + c^2} \tag{4.8}$$

$$r_{crit} = \sqrt{r_{pin}{}^2 - (l_{db} + r_{wheel})^2 + 2l_d x - l_d^2 + c^2 - l_t{}^2} - w_t/2 \tag{4.9}$$

$$\theta_{db} = \pi - \chi_1 - \chi_2 = \pi - atan\left(\frac{r_{front}}{x}\right) - atan\left(\frac{r_{rear}}{l_d - x}\right) \tag{4.10}$$

The drawbar length $l_{db,steer}$ in (4.4) is defined as the sum of the drawbar length l_{db} obtained from Table 3.3 and the wheel radius r_{wheel}. The parameters r_{front} and r_{rear} are the radii of the front and rear axle with respect to the instantaneous centre. The radius of the connection point of the drawbar at the chassis is represented by r_{con}. the geometry of the dolly is determined by the wheelbase l_d and the fifth wheel position with reference to the rear axle c. The drawbar angle with respect to the chassis is defined by θ_{db}. In the equations above, the distance between the front axle and the rotation point of the drawbar is defined by x.

It can be concluded from (4.9) that increasing the distance between the front axle and the rotating point at the dolly chassis, increases the critical radius of the innermost wheel. The largest critical radius is found for the largest possible value of x.
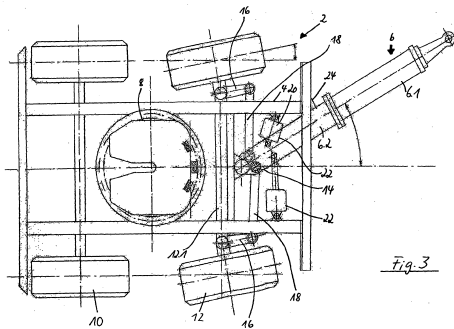
Krone steering

The second steering system that is evaluated for the 4x2 dolly continues on the previous system. This steering system is defined as the Krone steering system. In contrast to the drawbar steering system, the drawbar is connected to the axle via a mechanical linkage as shown in Fig. 4.6a. With this specially designed linkage, it is possible to define drawbar/steer angle ratios other than 1:1 as it is with the drawbar trailer steering. The gain between the drawbar angle θ_{db} and steer angle of the front axle δ_1, is defined by the parameter k as defined by:

$$\delta_1 = \theta_{db} \cdot k \tag{4.11}$$

By assuming steady state cornering at low velocities, it is approximated that the front and rear axles are oriented perpendicular to the instantaneous centre C of the corner. From the geometric design of the dolly in Fig. 4.7 it follows that the king pin radius $r_{kp,D}$ equals:

$$r_{kp,D} = \sqrt{\left(\frac{l_d}{tan(\delta_1)}\right)^2 + c^2} \tag{4.12}$$

The steer angle of the front axle is represented by δ_1 and the wheelbase of the dolly is represented by l_d. The distance between the centre of the rear axle and the fifth wheel coupling is represented by c. From (4.12) it follows that small steer angles are desired to increase the radius $r_{kp,D}$.

(a) Drawing of the krone steering system on a converter dolly [26].
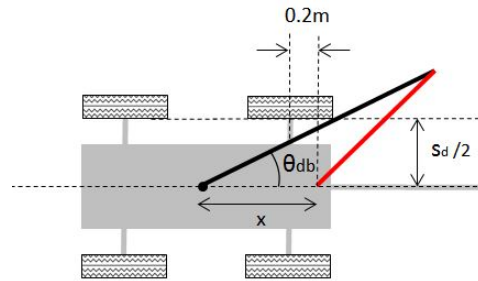
(b) Limitation on the maximum drawbar angle with Krone steering.

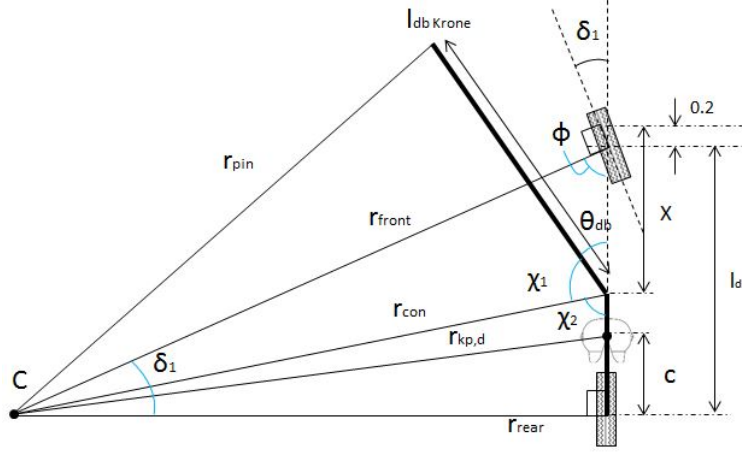Figure 4.6: Krone steering system design and the maximum drabwar angle.

Figure 4.7: Steady state cornering with Krone steering.

One way to decrease the steer angle δ_1 is to use a smaller gain k for the steer angle in (4.11). Another way to reduce the steer angle in (4.11), is to decrease the drawbar angle θ_{db}. This is realised by placing the revolute joint of the drawbar more at the rear of the dolly chassis, see Fig. 4.6b. In Fig. 4.6b the offset of the new rotating point with respect to the initial position is defined by x. From a blueprint of the Krone steering system [26], it is approximated that the initial drawbar rotating point is located 0.2 m in front of the centre of the first axle. From Fig. 4.6b it follows that the space available for the drawbar to rotate reduces for higher values of x, as defined by:

$$max(|\theta_{db}|) = atan\left(\frac{s_d/2}{r_{wheel} - 0.2 + x}\right) \tag{4.13}$$

This equation depends on the track width s_d of the dolly, which equals the dolly width w_d minus the width of the tires. When divided by two, this results in a value for half the track width of 0.87 m.

From (4.13) it follows that the maximum drawbar angle θ_{db} decreases for higher values of x. Combined with (4.11) and (4.12), this should result in a larger critical radius $r_{kp,D}$. However, (4.11) and (4.12) do not take the drawbar angle limit into account. For small drawbar angles θ_{db}, the dolly is actually positioned more to the inside of the turn. This dolly orientation is required to ensure that the front and rear axles are still oriented perpendicular to the instantaneous centre of the corner.

Simulations in the TU/e CVL and a brute force optimization, therefore, show that the optimal value for $r_{kp,D}$ is obtained for a value of x equal to zero. This can be explained by the two orientations of the dolly that are shown in Fig. 4.8. In this figure the king pin trajectories are shown for a given pin coupling radius of the first semi-trailer. At the left side of this figure, the dolly design has a large value of x; hence, small drawbar angle. At the right side of Fig. 4.8, the dolly has a small value of x, resulting in a large drawbar angle. From the orientations shown in Fig. 4.8 it can be obtained that large mounting distances x result in smaller king pin radii $r_{kp,D}$.
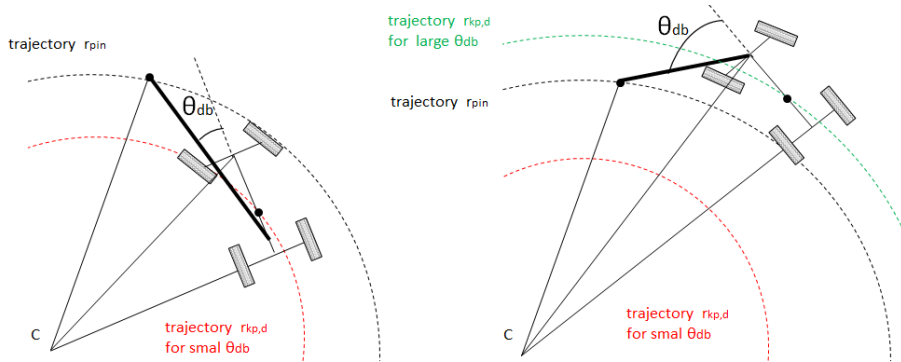

Figure 4.8: Influence of the drawbar angle θ_{db} on the dolly king pin radius for the Krone steering system.

A brute force optimization is used to retrieve the maximum achievable desired king pin radius $r_{kp,D}$ for the Krone steering system. This brute force optimization returns the optimal set of x and k that results in the largest critical radius $r_{kp,D}$. The optimization script ensures that the corresponding drawbar angle θ_{db} meets the limit defined in (4.13). Each iteration, the value of either x or k is incremented with 0.005. Next, the corresponding critical radius and drawbar angle are calculated. The set of x and k that result in the largest $r_{kp,D}$ are stored and updated when a larger critical radius $r_{kp,D}$ is found. For this brute force optimization the following equations are used:

$$\chi_1 = acos\left(\frac{r_{con}^2 + l_{db,Krone}^2 - r_{pin}^2}{2r_{con}l_{db,Krone}}\right) \tag{4.14}$$

$$\chi_2 = acos\left(\frac{l_d - (x - 0.2)}{r_{con}}\right) \tag{4.15}$$

$$\theta_{db} = \pi - acos\left(\frac{r_{con}^2 + l_{db,Krone}^2 - r_{pin}^2}{2r_{con}l_{db,Krone}}\right) - acos\left(\frac{l_d - (x - 0.2)}{r_{con}}\right) \tag{4.16}$$

$$r_{crit} = \sqrt{\left(\frac{l_d}{tan(\delta_1)}\right)^2 + c^2 - l_t^2} - w_t/2 \tag{4.17}$$

$$l_{db,Krone} = l_{db} + r_{wheel} - 0.2 + x \tag{4.18}$$

$$r_{con} = \sqrt{\left(\frac{l_d}{tan(\theta_{db} \cdot k)}\right)^2 + (l_d - (x - 0.2))^2} \tag{4.19}$$

The radius from the drawbar connection point to the instantaneous centre is represented by r_{con}. The length of the drawbar measured from pin coupling to the connection point at the dolly is represented by $l_{db,Krone}$ and is defined by (4.18). The length $l_{db,Krone}$ equals the sum of the: drawbar length l_{db}, wheel radius r_{wheel} and distance x, minus the offset of 0.2 m. The optimal sets of x and k for the different 360 degree turn manoeuvres are listed in Table 4.1.

Results 4x2 steering systems
In Table 4.1, the maximum achievable critical radii and swept paths of each steering system are listed for the EU and Dutch HCV 360 degree turns. The A-double HCV simulations in Table 4.1 are performed with empty semi-trailers without dolly propulsion, if not stated otherwise. For the EU legislation the critical radius r_{crit} needs to be greater than 5.3 m and for the Dutch HCV legislation r_{crit} needs to be greater than 6.5 m. Note from Chapter 2, the Swedish circle has the same outer radius as the EU circle, but for this test r_{crit} needs to be greater than 2.0 m. The radius of the pin coupling r_{pin} to the instantaneous centre C is the same for the Swedish HCV and EU 360 degree turns. Therefore, the Swedish 360 degree swept path performance equals the performance achieved during EU 360 degree turn manoeuvre.

In Chapter 2 it is explained that the 360 degree swept path is defined as the maximum radial distance between the outermost trajectory of the cabin and the innermost trajectory of the centre axle of the rear semi-trailer. For the analytical equations it is assumed that the frontal swing of the cabin during the EU and Dutch HCV 360 degree turns equals 0.7 m and 0.6 m, respectively. This distance is used to calculate the swept path for the analytical calculations listed in Table 4.1. The maximum swept path widths of the EU, Dutch and Swedish legislations are 7.2 m, 8 m and 10.5 m, respectively. The A-double HCV is not allowed to exceed these swept path limits. Simulation of the A-double HCV with a standard non-steered dolly shows a swept path width of 9.63 m on the Dutch HCV 360 degree turn test. This A-double with non-steered dolly is not able to complete the EU and Swedish 360 degree turn, since it will jackknife.

As can be concluded from Table 4.1, the dolly equipped with drawbar steering is not able to meet the European swept path legislation and exceeds the Dutch swept path legislation by 0.63 m. The Krone type steering, however, is able to meet the Dutch legislation. This is also shown in Fig. 4.9a, where the innermost path of the rear semi-trailer in the A-double stays within the limits set by the Dutch HCV legislation. The Krone steering system is not able to meet the EU legislation, since the simulation swept path is 2.2 m too large. This setup meets the Swedish HCV legislation, since the swept path stays within 10.5 m.

To achieve the maximum critical radius with the Krone steering system, a large drawbar angle with respect to the chassis is required. At this orientation, the drawbar almost hits the inner side of the front wheels. To ensure safe operation, it is chosen to increase the gain k, such that the required drawbar angle decreases. The final steering system parameters for the 4x2 dolly are chosen such that both the Swedish and Dutch HCV legislation are met, without reaching very large drawbar angles. The chosen design parameters are listed in Table 4.1. The simulation results are obtained from the TU/e CVL for empty semi-trailers. Dolly propulsion is enabled during these simulations. The A-double HCV equipped with 4x2 dolly has a swept path of 9.96 m at the EU/Sweden circle. The swept path during the Dutch 360 degree turn manoeuvre equals 8.03 m.

Table 4.1: Maximum achievable steering performance of different 4x2 dolly steering systems in the context of an A-double HCV.

		r_{crit} [m]	swept path [m]	δ_1 [deg]	δ_{db} [deg]	x [m]	gain [-]
drawbar trailer steering							
EU circle	analytical	1.79	11.14	19.68	19.68	1.79	1
NL circle	analytical	6.47	8.63	14.74	14.74	1.79	1
Krone steering (optimal)							
EU circle	analytical	4.63	8.57	16.43	68.17	0.00	0.24
	simulation	3.87	9.40	13.96	57.90	0.00	0.24
NL circle	analytical	8.61	6.49	12.77	67.98	0.00	0.19
	simulation	8.15	6.97	10.63	56.64	0.00	0.19
Krone steering (final design)*							
EU circle	simulation	3.31	9.96	18.70	50.99	0.00	0.37
NL circle	simulation	7.18	8.03	14.48	39.47	0.00	0.37

* Simulated with dolly propulsion and empty semi-trailers.

(a) Dutch HCV legislation   *(b) EU and Swedish HCV legislation.*
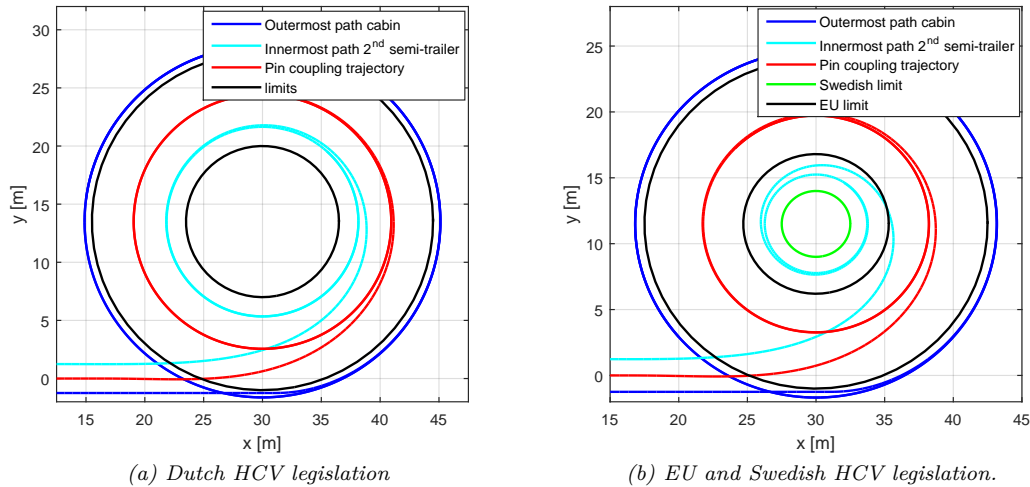
Figure 4.9: Inner- and outermost trajectories of the A-double HCV with 4x2 Krone steered dolly during different 360 degree turn manoeuvres. Simulated with dolly propulsion and empty semi-trailers.

4.2   Design of the 4x4 dolly

Link dolly steering

It follows from (4.3) that the radius of the fifth wheel coupling of the dolly should be increased, to improve the swept path behaviour of the vehicle. The first design of the 4x4 dolly is, therefore, a dolly which is rigidly connected to the rear of the first semi-trailer, see Fig. 4.10. This steering system limits the additional swept path introduced by the dolly with respect to the first semi-trailer. Theoretically, this should result in a larger king pin radius of the dolly in comparison with the standard dolly. For this steering system the first semi-trailer is extended with the dolly, making it a link trailer like is used by the B-double HCV. The four wheels of the dolly are steered to avoid large tyre side slip angles. The

required steer angles of the wheels are calculated by using Fig. 4.10 and the equations below. For this analysis, it is assumed that no forces are transmitted through the drawbar, so the critical radius of the first semi-trailer $r_{crit,1}$ is not affected by the dolly and second-semi-trailer. In reality, however, drawbar forces are transmitted to the chassis of the leading semi-trailer. With Pythagoras' theorem, the equations below are derived:

$$r_{crit,1} = \sqrt{r_{pin}^2 - l_{pin}^2} \tag{4.20}$$

$$r_{kp,D} = \sqrt{r_{crit,1}^2 + (l_{pin} + l_{db} + r_{wheel} + l_d - c)^2} \tag{4.21}$$

$$\delta_1 = \frac{\pi}{2} - \chi_1 = \frac{\pi}{2} - atan\left(\frac{r_{crit,1}}{l_{pin} + l_{db} + r_{wheel}}\right) \tag{4.22}$$

$$\delta_2 = \frac{\pi}{2} - \chi_2 = \frac{\pi}{2} - atan\left(\frac{r_{crit,1}}{l_{pin} + l_{db} + r_{wheel} + l_d}\right) \tag{4.23}$$

The required steer angles at the front and rear axle of the dolly are represented by δ_1 and δ_2, respectively. The radius to the front and rear axles are represented by r_{front} and r_{rear}. The wheelbase of the dolly is represented by l_d and the king pin radius by $r_{kp,D}$. The distance between the centre axle of the first semi-trailer and the front axle of the dolly is defined by the drawbar length l_{db}, wheel radius r_{wheel} and the distance between the centre axle of the semi-trailer and pin coupling location l_{pin}, as defined by (4.21). With the equations above, the required steer angles can be calculated for a given radius of the pin coupling or the critical radius of the first semi-trailer defined by $r_{crit,1}$.
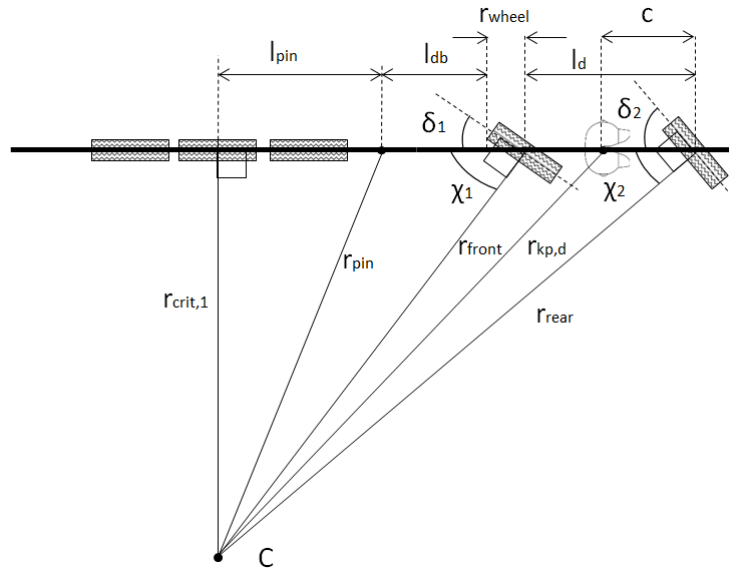

Figure 4.10: Steady state cornering with link dolly steering.

The gain between the articulation angle of the tractor/semi-trailer and the required steer angles of the dolly serve as input for the simulation model of the 4x4 link dolly. This gain is calculated for steady state cornering conditions. From (4.23) and (4.23) it follows that this steer angle depend on the critical radius of the first semi-trailer $r_{crit,1}$. For real life implementation, the steer controller should be able to calculate this radius and determine the required steer angles at the dolly axles accordingly. For now, a constant gain is assumed for both the Dutch HCV and EU 360 degree turn. The gain between the first articulation angle and steer angle of the wheels is calculated with:

$$k_i = \frac{\delta_i}{\theta_1} \tag{4.24}$$

The gain between the articulation angle and steer angles of each axle is represented by k_i. The required steer angles δ_i are calculated with (4.22) and (4.23). The steady state articulation angle between the tractor and first semi-trailer is represented by θ_1.

A large distance is present between the tractor's fifth wheel and the dolly axles. Therefore, the articulation angle θ_1 is delayed in the simulation model to ensure correct operation of this steering system. This delay equals the distance between both fifth wheel couplings l_{ff}, divided by the longitudinal velocity V_x. The required delay τ_{link} is defined by:

$$\tau_{link} = \frac{l_{ff}}{V_x} \tag{4.25}$$

One advantage of the link dolly steering is that the dolly can no longer yaw with respect to the first semi-trailer. The drawbar length of this dolly can be decreased to 1.5 m, since collisions between the dolly and rear bumper of the first semi-trailer cannot occur any more. This value of the drawbar length equals the distance from the pin coupling to the rear of the first semi-trailer, see Chapter 3.2. The reduction in the drawbar length reduces the interspace between the two semi-trailers and the air drag accordingly.

Path following steering

The second steering system for the 4x4 dolly that is evaluated is the path following steering system, as used in [17]. The basic idea of such a system is that a lead point and follow point are chosen at an arbitrary location on the truck. The trajectory of the lead point is sensed and stored, such that the follow point can be steered to follow this lead point trajectory. From the kinematic relations in Fig. 4.3 it follows that the critical radii r_{crit} of both semi-trailers are the same when the desired king pin radius $r_{kp,D}$ of the first and second semi-trailer are equal. Therefore, it is chosen to place the lead point position on the centre of the tractor's fifth wheel and the follow point at the centre of the dolly's fifth wheel. By doing so, the 4x4 dolly equipped A-double should achieve the same manoeuvrability performance as a tractor semi-trailer combination. In Fig. 4.11 the lead point trajectory is represented by the red line. The arrow in Fig. 4.11 represents the fixed drawbar distance l_{pf}, measured from pin coupling to the dolly's centre of the fifth wheel.
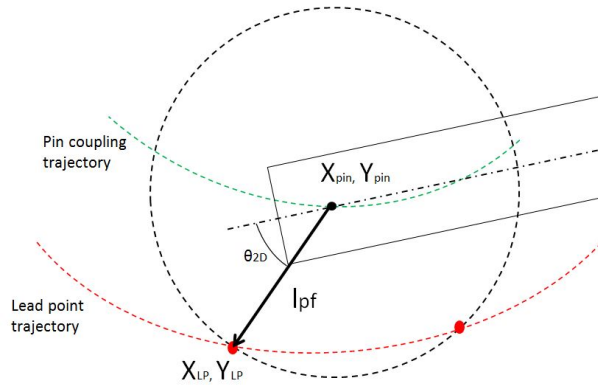

Figure 4.11: Lead point and follow point in the path following steering principle.

For this steering system, the tractor is equipped with position sensors or estimators that can estimate the longitudinal and lateral position of the tractor's fifth wheel in the global coordinate frame. This data is send to a memory storage device that stores these points for further computation. A similar sensor or estimator is placed at the pin coupling below the first semi-trailer. During driving, the distance between the pin coupling and dolly's fifth wheel l_{pf} is fixed. To determine the point towards the dolly should be steered, there is searched for the point on the lead point trajectory that is exactly at a distance of l_{pf} from the current pin coupling position. In the scenario shown in Fig. 4.11, this results in two feasible positions, which are denoted by the red dots.

The correct position for the follow point on the lead point trajectory satisfies the following relation:

$$(X_{pin} - X_{LP})^2 + (Y_{pin} - Y_{LP})^2 = l_{pf}^2 \tag{4.26}$$

The parameters X_{pin} and Y_{pin} are defined as the longitudinal and lateral coordinates of the current pin coupling position. The position on the lead point trajectory is defined by X_{LP} and Y_{LP}. The required articulation angle at the pin coupling to steer towards this lead point position is defined as θ_{2D}. Note, during certain manoeuvres, multiple points can be found on the lead point trajectory that satisfy (4.26).

These points are denoted by the red dots in Fig. 4.11. When the red rod in front of the pin coupling is used, a strange orientation of the dolly is obtained. In this orientation the rear of the dolly runs in front of the pin coupling. The maximum absolute value of the articulation angle θ_{2D} is set to π to eliminate these infeasible points.

An A-double HCV equipped with the path following steering system is shown in Fig. 4.12. The desired follow point coordinates are represented by X_{FPD} and Y_{FPD}. These coordinates are equal to the lead point coordinates X_{LP} and Y_{LP} obtained from (4.26). The articulation angles between the vehicles are represented by θ_i. In which θ_1 is the articulation angle between the tractor and semi-trailer and θ_{2D} is the desired articulation angle between the pin coupling and dolly drawbar. The yaw orientation of the vehicles are represented by ψ_i and are expressed in the global coordinate frame. For the yaw angles, the index i corresponds to the first, second and third vehicle, which are the tractor, first semi-trailer and dolly, respectively.

When the coordinates on the lead point trajectory are found, the desired yaw angle of the dolly, defined as ψ_{3D}, can be calculated with:

$$\psi_{3D} = atan2 \left(\frac{Y_{pin} - Y_{FPD}}{X_{pin} - x_{FPD}} \right) \tag{4.27}$$

With the global yaw orientation of the second semi-trailer ψ_2, the desired articulation angle θ_{2D} between the semi-trailer and dolly can be calculated with:

$$\theta_{2D} = \psi_2 - \psi_{3D} \tag{4.28}$$

Standard semi-trailers are used in the A-double configuration, so it is not likely that the trailers are equipped with a yaw sensor. Therefore, the yaw angle of the first semi-trailer can be calculated by using the yaw angle of the tractor and articulation angle as defined by the following equation:
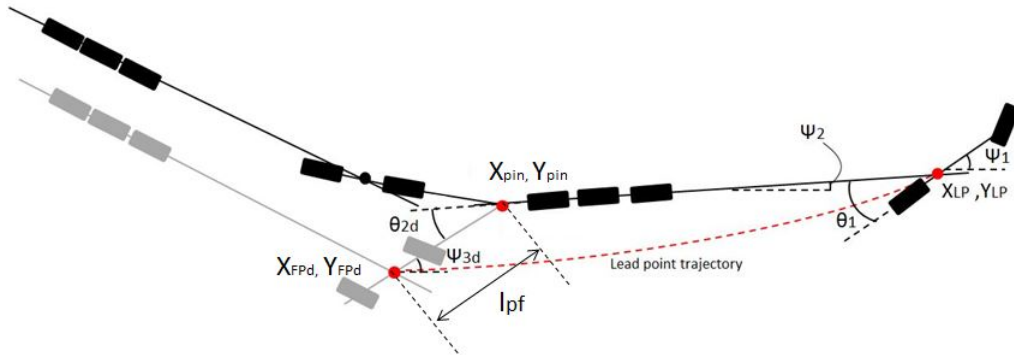
$$\psi_2 = \psi_1 - \theta_1 \tag{4.29}$$

Figure 4.12: Path following steering implemented on an A-double HCV.

The control variables of the path following steering system are the steer angles at the front and rear axle of the dolly, represented by δ_1 and δ_2. A problem may arise, because there are two control variables and only one control objective needs to be met. This means that the control problem is over-actuated, since there are multiple combinations of steer angles feasible that result in the same articulation angle θ_{2D} at the pin coupling. For the implementation of this steering system in [17], it is assumed that all the wheels on a vehicle are steered with equal steer angles. However, the link dolly steering design derived earlier, already shows that the magnitudes of both dolly steer angles differ a lot. This means that the approach as used by [17] cannot be used by the 4x4 smart dolly.

Another approach, as used in [36], is to determine the steer angles at the required positions by means of interpolation of the lateral velocities along the vehicle. When the lateral velocities of at least two points are known, the lateral velocity at other locations can be approximated via linear inter- and extrapolation. The tyre side slip angles α_i should be small under the assumption that steady state cornering at low longitudinal velocities is applied. With this assumption, it can be approximated that the steer angles of

both dolly axles are equal to the calculated body side slip angles at the axle positions. The body side slip angle β_i is defined as the angle between the velocity vector pointing in the direction of travel and the dolly chassis.

The longitudinal and lateral velocities at the axle locations are required to calculate the body side slip angles at the axles. The longitudinal velocity V_x is the same for all positions on the dolly and can be sensed with velocity sensors. The lateral velocity vectors at the axle locations are approximated by means of inter- and extrapolation. With the two position sensors/estimators the trajectories of the pin coupling and fifth wheel of the dolly are known. By using these trajectories, the corresponding velocity vectors that point in the direction of travel can be retrieved. For this approach, Fig. 4.13 is used. In this figure the trajectories of the pin coupling and fifth wheel of the dolly are shown, together with their corresponding velocity vectors.

To calculate the lateral velocities at the pin coupling and fifth wheel coupling, the body side slip angles at these two points must be retrieved first. The body side slip angle at the pin coupling can be calculated with:

$$\beta_{pin} = \psi_{3D} - \gamma_{pin} \tag{4.30}$$

The body side slip angle at the dolly's fifth wheel coupling can be calculated with:

$$\beta_{kp} = \psi_{3D} - \gamma_{kp} \tag{4.31}$$

In the equations above, the desired yaw orientation of the dolly is represented by ψ_{3D} and the angle between the longitudinal axis and the heading vector is represented by γ_i.

To reduce the memory usage and computation time, the controller is implemented such, that the lead point and pin coupling positions are only updated for every 10 cm travelled distance. To calculate the angles γ_{pin} and γ_{kp}, two consecutive positions on the pin coupling and lead point trajectory are required. This means that for the pin coupling heading angle the current coordinates X_{pin} and Y_{pin} and previous coordinates $X_{pin,prev}$, $Y_{pin,prev}$ are used. The coordinates of future positions of the pin coupling are unknown at the current position, so only the current and previous positions can be used for the pin coupling. When the interval between consecutive iterations is small, the heading angle γ_{pin} can be approximated with:

$$\gamma_{pin} = atan\left(\frac{Y_{pin} - Y_{pin,prev}}{X_{pin} - X_{pin,prev}}\right) \tag{4.32}$$

By assuming that the next desired fifth wheel position is located at the next position on the lead point trajectory defined by $X_{LP,next}$ and $Y_{LP,next}$, the fifth wheel heading angle γ_{kp} can be calculated with:

$$\gamma_{kp} = atan\left(\frac{Y_{LP,next} - Y_{LP}}{X_{LP,next} - X_{LP}}\right) \tag{4.33}$$
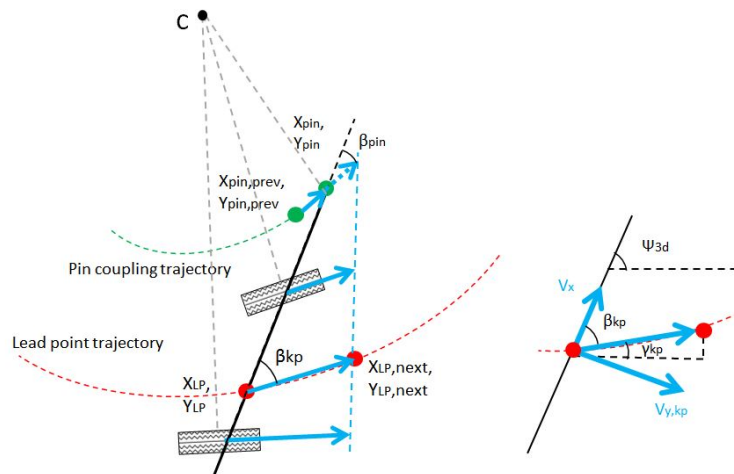

Figure 4.13: Interpolation of the velocity vectors.

43

The next step in this approach is calculating the magnitudes of the lateral velocity at the dolly's pin- and fifth wheel coupling. These lateral velocities are used in the lateral velocity inter- and extrapolation. Since the body side slip angles β_i are known from (4.30) and (4.31), the corresponding lateral velocities at the pin coupling and fifth wheel can be calculated with:

$$V_{y,pin} = \tan(\beta_{pin}) \cdot V_x \tag{4.34}$$

$$V_{y,kp} = \tan(\beta_{xp}) \cdot V_x \tag{4.35}$$

The lateral velocities derived in (4.34) and (4.35) are used to approximate the lateral velocities at the axle locations on the dolly. For the interpolation of the lateral velocity, a linear approximation is used, which is represented by:

$$V_{y,k} = \left(\frac{V_{y,kp} - V_{y,pin}}{l_{pf}} \right) \cdot z + V_{y,pin} \tag{4.36}$$

In this equation z is the distance from pin coupling to the axle positions of the front or rear axle. The subscript k stands for the axle positions denoted by *axle1* or *axle2*. The parameter l_{pf} is the length between the pin coupling and the fifth wheel of the dolly.

The lateral velocities at the axle positions $V_{y,axle1}$ and $V_{y,axle2}$ can be calculated with (4.36), by using axle positions of $z = 2.52$ m and $z = 5.30$ m for the front and rear axle respectively. With these lateral and longitudinal velocities of both axles, the required body side slip angles and hence; steer angles can be calculated with:

$$\beta_1 = \delta_1 = atan\left(\frac{V_{y,axle1}}{V_x} \right) \tag{4.37}$$

$$\beta_2 = \delta_2 = atan\left(\frac{V_{y,axle2}}{V_x} \right) \tag{4.38}$$

In these equations δ_i denotes the steer angle of the front (1) and rear (2) axle.

Implementation of the path following steering in the TU/e CVL

The steer controller uses two methods to reduce the computation time and memory usage. First of all, positions of the lead point and pin coupling are only updated for every 10 cm travelled distance. Accordingly, the required steer angles δ_i are updated for every 10 cm travelled distance. The second method distinguishes feasible lead points from infeasible lead points. Due to the large distance between the fifth wheels on the A-double HCV, the last set of added lead points are more than a full semi-trailer length in front of the current dolly position. To reduce the computation time further, the last added set of lead points and the lead points that already have been used by the steer controller, are not evaluated by the searching algorithm in (4.26).

The implemented steer controller in the simulation model, searches along the lead point trajectory for the desired point towards the follow point should be steered. The controller can only find desired lead points after the tractor has travelled 17.63 m, which equals the distance between the fifth wheel of the tractor and the fifth wheel of the dolly. The lead point trajectory during the EU 360 degree turn and the selected follow points are shown in Fig. 4.14. The follow points in this figure are plotted with intervals of 1 m for visibility reasons.

The output of the steer controller for the EU 360 degree turn is shown in Fig. 4.15. It is obtained from Fig. 4.15b that the steering angles are calculated correctly, since the fifth wheel trajectory of the dolly follows the fifth wheel trajectory of the tractor well. It follows from Fig. 4.15a that the dolly initially steers in the same direction as the steered wheels of the tractor. A few moments later the wheels are steered with opposite signs. This causes the dolly to move to the outside of the turn. The initial steering manoeuvre towards the centre of the turn, can be explained by the fact that when the tractor and semi start entering the roundabout, articulation angles at the couplings are generated. Because of this, the dolly needs to be steered to the inside of the turn to follow the same path as the tractor. At approximately t=25 s, the lateral tyre forces at the dolly increase and side slip angles are generated. Without steering, the radius from dolly to the instantaneous centre decreases. To counteract this behaviour, both wheels on the dolly are steered with opposite sign to move the fifth wheel coupling to the outside of the turn.
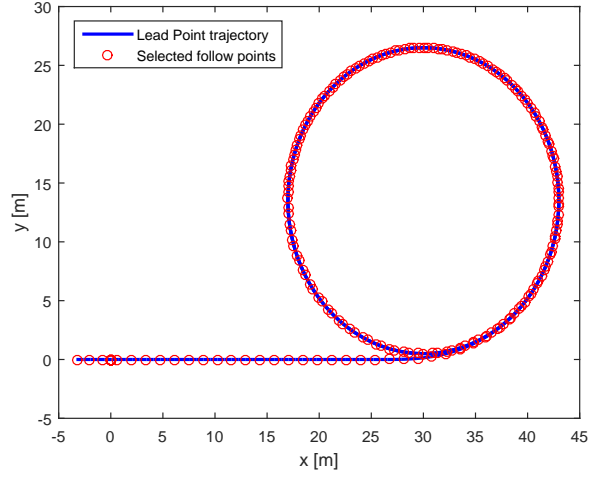
Figure 4.14: Lead point trajectory of the tractor and selected desired follow points by the path follower steer controller.

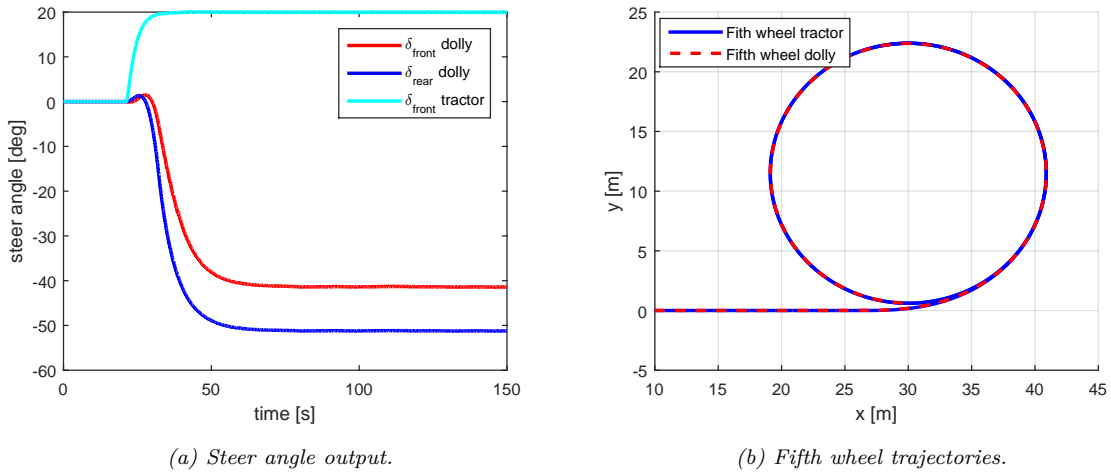*(a) Steer angle output.*

(b) Fifth wheel trajectories.

Figure 4.15: Calculated steer angles by the 4x4 path follower controller and fifth wheel trajectories of the tractor and dolly for the EU 360 degree turn, simulated with dolly propulsion.

Results 4x4 steering system

The steady state circular steer performance results of the 4x4 link dolly steering and path following steering are shown in Table 4.2. For the analytical determined swept paths, the additional frontal swing of the cabin is assumed to be 0.7 m and 0.6 m for the EU and Dutch HCV 360 degree turns, respectively. Furthermore, the A-double HCVs are simulated with empty semi-trailers. Dolly propulsion is enabled in the 4x4 path following steering simulations. The link dolly simulations are performed without dolly propulsion.

From the analytical results in Table. 4.2 it can be concluded that the swept path of the link dolly steering on the EU 360 degree turn is 0.34 m smaller than swept path of the path following steering. The Dutch HCV swept path of the link dolly steering is 0.60 m smaller than the path following controller. However, large differences can be found between the analytical and simulation results of the link dolly steering system. This is explained in the next section. Based on the simulation results, the path following steering system achieves the best performance for the 4x4 dolly equipped A-double.

From simulation it is obtained that the EU 360 degree swept path of a fully loaded tractor semi-trailer combination equals 6.70 m. Comparing this value with the 4x2 dolly A-double performance in Table 4.1, results in an increased swept path value of 48.7 %. However, the increase in swept path for the 4x4 dolly A-double is only 1.19 %. This implies that the A-double equipped with 4x4 dolly is able to meet the swept path performance of the tractor semi-trailer combination better.

Table 4.2: Maximum achievable steering performance of different 4x4 dolly steering systems in the context of an A-double HCV.

		r_{crit} [m]	swept path [m]	δ_1 [deg]	δ_2 [deg]	δ_1/θ_1 [-]	δ_2/θ_1 [-]
Link dolly steering							
EU circle	analytical	6.76	6.44	32.80	45.15	0.89	1.23
	simulation	5.61	7.59	34.43	47.47	0.89	1.23
NL circle	analytical	9.80	5.30	25.39	36.51	0.69	0.99
	simulation	8.36	6.74	24.20	34.79	0.69	0.99
Path following steering*							
		r_{crit} [m]	swept path [m]	δ_1 [deg]	δ_2 [deg]	δ_{pin} [deg]	
EU circle	simulation	6.53	6.78	41.42	51.24	8.30	
NL circle	simulation	9.30	5.90	32.97	42.46	7.06	

* Simulated with dolly propulsion.

4.3 Performance comparison with the TU/e CVL

For the proposed steering system designs in this chapter, the steering performance that are listed in Table 4.1 and Table 4.2 are calculated analytically and by means of simulations in the TU/e CVL. From Table 4.1 and Table 4.2 it follows that the swept path performances retrieved via simulation are worse than using analytical equations. To understand the differences between the analytical and simulation results, the swept path behaviour of a vehicle is explained first.

The swept path behaviour of a vehicle can be explained in two ways. First there is the kinematic model of a vehicle during steady state cornering. Kinematic models are used for the derivations of the analytical equations in the steering systems above. As already shown in Fig. 4.3, under the assumption that the tyre side slip angles are small and neglecting the outermost axles of the semi-trailer axle set, the wheels of a tractor semi-trailer combination are orientated perpendicular to the instantaneous centre of the turn. To achieve this, articulation angles between the vehicles are present. Together with the wheelbases of the vehicles, swept paths are induced by each vehicle. Extending Fig. 4.3 with all the vehicles in the A-double configuration, results in Fig. 4.16. It follows from this figure that each vehicle introduces a swept path with respect to the preceding vehicle. The critical radius of the innermost tyre on the rearmost semi-trailer is, therefore, much smaller than the critical radius of the first semi-trailer.
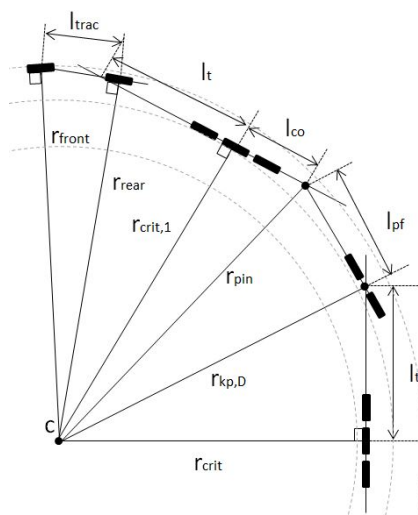

Figure 4.16: Kinematics of a baseline A-double HCV in steady state cornering position.

The second way in which the swept path behaviour of an articulated vehicle can be explained is by means of the tyre side slip angles. As mentioned in Chapter 4.1, the tyres on a vehicle need to generate lateral tyre forces when cornering. Tyre side slip angles are required to generate this lateral tyre force. In Fig. 4.17 a semi-trailer with increased tyre side slip angles is shown. The increased tyre side slip angles change the position of the semi-trailer with respect to the instantaneous centre. The centre axle of the

semi-trailer in Fig. 4.17 is closer to the instantaneous centre than shown in Fig. 4.2. For increasing tyre side slip angles, smaller critical radii $r_{crit,1}$ between the centre axle of the semi-trailer and instantaneous centre of the turn are found. Furthermore, when an articulated vehicle is cornering, articulation angles are induced at the coupling and lateral coupling forces are generated. These forces act on the chassis of the vehicles, which require an additional lateral tyre force to be generated. When a dolly and second semi-trailer are attached to the tractor semi-trailer combination, a large lateral pin coupling force is present at the first semi-trailer. Because of this, the required lateral tyre forces of the first semi-trailers increase even more. This requires even larger tyre side slip angles to be generated.
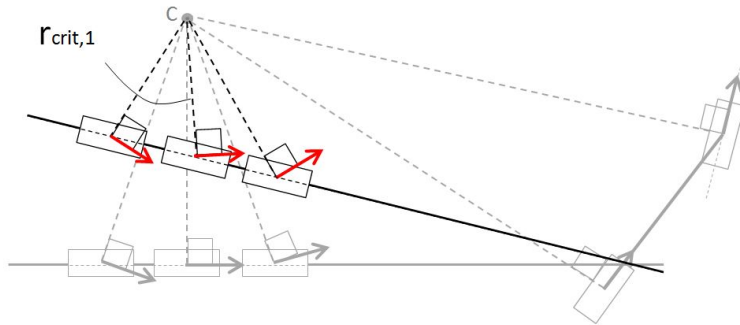

Figure 4.17: Effect of large semi-trailer tyre side slip angles on the critical radius $r_{crit,1}$.

The following observations are found from the simulations results:

1. Positive tyre side slip angles are present at the centre axles of both semi-trailers in the A-double HCV simulations.

2. Longitudinal and lateral forces are present at the pin coupling for the A-double configuration

3. Larger tyre side slip angles are present at the first semi-trailer in the A-double HCV in comparison with the tractor semi-trailer combination.

First of all, the non-zero tyre side slip angles at the centre axles of the semi-trailers and dolly axles conflict with the assumption of a zero tyre side slip angle during steady state cornering. This indicates that the analytically determined critical radii r_{crit} are too optimistic. Secondly, the presence of pin coupling forces actually indicates that there is a lateral force acting on the first semi-trailer's chassis. As explained above, to counteract this lateral force, larger tyre side slip angles at the first semi-trailer are required. From Fig. 4.17 it follows that this decreases the critical radius of the first semi-trailer. Accordingly, the radius of the pin coupling below the first semi-trailer r_{pin} in the A-double simulation is actually smaller than obtained with the tractor semi-trailer simulation. To match the performance of the simulation models better, the gains calculated with the analytic equations above should be adapted for the difference in r_{pin}.

Furthermore, note that the gains for e.g. the 4x4 link dolly steering have been determined for steady state cornering. When entering the 360 degree turn, the wheels should be steered with different gains to ensure that the trajectories of the tractor and first semi-trailer are not affected by the dolly and second semi-trailer. This can be explained by the typical steering behaviour during a 360 degree turn as shown in Fig. 4.15a. Using the steady state determined gains when entering the roundabout in the simulation, may result in larger steer angles than required, which results in large tyre side slip angles at the dolly. This causes a difference in the steady state value of r_{pin} of the first semi-trailer in the A-double simulation in comparison with the value obtained from the tractor semi-trailer simulation.

The mismatch between the performance obtained from the analytical- and simulation models can be reduced via two ways. The problem of the large tyre side slip angles of the first semi-trailer can be solved by propulsion of the dolly wheels. By doing so, the transferred pin coupling forces are reduced and the tyre side slip angles at the first semi-trailer can be reduced too. This solution is explored in the next chapter. Additionally, to reduce the side slip angles at the front axles, Ackermann steering can be implemented. With Ackermann steering the steering angles of the left and right wheel are correct with the dolly's wheelbase, instead of using the single track steer angle [3].

4.4 High speed steer controller design

The aim of this chapter is to design a steering system for the dolly in the A-double configuration to improve the low speed manoeuvrability of the vehicle. Although, extra articulation points and steered axles are beneficial for the low speed manoeuvrability, the high speed stability of the vehicle may be negatively influenced by the steering systems [2], [18]. In this section two high speed control approaches are proposed for the smart dolly designs. These high speed controllers aim to improve the high speed stability, while maintaining the same low speed manoeuvrability performance.

High speed steer control approach 4x2 dolly

A common approach to improve the high speed stability of vehicles with steered axles is to lock the axles at high velocities in order to prevent any steering [17]. By doing so, the benefit of the additional articulation joint introduced by the steered axle can be used during low speed manoeuvring. However, at high velocities the steer axles are locked and the vehicle is considered to have one articulation joint less in comparison with the low speed operation. This approach is used in the 4x2 dolly, such that the drawbar angle can no longer yaw with respect to the chassis of the dolly.

The lateral acceleration a_y acting on the CoG of a vehicle in the A-double configuration is defined as [31]:

$$a_y = \dot{v} + ur \tag{4.39}$$

The lateral acceleration in (4.39) depends on the derivative of the lateral velocity v acting on the CoG, the yawrate of the vehicle r and the longitudinal velocity u. According to [31], the yawrates of trailing vehicles in the global coordinate frame are defined as:

$$r_i = r_1 + \sum_{j=1}^{N} \dot{\theta}_j \tag{4.40}$$

In this equation, r_1 represents the yawrate of the tractor, θ_j represents the angular velocity of the articulation joint j. The index i represents the vehicle id. The maximum number of articulations is represented by the parameter N. Due to the krone steering systems, N equals 4 for the 4x2 dolly and N equals 3 for the 4x4 dolly. From the substitution of (4.40) in (4.39) it follows that the lateral acceleration of the trailing vehicles is influenced by every articulation angle preceding the vehicle of interest. Depending on the orientation of the vehicles, this will increase or decrease the yawrate of the rearmost vehicle. Reducing the number of articulations, by e.g. locking the steering system in the 4x2 dolly design, reduces the yawrate and lateral acceleration of the 4x2 dolly and the second semi-trailer.

High speed steer aproach 4x4 dolly

The approach to improve the high speed stability of the path following steering system is explained in [17]. The idea of this approach is to move the lead point more towards the CoG of the tractor. As shown for the D-type HCV single-sine trajectory in Fig. 4.18, moving the lead point more towards the truck's CoG, results in a more smooth lead point trajectory. For this new lead point trajectory, the desired articulation angle in (4.28) evolves more smoothly and the lateral accelerations decrease accordingly.

The CoG location of the tractor is assumed to be 2 m in front of the fifth wheel. It can be chosen to mount an additional position sensor or estimator at this location or compute the position based on the yaw orientation ψ_1 and tractor's fifth wheel coordinates X_{LP} and Y_{LP}. In comparsion with using a single sensor, the memory storage device always stores twice as much data for two sensors. If the second approach is used, the controller can calculate the required lead point positions when needed. To reduce the computation time and memory usage, the second approach is chosen.
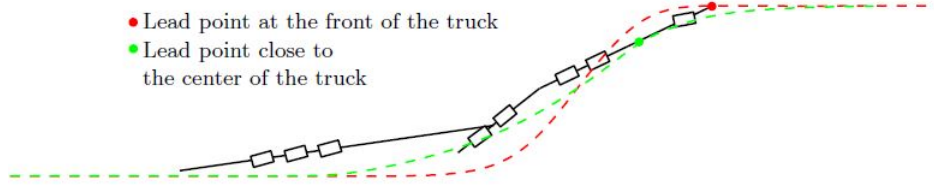
Figure 4.18: Lead point shift for high speed stability improvement of a D-configuration HCV [17]

In Fig. 4.19 the high speed and low speed lead points of a tractor are shown. The coordinates of the new high speed lead point are represented by X_{HSLP} and Y_{HSLP}. The parameter l_{shift} represents the distance of the longitudinal shift between the old and new lead point position. The old, low speed lead points are represented by X_{LP} and Y_{LP} and the yaw orientation of the tractor is represented by ψ_1. From Fig. 4.19 it follows that the coordinates of the high speed lead point can be calculated with:

$$X_{HSLP} = X_{LP} + cos(\psi_1)l_{shift} \tag{4.41}$$

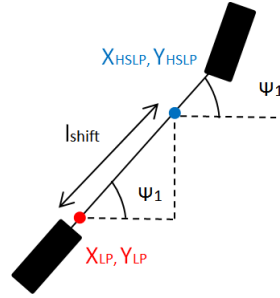$$Y_{HSLP} = X_{LP} + sin(\psi_1)l_{shift} \tag{4.42}$$

Figure 4.19: High speed and low speed lead point positions.

It is desired to gradually increase the distance l_{shift}, to avoid rapid changes in the steer angles for increasing velocities. Therefore, the lead point shift distance l_{shift} is gradually increased from 0 to 2 m for velocities in the range of 30 km/h to 80 km/h. The lead point shift value for increasing velocities is shown in Fig. 4.20. It follows from Fig. 4.20 that for velocities ranging from 30 to 80 km/h the value for l_{shift} increases linearly with the longitudinal velocity V_x of the tractor. The shift distance l_{shift} is kept constant for velocities outside this range. This implementation improves the high-speed stability and ensures that the low speed manoeuvrability till 30 km/h is not affected.
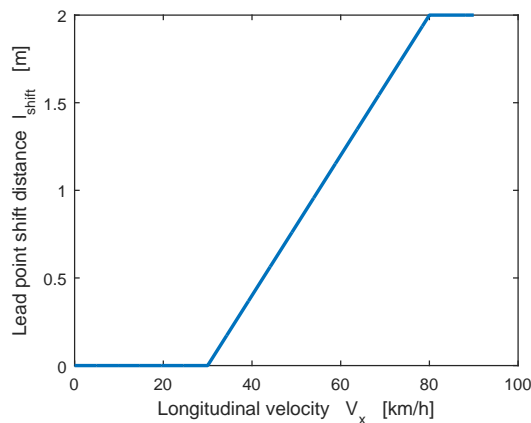

Figure 4.20: Velocity dependent lead point shift distance for the 4x4 high speed steer controller approach.

High speed steer controller results

The performance values for the single sine PBS manoeuvres with- and without high speed controller are listed in Table 4.3 and Table 4.4. The simulations are performed with fully loaded A-double HCVs. The low speed manoeuvrability performance of both dollies is not affected by these high speed controllers, since both high speed controllers are enabled for velocities above 30 km/h. In this section emphasis only lies on the single sine PBS improvements caused by the high speed controllers. A detailed performance comparsion between all dollies is made at the end of this report.

The high speed control approach for the 4x2 dolly design eliminates the articulation point between the drawbar and dolly chassis. From Chapter 2 it follows that small values for the high speed off-tracking and rearward amplification are desired, since this increases the stability of the vehicle. However, the yaw damping coefficient should be increased to improve the stability, such that sway oscillations of the vehicles are better damped. From Table. 4.3 it can be concluded that the high speed control approach on the 4x2 dolly improves yaw damping, high speed off-tracking and rearward amplification. From Fig. 4.21a it follows that enabling the high speed controller of the 4x2 dolly reduces the lateral acceleration compared to the standard and 4x2 dolly with disabled high speed controller. The reduced lateral acceleration and yawrate of the dolly reduces the yawrate of the second semi-trailer in the A-double HCV configuration, as shown in Fig. 4.21b.

Table 4.3: Comparison of the high speed stability of the 4x2 smart dolly in the A-double configuration with and without high speed (HS) control approach.

PBS	unit	4x2 dolly	4x2 dolly HS	improvement
Yaw damping coefficient	[-]	0.10	0.13	+ 30.0 %
High speed off-tracking	[m]	1.55	1.37	- 11.6 %
Rearward amplification	[-]	3.08	2.92	- 5.19 %

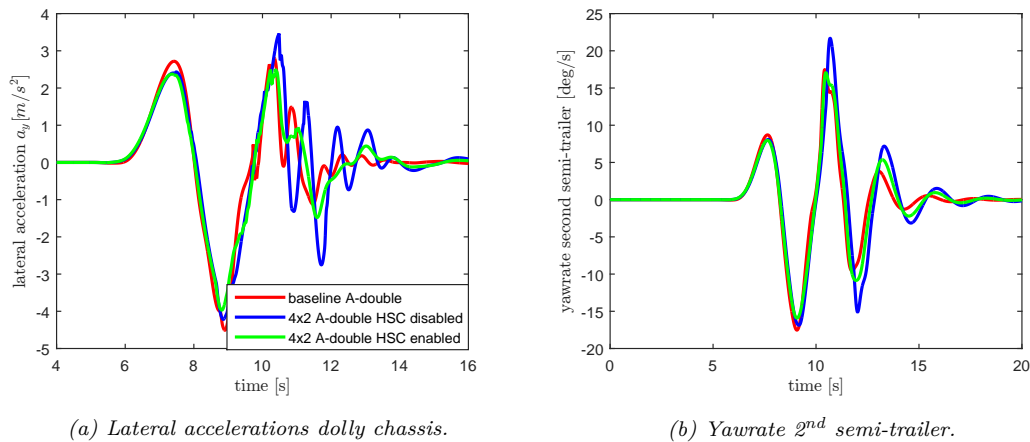*(a) Lateral accelerations dolly chassis.*   *(b) Yawrate 2nd semi-trailer.*

Figure 4.21: Lateral acceleration of the dolly and yawrate of the 2nd semi-trailer for the 4x2 A-double with and without high speed control approach during the single sine manoeuvre. Simulated with fully loaded semi-trailers.

From Table 4.3 and Table 4.4 it can be concluded that the high speed stability performance improves more for the 4x4 dolly compared to the 4x2 dolly. The high speed controlled 4x4 dolly follows a lead point closer to the CoG of the truck. The new set of high speed lead points result in a more smooth lead point trajectory to be followed. This results in decreased lateral accelerations at the dolly. The high speed controlled 4x4 dolly reduces the lateral accelerations peaks compared to the standard and 4x4 dolly without high speed controller, see Fig. 4.22a. The reduction in lateral acceleration reduces the yawrate of the second semi-trailer as shown in Fig. 4.22b. In comparison with the 4x4 dolly with disabled high speed controller, the high speed controlled 4x4 dolly improves the rearward amplification with 18% and the high speed off-tracking with 19%.

Table 4.4: Comparison of the high speed stability of the 4x4 smart dolly in the A-double configuration with and without high speed (HS) control approach.

PBS	unit	4x4 dolly	4x4 dolly HS	improvement
Yaw damping coefficient	[-]	0.19	0.21	+ 10.5 %
High speed off-tracking	[m]	0.88	0.71	- 19.3 %
Rearward amplification	[-]	2.35	1.92	- 18.3 %

(a) Lateral accelerations dolly chassis.
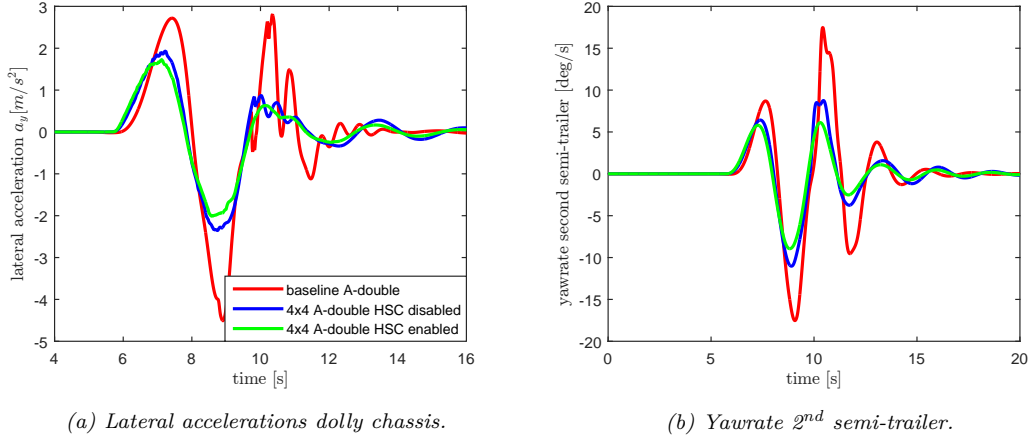

(b) Yawrate 2nd semi-trailer.

Figure 4.22: Lateral acceleration of the dolly and yawrate of the 2nd semi-trailer for the 4x4 A-double with and without high speed control (HSC) approach during the single sine manoeuvre. Simulated with fully loaded semi-trailers.

4.5 Summary

Simulation of the baseline A-double HCV with non-steered dolly shows that the vehicle is not able to meet the Dutch and EU legislation regarding the 360 degree swept paths. The design objective for the dolly steering system is to improve the low speed swept path of the vehicle by increasing the dolly's fifth wheel radius to the instantaneous centre. The Krone steering system appears to be the best design for the 4x2 dolly. This steering systems allows the drawbar not only to rotate with respect to the vertical axis of the pin coupling, but also with respect to the vertical axis of the dolly chassis. The optimal steady state gain is determined and is used to steer the front wheels of the 4x2 dolly. This setup is able to meet the Dutch and Swedish HCV swept path legislation for the 360 degree turn manoeuvre. However, the 4x2 dolly equipped A-double fails to meet the EU 360 degree swept path legislation.

The best solution for the 4x4 dolly was found to be the path following steering. The principle of this system is that the wheels of the dolly are steered such that the follow point follows the lead point trajectory. The lead point has been chosen to be located at the fifth wheel of the tractor and the follow point is located at the fifth wheel of the dolly. By doing so, both fifth wheels follow the same trajectory. This results in matching manoeuvrability performance of the first and second semi-trailer in the A-double configuration. The 4x4 dolly equipped A-double is able to meet all three swept path legislations.

Different approaches are available to improve the high speed stability. For the 4x2 dolly it is chosen to lock the wheels at high velocities. For the 4x4 dolly the lead point is gradually shifted towards the CoG of the tractor for high velocities. The longitudinal distance of this shift is gradually increased with the forward velocity of the vehicle. By shifting the lead point towards the CoG of the tractor, a more smooth lead point trajectory is obtained. Steering the dolly towards this high speed lead point trajectory, reduces the lateral accelerations of the dolly and improves the high speed stability.

The low speed swept path performance of a 360 degree turn and high speed stability performance improvement of the two dolly designs are summarized in Table. 4.5. The results listed in this table are retrieved from simulations with dolly propulsion for low speed operation and enabled high speed controllers for the 4x2 and 4x4 dollies.

Table 4.5: Low speed manoeuvrability performance achieved by the 4x2 and 4x4 dolly steering systems and high speed stability controller (HSC) improvement in the context of an A-double HCV.

		4x2 dolly A-double	4x4 dolly A-double	limit
Low speed manoeuvrability				
EU swept path	[m]	9.96	6.78	7.2
Sweden HCV swept path	[m]	9.96	6.78	10.5
NL HCV swept path	[m]	8.03	5.90	8.0
High speed stability				
Yaw damping increase i.c.w disabled HSC		30.0 %	10.5 %	
Rearward Amplification reduction i.c.w disabled HSC		11.6 %	19.3 %	
High speed Off-tracking reduction i.c.w. disabled HSC		5.19 %	18.3 %	

Chapter 5
Driveline design

In this chapter a preliminary design of the driveline is made. Dolly propulsion can be beneficial in two ways. Firstly, the dolly can assist the tractor's engine in high power demanding scenarios. Secondly, the low speed swept path performance can be improved further. From Chapter 4.3 it follows that large tyre side slip angles are present at the axles of the dolly and last semi-trailer. By propelling the dolly, the pin coupling forces can be reduced. This improves the swept path performance of the vehicle. Equipping an A-double HCV with a smart dolly makes it possible to use a standard 4x2 tractor. Preferably, the A-double HCV should achieve the same driveline performance as a standard tractor semi-trailer combination. To ensure that the performance of the tractor and first semi-trailer is not affected by the dolly and second semi-trailer, a powertrain controller needs to be implemented. The powertrain controller aims to reduce the pin coupling forces. This chapter starts with the derivations of the road load equations. Next the required powertrain performance is determined, followed by the controller design.

5.1 Motor sizing

The required drivetrain performance of the dolly is determined for some typical driving conditions. The tractor semi-trailer performance is used as a starting point to evaluate the required motor performance of the dolly. The road load equations are derived first, to calculate the driveline performance of the tractor semi-trailer during several driving conditions. These driving conditions include highway driving at different constant velocities and startability of the A-double HCV on inclined roads. The aim of the driveline calculations is to ensure that the dolly does not limit the driveline performance of the tractor semi-trailer combination.

Road load equations
The force required from the motor to propel the A-double HCV in longitudinal driving conditions is determined by the road load and efficiencies of the driveline [16]. The road load equations below are derived such that the equations hold for both the ICE propelled tractor and electric motor driven dollies. The road load of the vehicle can be separated into four forces, which are: the gradient force F_{grad}, the air drag force F_{drag}, the tyre rolling resistance force F_{rr} and inertial force F_{inert}. Combining these forces results in the following road load equation:

$$F_{tractive} = F_{grad} + F_{rr} + F_{drag} + F_{inert} \tag{5.1}$$

The equivalent tractive power P and torque T are defined by:

$$P = F_{tractive} \cdot v_x \tag{5.2}$$

$$T = F_{tractive} \cdot r_{wheel} \tag{5.3}$$

More power is requested from the engine or motor P_{engine}, for non-zero total driveline efficiencies. The driveline efficiency $\eta_{driveline}$ can be approximated to 0.95% [33]. Including the driveline efficiency in the road load calculation yields:

$$P_{engine} = \frac{P}{\eta_{driveline}} \tag{5.4}$$

The gradient force in (5.1) originates from the gravity that is acting downwards when the vehicle is driving on an inclined road. The gradient force is calculated with:

$$F_{grad} = m_v \cdot g \cdot sin(\phi) \tag{5.5}$$

The vehicle mass is represented by the parameter m_v, the gravitational constant is represented by g and the road slope angle is represented by ϕ.

The rolling resistance between the tyres and the road can be approximated with:

$$F_{rr} = c_r \cdot m_v \cdot g \cdot cos(\phi) \tag{5.6}$$

The most important parameter for this equation is the roll resistance coefficient c_r of the tyre. This parameter depends on the velocity, temperature, tyre pressure, tyre tread and road surface. In most calculations this parameter is approximated by a constant value. In the TU/e CVL this value equals 0.0065 [-] for a Goodyear R22.5 semi-trailer tyre. Besides the rolling resistance coefficient, also the vertical force on the tyres plays a role in the rolling resistance force, as represented by $m_v \cdot g$. On an inclined road the vertical force on the tyres decreases, which follows from (5.6) by the multiplication with $cos(\phi)$.

The air drag force originates from the viscous friction of the air on the vehicle's surface and the pressure difference between the front and the rear of the vehicle. The air drag force is calculated with the following equation:

$$F_{drag} = 1/2 \cdot \rho_a \cdot A_f \cdot c_d \cdot v_x^2 \tag{5.7}$$

In this equation, A_f is the frontal area of the vehicle, c_d is the air drag coefficient of the vehicle, ρ_a is the air density and v_x is the longitudinal velocity of the vehicle. The air drag coefficient describes the flow conditions and represents how easy or hard it is to overcome the air drag. This value can be approximated with 3D programs or wind tunnel testing. In combination with the large frontal area and gaps between adjacent vehicles in commercial vehicles, large air drag forces are present. From [33] it follows that the MAN TGX has a frontal area of 7.0 m^2 and an air drag coefficient of 1.0.

The inertia force of the vehicle is the last force that is used in the road load calculation and represents the force required to accelerate the total mass m_{tot} of the vehicle. The total mass m_{tot} is the sum of the vehicle mass m_v and the added equivalent rotating mass of the wheels and engine/motor. The equivalent rotating mass of the wheels is represented by $m_{r,w}$ and the equivalent rotating mass of the engine/motor is represented by $m_{r,e}$. The induced inertial torque by these rotating parts needs to be derived first, to determine the equivalent rotating mass of the wheels and engine.

All the rotating parts in the vehicle induce an additional torque that needs to be counteracted by the engine torque. The wheels and engine inertia of an ICE vehicle have the largest influence on the inertial force F_{inert}, as stated in [16]. The inertia torque of the wheels $T_{m,w}$ and the inertial torque of the engine/motor $T_{m,e}$ are calculated with:

$$T_{m,w} = I_w \cdot \dot{\omega}_w \tag{5.8}$$

$$T_{m,e} = I_e \cdot \frac{\gamma}{r_{wheel}} \dot{\omega}_e \tag{5.9}$$

In these equations I_w and I_e are the total moments of inertia at the wheel- and engine side of the gearbox, respectively. The angular velocities of the wheel and engine are defined by ω_w and ω_e. The parameter γ in (5.9) represents the total transmission ratio from engine to wheels. The wheel radius is defined by r_{wheel}.

Assuming no longitudinal tyre slip, it is assumed that:

$$v_x = \omega_w \cdot r_{wheel} \tag{5.10}$$

Furthermore, the required force to overcome this inertia torque can be calculated by dividing the inertia torques in (5.8) and (5.9) with the wheel radius r_{wheel}. This results in:

$$F_m = \frac{T_m}{r_{wheel}} \tag{5.11}$$

Combining (5.10) and (5.11) in (5.8) and (5.9), yields:

$$F_{m,w} = \frac{I_w}{r_{wheel}^2} \dot{v}_x \tag{5.12}$$

$$F_{m,e} = I_e \frac{\gamma^2}{r_{wheel}^2} \dot{v}_x \tag{5.13}$$

The equations above are used to calculate the inertial forces that are acting on the vehicle. The inertial force originating from the wheels is defined by (5.12). The inertial force induced by the engine on the vehicle is defined by (5.13).

Both forces act as an equivalent, to be accelerated mass, for the equation as shown in (5.1). Therefore, the total vehicle mass m_{tot} equals:

$$m_{tot} = m_v + m_{r,w} + m_{r,e} = m_v + \frac{I_w}{r_{wheel}^2} + I_e \frac{\gamma^2}{r_{wheel}^2} \tag{5.14}$$

The resulting inertial force equals:

$$F_{inert} = m_{tot} \dot{v}_x \tag{5.15}$$

For ICE vehicles operated in high gear ratios (low gears), the additional mass added by the inertial forces are significant and should not be neglected [16].

Gearbox ratio

At low speed scenarios like startability and driving on an inclined road, the required power to overcome the road load is low, but the required torque is high. For these high torque demanding scenarios, a gearbox can be mounted between the engine or motor and the wheels to amplify the torque when needed.

Assuming no gearbox losses, the power entering the gearbox equals the power leaving the gearbox. This results in the following equation:

$$T_{engine} \cdot \omega_{engine} = T_{driveshaft} \cdot \omega_{driveshaft} \tag{5.16}$$

In this equation T_{engine} represents the torque at the engine/motor side and $T_{driveshaft}$ represents the torque at the driveshaft. Although the input and output shaft gears have different radii, defined by r_{engine} and $r_{driveshaft}$, the velocity at the point where the gears make contact is equal. Due to this, the following relation holds:

$$\frac{\omega_{driveshaft}}{\omega_{engine}} = \frac{r_{driveshaft}}{r_{engine}} \tag{5.17}$$

The gear ratio γ is defined as the ratio between the numbers of teeth at the output and input shaft, as represented by:

$$\gamma = \frac{r_{driveshaft}}{r_{engine}} = \frac{\#\ teeth\ output\ shaft}{\#\ teeth\ input\ shaft} \tag{5.18}$$

With the gear ratio included in (5.16), the following relation is obtained:

$$\frac{T_{driveshaft}}{T_{engine}} = \gamma \tag{5.19}$$

For gear ratios greater than one, the torque is amplified at the output shaft, whereas the rotational speed is decreased. In the entire driveline of a standard ICE driven tractor two gear ratios can be obtained. These gear ratios are the final drive ratio at the differential and the gear ratio at the gearbox.

Comparison with standard tractor semi-trailer

The design aim for the dolly driveline is that it should meet the performance of the tractor semi-trailer combination for different driving scenarios. When the dolly is able to meet the performance of the tractor, no forces are transmitted via the drawbar for longitudinal driving scenarios. To determine the required motor performance of the dolly, the drivetrain performance of the MAN TGX 4x2 BLS tractor is evaluated during several (longitudinal) driving conditions. The required drivetrain parameters are listed in Table 5.1.

The EU Directive 97/27/EC states two important requirements on the engine or motor performance of commercial vehicles in points 7.9 and 7.10 of [8]. First of all, the maximum loaded vehicle should be able to start five consecutive times on an inclined road with a gradient of at least 12 percent, within five minutes. Secondly, motor vehicles should have an engine power output of at least 5 kW/t of the technically allowed GVW. This requirement should be met to ensure that the vehicle is able to maintain speed on an inclined road. The second requirement already implies that a powertrain is required on the dolly to meet the legislation. When the dolly and last semi-trailer are disconnected from the tractor and first semi-trailer, the

required minimum dolly motor power equals 206 kW. This value results from the total mass of the dolly and second semi-trailer (37+4.2=41.2 t), multiplied with the 5 kW/t requirement. Taking into account the reserve of the tractor's engine in the A-double configuration of 85.2 t, this reduces to 426-328=98 kW.

The desired drivetrain performance of the dolly is determined by means of five different tests that are used in the performance assessment of the A-double HCV. For these test the following performance criteria are calculated:

1. Required power for highway driving on a flat road at 90 km/h

2. Required power for highway driving, on a 4% grade road at the maximum achievable velocity

3. Required power for driving on a 12% grade road at the maximum achievable velocity

4. Required torque for startability on a 12% grade road

5. Required torque for startability on the maximum achievable road slope

During the first three tests the acceleration equals zero, since the vehicle is driving at a constant velocity. Furthermore, it is assumed that the air drag does not increase for the A-double HCV, since the second semi-trailer is couple close to the first semi-trailer. This means that air drag force F_{drag} acting on the dolly can be neglected in the road load calculation defined in (5.1). The 4% slope in the second test originates from the maximum allowed grade on European motorways as determined by the United Nations Economic Commission for Europe (UNECE) [59]. The aim of the third test is to maintain motion on a 12 % grade road. For the first three tests, it is assumed that the engine power is the limiting factor and the tyres can transfer this propulsion force to the road. Furthermore, a driveline efficiency of 95% is used for both the electric motor propelled dolly and ICE propelled tractor.

The fourth test originates from the requirement as stated in the European directive [18]. The fifth test evaluates the additional performance in terms of startability. For both the fourth and fifth test, the performance is limited by the force the tyres can transfer to the road. The maximum required motor torque of the dollies, should therefore be equal to the maximum torque that the tyres can transfer at a given inclination angle. For test 4 and 5, it is assumed that the initial longitudinal acceleration equals 0.01 m/s^2. The air drag is assumed to be negligible, due to the low velocity during startability. The amount of force the tyres can transfer is calculated with (3.9) and (3.10). From (3.9) and (3.10) it follows that the 4x4 dolly has a major advantage compared to the tractor and 4x2 dolly. The total vertical force on the driven axles of the 4x4 dolly is much larger than the vertical force of the 4x2 dolly and tractor. Furthermore, four wheels are driven, so the total required torque can be split over four wheels instead of two.

Table 5.1: MAN TGX 4x2 BLS, D2676 EGR 440PS engine and Tipmatic 12 speed automated gearbox parameters [32].

parameter			value
Maximum engine power	$P_{engine,max}$	$[kW]$	328
Maximum engine torque	$T_{engine,max}$	$[Nm]$	2100
Final drive ratio	γ_{FD}	$[-]$	2.85:1
1st gear ratio gearbox	r_1	$[-]$	15.86
Engine moment of inertia	I_e	$[kg \cdot m^2]$	1.05*
Flywheel moment of inertia	$I_{flywheel}$	$[kg \cdot m^2]$	1.44*
Roll resistance coefficient of the tyres	c_r	$[-]$	0.0065
Efficiency of the driveline	$\eta_{driveline}$	$[-]$	0.95

* MAN engine values can not be found, so the inertias of the Iveco engine are used [39].

Results

The required performances for the five driving tests are listed in Table 5.2 and Table 5.3. Three configurations are evaluated, which are a 4x2 tractor with semi-trailer, 4x2 tractor A-double with non-driven dolly and a smart dolly semi-trailer combination. The required torque at each wheel in Table 5.3 and Table 5.2 is calculated as the total required tractive torque, divided by the number of driven wheels on the motor vehicle.

From Table 5.2 it follows that for highway driving on a flat road at 90 km/h, the tractor semi-trailer combination has a power reserve of 185 kW. Including the drivetrain efficiency of 0.95 %, this results in a power reserve at the wheels of 176 kW. The dolly with semi-trailer only requires 69 kW at the wheels for the same driving scenario, see Table 5.2. For driving at constant velocities, the tractor has sufficient power reserve to haul the dolly and second semi-trailer.

It follows from Table 5.2 that the maximum achievable velocity of the A-double without dolly propulsion drops significantly on 4% and 12% grade roads compard to a tractor semi-trailer combination. To meet the velocities of the tractor with semi-trailer better for these two driving scenarios, it is recommended to perform hill assist by means of dolly propulsion. If it is desired that no forces are transmitted through the drawbar in all three tests listed in Table 5.2, (the sum of) the motor power on the dolly should be equal to 307 kW. This is the maximum required power listed in Table 5.2 and originates from the driving scenario on the 12% grade road for maximum velocity. This is 307-98=209 kW more than required by the EU legislation in [8].

The over-scaling of the tractor engine can immediately be noticed from the maximum achievable startability grades in Table 5.3. Although legislations state that the vehicle should be able to start on a road with 12 % grade, the maximum startability grade of the tractor semi-trailer combination equals 22.7%. To meet the startability performance, the electric motor(s) should deliver 25.2 kNm and 12.6 kNm to each driven wheel on the 4x2- and 4x4 dolly, respectively.

From the above it can be concluded that the dolly motor (set) should have a total output power of 307 kW. This ensures that the dolly and second semi-trailer do not decrease the performance of the tractor semi-trailer combination during the five listed driving scenarios. The selection of the gearbox and motor should be chosen such that the maximum torque at the driven wheels equals 25.2 kNm and 12.6 kNm for the 4x2- and 4x4 dolly, respectively.

Table 5.2: Requested driveline performance for constant velocity highway driving scenarios on roads with different slopes.

		highway 0%	highway 4%	highway 12%
4x2 Tractor with semi-trailer				
P_{engine}	[kW]	143	328	328
Power reserve	[kW]	185	0	0
$T_{per\ wheel}$	[kNm]	1.48	5.73	14.8
V_x **during test**	[km/h]	90.0	53.5	20.7
A-double with non-driven dolly, only using tractor propulsion				
Required power	[kW]	212	328	328
Power reserve	[kW]	116	0	0
$T_{per\ wheel}$	[kNm]	2.20	10.7	28.7*
V_x **during test**	[km/h]	90.0	28.7	10.7
Dolly with semi-trailer				
P_{motor}	[kW]	69	294	307
$T_{per\ wheel}$ **(4x2/ 4x4)**	[kNm]	0.72/0.36	5.13/2.56	13.9/6.93
V_x **during test**	[km/h]	90.0	53.5	20.7

* This required tractive force is found to be higher than the force that can be transferred to the road, so the vehicle is not able to complete this test.

Table 5.3: Required torque at the wheels for startability with 0.01 m/s^2 on a 12% grade road and maximum achievable grade road.

	unit	tractor+semi	baseline*	4x2	4x4
$T_{per\ wheel}$ **12 % grade road**	[kNm]	15.0	28.9**	14.0	6.98
$T_{per\ wheel}$ **max grade road**	[kNm]	27.0	25.9	25.2	12.6
Maximum grade	[-]	22.7%	10.7%	22.7%	22.7%

* A-double HCV without dolly propulsion.
** This required tractive force is found to be higher than the force that can be transferred to the road, so the vehicle is not able to complete this test.

5.2 Controller design

The weight of the dolly is partially be determined by the size of the batteries. A powertrain controller ensures that the wheels of the dolly are only propelled when needed to reduce the battery size and weight of the dolly accordingly. Dolly propulsion is needed for high power demanding scenarios like e.g. startability on an inclined road. Furthermore, dolly propulsion can also be used to improve the swept path performance of the A-double HCV. As mentioned in Chapter 4.3, large tyre side slip angles and coupling forces are present during the 360 degree turns. The forces acting on the pin coupling can be reduced with dolly propulsion. Doing so, improves the swept path of the rearmost semi-trailer even more.

The control objective of the powertrain controller is to cancel the pin coupling forces. When this control objective is met, the dolly and second semi-trailer in the A-double HCV do not decrease the driveline performance of the leading tractor semi-trailer combination. In theory, this also means that infinitely many dollies and semi-trailers can be coupled without affecting the driveline performance of the tractor semi-trailer combination. For this implementation, the longitudinal and lateral forces at the pin coupling are measured with a force sensor. The control variables in this approach are the tractive force at the wheels. For now, emphasis lies on the reduction of the large longitudinal pin coupling force. In a future research a lateral controller should be added to reduce the lateral pin coupling force. Two proposed design approaches of this lateral controller are explained in Appendix D.

The free body diagram of the dolly, coupled in an A-double HCV configuration, is shown in Fig. 5.1. With Newton's second law the following equations are derived:

$$m_3(\dot{u}_d - v_d r_d) = \sum_{n=1}^{4} F_{xn,chas} - F_{c3x} + F_{c2x} \tag{5.20}$$

$$m_3(\dot{v}_d + u_d r_d) = \sum_{n=1}^{4} F_{yn,chas} - F_{c3y} + F_{c2y} \tag{5.21}$$

The pin coupling and fifth wheel forces are represented by F_{c2x}, F_{c2y}, F_{c3x} and F_{c3y} for the longitudinal and lateral directions, respectively. The yaw velocity of the dolly is represented by r_d and the dolly mass is represented by m_3. The longitudinal and lateral velocity of the dolly are defined by the parameters u_d and v_d.

The forces generated by the tyres needs to be transformed into the coordinate frame of the dolly to obtain the longitudinal and lateral forces that are acting on the chassis of the dolly. This force transformation is derived for the rear left tyre in Fig. 5.1. From this tyre it follows that the tyre forces can be transferred to the dolly chassis frame by using:

$$F_{xn,chas} = F_{xn} \cdot cos(\delta_n) + F_{yn} \cdot sin(\delta_n) \qquad n = 1, .., 4 \tag{5.22}$$

$$F_{yn,chassis} = F_{yn} \cdot cos(\delta_n) - F_{xn} \cdot sin(\delta_n) \qquad n = 1, .., 4 \tag{5.23}$$

In which the longitudinal and lateral force in the tyre coordinate frame are represented by F_{xn} and F_{yn}, respectively. The total resulting force of each tyre acting on the chassis in the dolly coordinate frame is represented by $F_{xn,chas}$ and $F_{yn,chas}$, for the longitudinal and lateral component respectively. The front left tyre is represented by the subscript $n = 1$, the front right by $n = 2$, the rear left by $n = 3$ and rear right by $n = 4$. The corresponding steer angle at the wheels is represented by the parameter δ_n. The distance between the centre of the pin coupling and the fifth wheel coupling at the dolly is represented by the distance l_{fw}. The inertia around the vertical axis is represented by $I_{zz,d}$.

To reduce the longitudinal force transmitted via the drawbar, the individual wheels needs to be driven such that the sum of the transformed forces $F_{xn,chas}$ equals the longitudinal coupling force measured at the pin coupling. This reguirement yields the following equation:

$$\sum_{n=1}^{n=4} F_{xn,chass} = F_{x,pin} \tag{5.24}$$

The parameter $F_{x,pin}$ is the measured resulting longitudinal force in the dolly coordinate frame. From Fig. 5.1 it follows that F_{c2x} is the resultant force originating from the longitudinal fifth wheel force F_{c3x} minus all the transformed longitudinal tyre forces $F_{xn,chas}$ and the longitudinal inertial force $m_3(\dot{u}_d - v_d r_d)$.
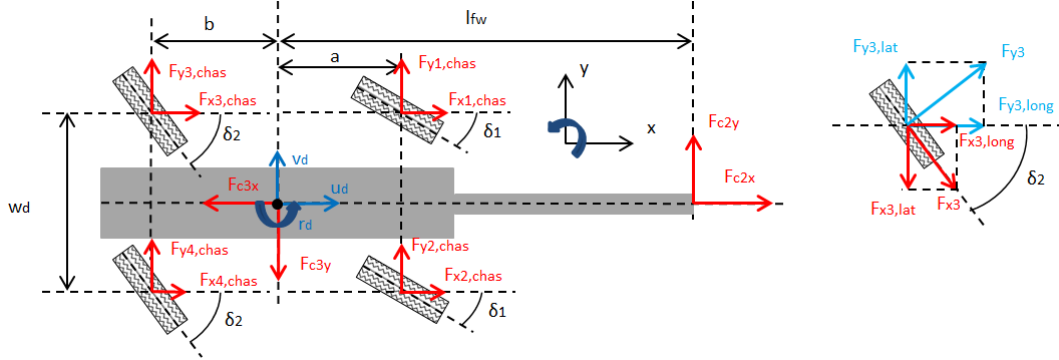

Figure 5.1: Free body diagram of the 4x4 dolly, coupled in an A-double HCV.

The longitudinal pin coupling force equals zero, when the sum of the transformed longitudinal tyre forces equals the measured longitudinal pin coupling force $F_{x,pin}$. This results in:

$$F_{x,pin} = \frac{cos(\delta_1)}{F_{x1}} + \frac{cos(\delta_1)}{F_{x2}} + \frac{cos(\delta_2)}{F_{x3}} + \frac{cos(\delta_2)}{F_{x4}} \tag{5.25}$$

With this control approach there are four control variables, which are the longitudinal forces in the tyre coordinate frames F_{xn}. However, only one control objective has been defined. This means that the system has infinitely many solutions. To solve this problem, it is assumed that each wheel should counteract a fourth of the total longitudinal measured pin coupling force $F_{x,pin}$, yielding:

$$F_{xn} = \begin{cases} \frac{1}{4}\frac{1}{cos(\delta_1)}F_{xpin} & n = 1,2 \\ \frac{1}{4}\frac{1}{cos(\delta_2)}F_{xpin} & n = 3,4 \end{cases} \tag{5.26}$$

For the implementation of the driveline controller in the 4x2 dolly simulation model, the relation shown in (5.26) changes slightly. Since the 4x2 dolly is two-wheel-driven, only the rear wheels can be propelled, such that the tractive force controller uses the following equation:

$$F_{xn} = \frac{1}{2}F_{xpin} \quad n = 3,4 \tag{5.27}$$

Multiplying the required tractive force in (5.26) and (5.27) with the wheel radius r_{wheel}, results in the required torque T_n at each wheel.

$$T_n = F_{xn} \cdot r_{wheel} \tag{5.28}$$

The longitudinal drive controller is implemented as a PI-controller and the implementation of this controller in Simulink is shown in Fig. 5.2. From Fig. 5.2. it follows that the longitudinal pin coupling force is subtracted from the reference value of zero to retrieve the error. This force error is divided by four and transformed to the wheel coordinate frame by means of the steer angles at each wheel. The multiplication with the wheel radius results in the required torque for the front and rear wheels at the dolly.
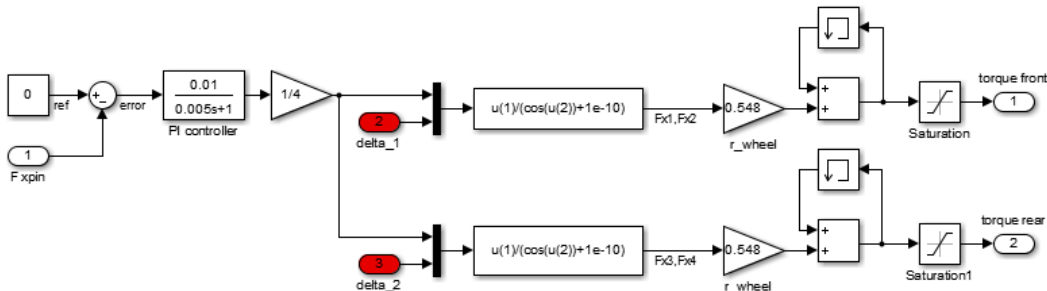

Figure 5.2: longitudinal drive controller implemented on the 4x4 dolly in the A-double HCV.

The longitudinal pin coupling force acting on the 4x4 dolly during the EU 360 degree turn test is shown in Fig. 5.3. Four different responses are shown in Fig. 5.3 to evaluate the effect of the gain and integral settings of the PI controller. From Fig. 5.3 it can be obtained that for small gains k, the peak that starts at around t= 29 s reaches a higher amplitude at t=40 s compared to large gains k. This can be explained by the fact that for smaller gains, the controller needs more time to reduce the error between the reference value and longitudinal pin coupling force. The maximum pin coupling force, therefore, can reach higher values and it takes longer before the pin coupling force is reduced to zero. However, too large gains, as represented by the black line in Fig. 5.3, can lead to instability of the system. Any oscillation or disturbance in the pin coupling force signal is amplified more, such that the required tractive force increases. This increases the oscillations in the pin coupling force even more. From Fig. 5.3 it follows that for larger values of I, represented by the green line, the oscillations in the pin coupling force are less damped and reach higher amplitudes. Manual tuning of the PI controller results in a gain value of 0.010 and integral value of 0.005. This ensures a fast reaction and reduces the steady state error sufficiently fast.
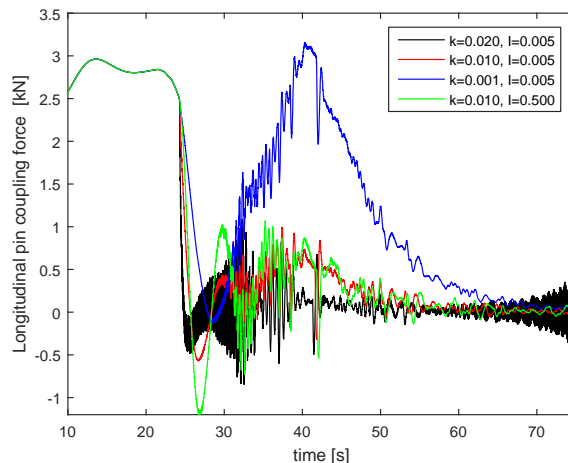

Figure 5.3: Effect of the controller settings on the longitudinal pin coupling forces at the 4x4 dolly, during the EU 360 degree turn.

5.3   Controller results

In this section the results of the longitudinal powertrain controller are presented. First the uncontrolled pin coupling forces are explained in detail, after which the results of the longitudinal pin coupling force controller are explained.

The forces that are present at the pin coupling of the 4x4 dolly during the EU 360 degree manoeuvre are shown in Fig 5.4a. At the start of the 360 degree turn simulations, the vehicle is driving on a straight road segment for 30 meters. Since the articulation angles are zero before entering the roundabout, only a longitudinal force is present at the pin coupling. However, when the tractor and first semi-trailer initiate the turn at approximately t = 25 s, a lateral pin coupling force is present too, because of the non-zero articulation angle between the first semi-trailer and dolly. When the semi-trailer initiates cornering at t=25 s, the lateral pin coupling force and articulation angle are relatively small. Initially, the drawbar of the dolly rotates with respect to the pin coupling, since it takes some time to generate the desired lateral tyre forces. Therefore, the longitudinal pin coupling force reduces slightly till t=30 s. After t=30 s, the dolly generates sufficient lateral tyre forces to initiate cornering. The dolly starts to turn and the articulation angle and according lateral and longitudinal pin coupling forces are increased again. The pin coupling force increase until an equilibrium has been found between the tyre forces and the forces at the couplings between adjacent vehicles.

From Fig. 5.4a it follows that the steady state value of the longitudinal pin coupling force for the 4x4 dolly is greater than the steady state value of the lateral pin coupling force. This is caused by the relative small pin articulation angle of -4.2 degree. From Fig. 5.4a is obtained that the longitudinal force reaches a value of 35 kN, whereas the lateral force only reaches a value of 11 kN.
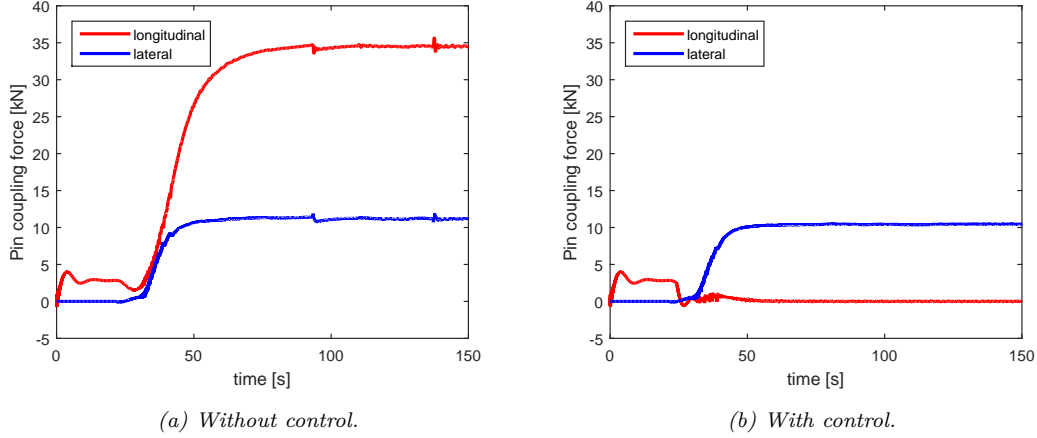
(a) Without control.   *(b) With control.*

Figure 5.4: Longitudinal and lateral pin coupling force during the EU 360 degree test for the 4x4 dolly in the A-double HCV.

This research mainly focuses on the low speed manoeuvrability of the A-double HCV. Therefore, dolly propulsion is enabled for velocities below 30 km/h. Furthermore, the articulation angles between the tractor and semi-trailer should be greater than 5 deg. This simple on/off switch cannot determine whether the vehicle is driving on an inclined road, so more research on the powertrain controller is needed to perform e.g. hill assist in high-power demanding scenarios.

The measured pin coupling forces with enabled powertrain controller during the EU 360 degree turn are shown in Fig 5.4b. From Fig 5.4b it follows that at t=25 s, the powertrain controller is switched on and is able to decrease the longitudinal component of the pin coupling force to zero. Note that some oscillations occur at the moment where the driveline and steer controller are switched on. The enabled steer controller introduces steer angles at the dolly which changes the magnitude of the lateral tyre forces. These lateral tyre forces are transferred to the pin coupling and counteracts the powertrain controller. This contradictive behaviour induces the oscillations shown in Fig 5.4b.

The swept path performance for the 4x2 and 4x4 dolly with and without dolly propulsion are shown in Table 5.4. From Table 5.4 it follows that the swept path of both dollies can be improved with dolly propulsion. The swept path values improve as a result of the reduction in the longitudinal pin coupling force. The tyre side slip angles of the centre axle of both semi-trailers with and without 4x4 dolly propulsion are shown in Fig 5.5a. From Fig 5.5a it follows that the side slip angles at both trailers decrease, which has several benefits. As explained in Chapter 4.3, the decrease in the side slip angle of the rearmost trailer shows that the critical radii r_{crit} of this semi-trailer increases for the simulations with dolly propulsion. Furthermore, the lateral tyre forces decrease, since the lateral tyre forces F_y depend on the magnitude of the tyre side slip angles. This decreases the lateral forces transferred to the couplings, such that the trajectories of leading vehicles are further from the instantaneous centre.

Table 5.4: Swept path values during the 360 degree turn test of a fully loaded A-double HCV equipped with either the 4x2- or 4x4 smart dolly.

	4x2 without propulsion	4x2 with propulsion	reduction	4x4 without propulsion	4x4 with propulsion	reduction
EU	10.73 m	9.84 m	- 8.29 %	6.81 m	6.64 m	- 2.50 %
NL HCV	8.30 m	7.94 m	- 4.34 %	5.87 m	5.83 m	- 0.70 %

The swept path on the EU circle for the 4x2 dolly A double with propulsion and fully loaded trailers equals 9.84 m, whereas the swept path of the one without drive controller is 10.73 m. Based on this observation, it can be concluded that the powertrain controller reduces the swept path at the EU 360 degree turn test with 0.89 m. This is also shown in Fig. 5.5b, since the red trajectory of the innermost path of the second semi-trailer is closer to the centre of the circle than the innermost path of the second semi-trailer without dolly propulsion. The improvement of the 4x2 dolly A-double swept path during the

Dutch 360 degree turn equals 0.36 m. Based on this observation, it can be concluded dolly propulsion improves the low speed swept path more for sharp turns.

(a) Tyre side slip angles of the semi-trailers centre axles.

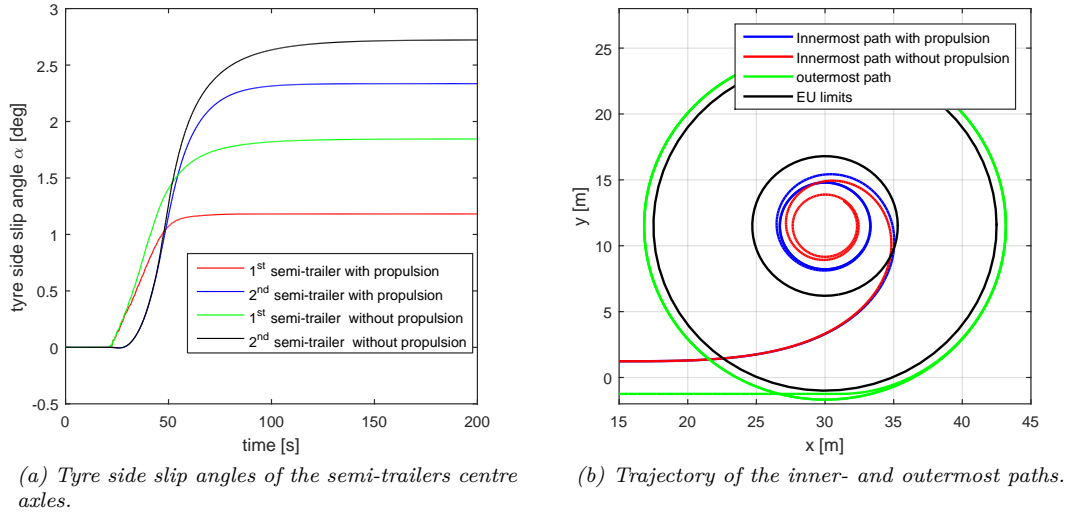(b) Trajectory of the inner- and outermost paths.

Figure 5.5: Semi-trailer centre axle tyre side slip angles and swept path trajectory during the EU 360 degree test for the fully loaded 4x2 dolly A-double HCV with and without propulsion.

5.4   Summary

In this chapter the motor sizing and powertrain controller have been derived and explained. Road load calculations show that the tractor has enough power to haul the second semi-trailer and dolly for 90 km/h highway driving on a 0% grade road. On inclined roads with slopes of 4% and 12%, the tractor's engine still delivers enough power, only very low velocities can be achieved and may result in dangerous scenarios. Although the EU directive states that the vehicle should be able to start on an inclined road of 12%, the tractor semi-trailer combination is able to start on a 22.7% grade road. To ensure that the performance of the tractor semi-trailer combination is not affected by the dolly and second semi-trailer, the required torque per wheel equals 25.5 kNm and 12.6 kNm for the 4x2 and 4x4 dolly, respectively. Furthermore, the total motor output power of the dolly should be 307 kW, as shown in Table 5.5.

Table 5.5: Requested motor/powertrain performance of the dolly for different operating modes

Required performance, operating mode	value
Power by legislations, coupled in A-double HCV	98 kW
Power by legislations, autonomous operation dolly & semi-trailer	208 kW
Power, ensuring drawbar forces equal to 0	307 kW
Torque per wheel, ensuring drawbar forces equal to 0 [4x2/4x4]	25.5/12.6 kNm

The control objective for the dolly powertrain controller is to limit the lateral and longitudinal forces transferred to the first semi-trailer via the pin coupling. By doing so, the dolly will not limit the performance of the tractor and first semi-trailer in terms of manoeuvrability and drivetrain performance. In this research only the longitudinal pin coupling force controller has been evaluated. For the longitudinal controller, each wheel counteracts a fourth of the total pin coupling force, taking into account the steering angles of each wheel. Via a PI controller with a gain of 0.01 and integral value of 0.005, the longitudinal pin coupling force can be controlled to zero sufficiently fast.

Simulations show that implemented powertrain controller is able to further reduce the low speed swept paths of the A-double HCV. The fully loaded A-double 360 degree swept path can be reduced with values up to 0.89 m and 0.17 m, for the 4x2 dolly and 4x4 dolly, respectively. The benefit of dolly propulsion in terms of swept path reduction decreases for less sharp turns.

Chapter 6

Performance comparison between the standard and smart dollies

In this chapter three different A-doubles are compared with a tractor semi-trailer combination to evaluate the manoeuvrability and high speed stability performance. First of all, a baseline A-double with a standard dolly is compared with the tractor semi-trailer combination to understand the decrease in performance caused by the dolly and second semi-trailer. Next, the two smart dolly designs are compared, after which the best dolly setup in terms of manoeuvrability and stability is chosen. The dolly design that matches the tractor semi-trailer combination performance best is chosen. The comparison between the vehicles is made based on the PBS criteria as explained in Chapter 2. At the end of this chapter basic 3D sketches of the dolly are shown.

6.1 PBS results

The PBS performance values of the tractor semi-trailer combination and A-double HCVs are listed in Table 6.1. For each PBS test the worst case value, as determined by the loading condition of the vehicle, is listed in Table 6.1. The values are retrieved by simulation of the four vehicles in MATLAB Simulink with the TU/e CVL. The four evaluated vehicles are: a standard tractor with semi-trailer, a baseline A-double with a non-steered, non-driven dolly and the two A-doubles equipped with either the 4x2 smart dolly or 4x4 smart dolly. All vehicle configurations use a MAN TGX BLS 4x2 tractor [32] and SDC 27 eL 45' 45 ft. Krone container semi-trailer(s) [12] to make a fair comparison. The baseline A-double uses the standard non-steered ZZB 18 eL Krone dolly [12].

All four configurations are simulated in the TU/e CVL for three different loading conditions. These loading conditions include: fully loaded semi-trailers, semi-trailers with empty containers on top and semi-trailer chassis without containers. For the fully loaded mass of the vehicles it is assumed that each semi-trailer is loaded to the maximum allowed payload. The GVW of the tractor semi-trailer combination is used to determine the maximum allowed payload. The maximum GVW of the tractor semi-trailer equals 44 t. When the tractor mass of 7 t [32] is subtracted from the GVW, 37 t remains available for the total semi-trailer weight. As found in [12] and [18] the mass of the empty semi-trailer chassis and 45 ft. container are 5 t and 4.3 t, respectively. This means that resulting payload of each semi-trailer equals 27.7 t. For the performance listed in Table 6.1, dolly propulsion is enabled during the low speed manoeuvrability tests. The smart dollies are steered by means of the steering systems that are derived in Chapter 4.

Table 6.1: Worst case PBS performances of tractor semi-trailer combination, baseline A-double, 4x2 smart dolly A-double and 4x4 smart dolly A-double.

PBS	unit	tractor+semi	baseline A-double	4x2 dolly A-double	4x4 dolly A-double
low speed sept path	[m]	5.70	7.61	6.91	5.70
Frontal swing	MoD* [m]	0.38	0.35	0.37	0.36
	DoM* [m]	0.10	0.07	0.09	0.08
	max width [m]	0.66	0.66	0.66	0.66
Tail swing	[m]	0.28	0.24	0.19	0.26
EU 360 degree swept path	[m]	6.70	NA	9.96	6.78
NL 360 degree swept path	[m]	5.88	9.63	8.03	5.90
static roll-over threshold	[-]	0.35	0.32	0.37	0.33
Yaw damping coefficient	[-]	0.27	0.19	0.13	0.21
High speed off-tracking	[m]	0.35	1.46	1.37	0.71
Rearward amplification	[-]	1.26	2.93	2.92	1.92
GVW	[t]	44.0	83.7	85.2	85.2

* Calculated between the tractor and first semi-trailer.

6.2 Low speed PBS comparison

In this section the low speed PBS performance is evaluated for the tractor semi-trailer combination, baseline A-double and A-doubles equipped with the 4x2 and 4x4 smart dolly. From the low speed PBS values listed in Table 6.1 it follows that the baseline A-double performs worse than the tractor semi-trailer combination. The PBS values from Table 6.1 are reviewed in detail in the next sections to explain this decrease in performance. Next the performance comparison is extended with the results obtained for the smart dolly equipped A-doubles.

Low speed swept path
The first PBS value is the low speed swept path during a 90 degree turn. The low speed 90 degree turn trajectories of the innermost and outermost wheels in the vehicle are shown in Fig. 6.1. It follows from the swept path performance of the tractor semi-trailer combination listed in Table 6.1 and shown Fig. 6.1 that the relatively large wheelbase of the semi-trailer introduces a swept path of 5.7 m. From Table 6.1 it follows that the low speed swept path increases with 1.89 meter for the baseline A-double HCV compared to the tractor semi-trailer combination.

As explained in Chapter 4.3, the kinematics of the A-double HCV already show that each trailing vehicle is oriented closer to the instantaneous centre than preceding vehicles. Furthermore, coupling a dolly and semi-trailer to the first tractor and semi-trailer, introduces pin coupling forces. These forces act on the chassis of the first semi-trailer and needs to be counteracted by the tyre forces on the first semi-trailer. Larger tyre side slip angles are required to increase the lateral tyre forces. From Fig. 4.17 it follows that larger tyre side slip angles increase the swept path of the A-double HCV even more.
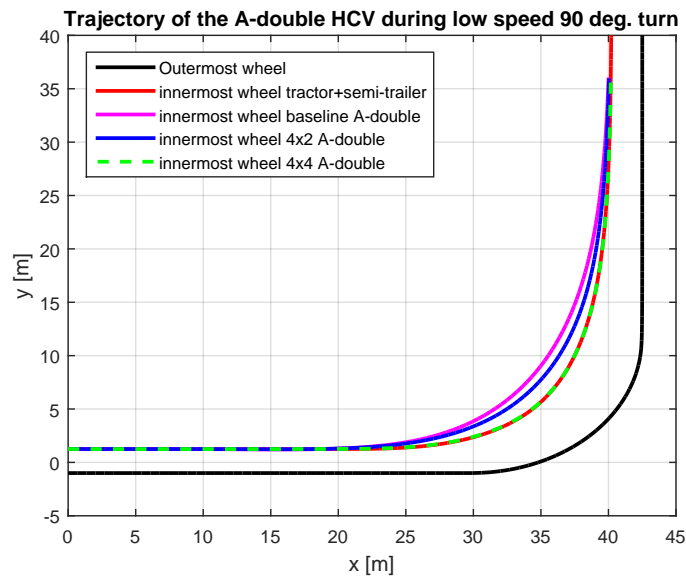

Figure 6.1: Trajectories of the inner- and outermost wheels of the tractor with semi-trailer, baseline-, 4x2- and 4x4 A-double HCV during a 90 deg. turn at low speed.

From Table 6.1 and Fig. 6.1 it can be concluded that the 90 degree swept path improves for the A-double HCVs equipped with smart dollies in comparison with the baseline A-double. The improvement originates from the dolly propulsion and steering of the smart dollies. As mentioned in Chapter 5.3, propulsion of the dolly reduces the forces acting on the pin coupling. This decreases the required tyre side slip angles of the preceding vehicles, such that the swept path improves in comparsion with the non-driven dolly in the baseline A-double HCV.

The improvement by the steering system can be explained by the tyre side slip angles of the dollies, which are shown in Fig. 6.2a. By steering the axle(s) of the dollies, the magnitude and/or sign of tyre side slip angles can be changed. From Fig. 6.2a it follows that the 4x2 dolly steering systems reduces the tyre side slip angles of both axles in comparison with the baseline non-steered dolly. As explained in Chapter 4.3, increasing the magnitude of the tyre side slip angles, decreases the distance to the instantaneous centre.

From Fig. 6.2a it follows that the 4x4 dolly steering system increases the absolute magnitude of the tyre side slip angles. Note, however, that this steering system changes the sign of the tyre side slip angle of the front axle. Therefore, both tyre side slip angles of the 4x4 dolly become negative, indicating that the dolly is actively steered to the outside of the corner. From the fifth wheel trajectories of the smart dollies in Fig. 6.2b it follows that the fifth wheel of the 4x2 dolly follows a path closer to the instantaneous centre compared to the 4x4 dolly. As already shown in Fig. 4.3, this increases swept path of the second semi-trailer.
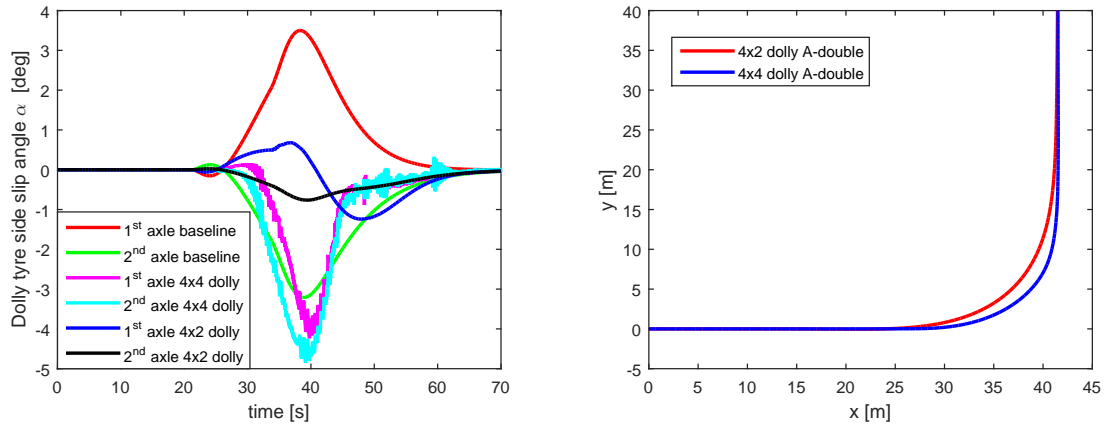
(a) Dolly tyre side slip angles of the three A-doubles.

(b) Fifth wheel trajectory of the 4x2 and 4x4 dolly.

Figure 6.2: Dolly tyre side slip angles of the three A-doubles and fifth wheel trajectories of the 4x2 and 4x4 dolly A-doubles during the 90 degree swept path test.

The worst case swept path values are found for operation with empty semi-trailer chassis. As shown in Fig. 3.9, the maximum shear force that a tyre can generate is limited by the vertical force acting on the tyre. The vertical tyre forces on the A-double's axles are smaller for operation with empty semi-trailer chassis. This indicates that the maximum forces that can be generated by the tyres in the longitudinal and lateral direction are also smaller. Larger tyre side slip angles are required on the axles of the vehicle to generate sufficient lateral force during empty operation. In Fig. 6.3b the semi-trailer tyre side slip angles are shown for fully loaded and empty operation of the tractor semi-trailer combination during the 90 degree swept path manoeuvre. Although the effect is small, it can be seen that the tyre side slip angles for empty operation of the vehicle are slightly larger than for fully loaded conditions. As is explained in Chapter 4.3, this implies that the critical radius of the trailing vehicles becomes smaller and the swept path increases for decreasing load. The difference between the swept path values of a fully loaded tractor semi-trailer combination and tractor with empty semi-trailer chassis is only 4 cm for a 90 degree turn.
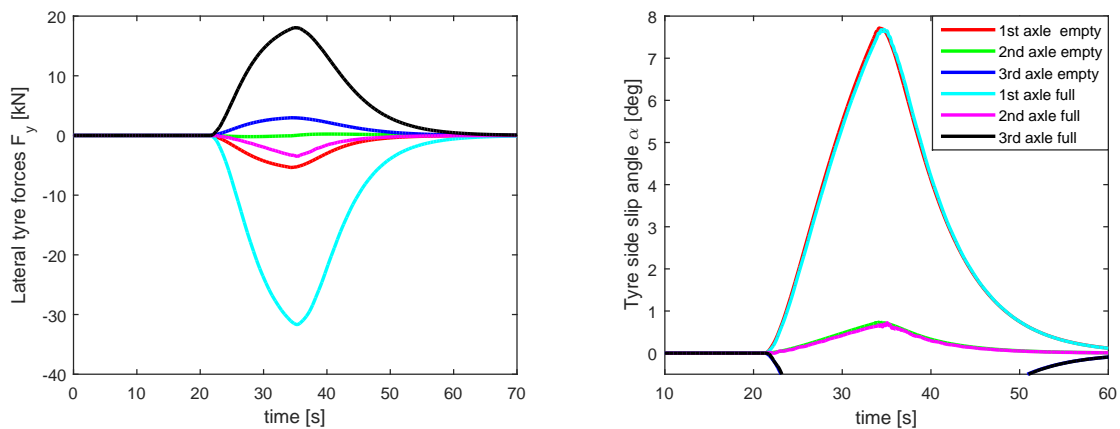
(a) Lateral tyre force first semi-trailer axles.


(b) Tyre side slip angle α.

Figure 6.3: Lateral tyre forces and side slip angles of the semi-trailer in the tractor semi-trailer combination. Simulated with fully loaded and empty semi-trailer during the 90 degree swept path test.
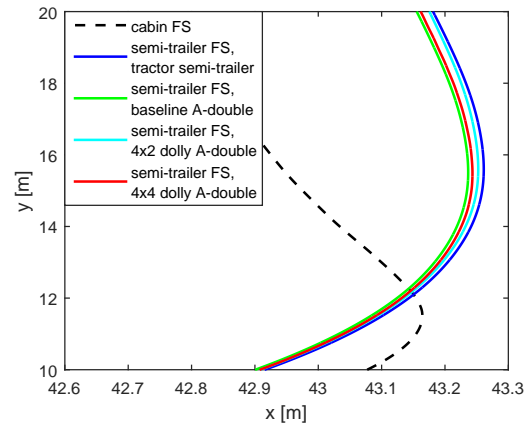
Frontal swing

From Table 6.1 it follows that the frontal swing maximum width performance is the same for all vehicles. This can be explained by the fact that the path following controller in the simulation model ensures that the tractor's steer axle always follows the same input trajectory. Combined with the fact that the cabin overhang is the same for all configurations, it follows that the frontal swing swept path width does not change.

The performance values of the MoD and DoM are mainly determined by the frontal overhang of the semi-trailer and the orientation of the tractor. As shown in Table 6.1 and Fig. 6.4b, small differences are present in the MoD and DoM performance of the different vehicles. These differences originate from the increased forces at the couplings for the A-double HCVs. Due to the additional forces transferred via the couplings in the three A-double configurations, the required lateral tyre forces at the rear axle of the tractor increases compared to the tractor semi-trailer combination. This indicates that larger tyre side slip angles are present at the rear axle of the tractor in the A-double configurations. Therefore, the rear of the tractor is oriented more to the inside of the corner compared to a tractor semi-trailer combination. Accordingly, the fifth wheel of the tractor is oriented more towards the inside of the corner.

The tractor yaw orientations of the baseline A-double and tractor semi-trailer combination are shown in Fig. 6.4a. From this figure it can be obtained that the yaw angle of the tractor in the baseline A-double combination is smaller than the one obtained from the tractor semi-trailer combination. This indicates that the rear of the tractor is oriented more to the inside of the corner. The frontal swing trajectories of the four different vehicles are shown in Fig. 6.4b. If follows from Fig. 6.4b that the baseline A-double achieves the best DoM and MoD performance. The baseline A-double uses a standard, non-driven dolly. Without dolly propulsion, the pin coupling forces cannot be reduced to zero, such that the rear of the tractor is oriented more to the inside of the corner. This results in a smaller DoM and MoD. Both smart dolly equipped A-doubles, however, are simulated with dolly propulsion, resulting in decreased DoM and MoD performance.
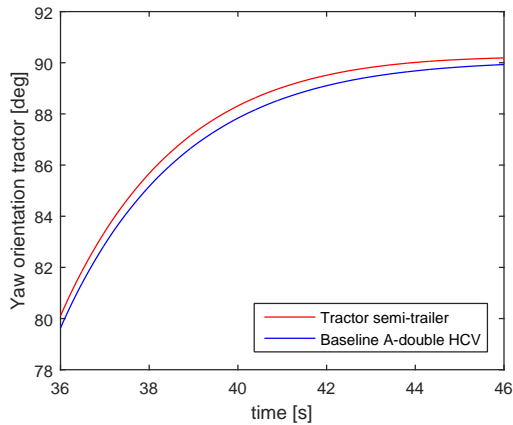
(a) Yaw orientation of the tractors of the tractor semi-trailer combination and baseline A-double.

(b) Frontal swing (FS) trajectories of the cabin and semi-trailers.

Figure 6.4: Tractor yaw orientation and outermost trajectories of the semi-trailers of the tractor semi-trailer combination, baseline-, 4x2- and 4x4 dolly A-doubles during the 90 degree turn manoeuvre with fully loaded semi-trailers.

Tail swing

The tail swing of an articulated vehicle mainly depends on the rear overhang of the semi-trailer, measured from centre axle to the rear of the semi-trailer. Furthermore, the initial fifth wheel trajectory, when entering the 90 degree turn, plays an important role in the tail swing performance of the vehicle. Small articulation angles between the last two vehicles in the vehicle configuration are desired, since smaller articulation angles indicate that the tail swing reduces. Loading conditions have negligible influence on the tail swing performance of the vehicle. The tail swing performance and rearmost articulation angles of the tractor semi-trailer and three A-double configurations are shown in Fig. 6.5.

The articulation angle between adjacent vehicles is typically measured between the chassis of the preceding and trailing vehicle. For e.g. the tractor, non-steered dolly and 4x2 dolly, it can be assumed that the pulling force at the king pin of the semi-trailer is oriented parallel to the longitudinal axis of the hauling vehicle. At low velocities, it can be assumed that king pin direction of travel has the same orientation as the pulling force. In the 4x4 dolly design all four wheels are steered, so the king pin force is no longer oriented parallel to the longitudinal axis of the 4x4 dolly chassis. Therefore, the measured articulation angle needs to be corrected with the steer angles of the dolly to evaluate the semi-trailer's direction of travel. The corrected articulation angle of the 4x4 dolly is represented by the red dashed line in Fig. 6.5b. This corrected articulation angle originates from the measured articulation angle, minus the average steer angle of dolly axles.

From Table 6.1 and Fig. 6.5a it follows that the tail swing of the baseline A-double is smaller than the tail swing of the tractor semi-trailer combination. This can be explained by the trajectories of the first semi-trailer and dolly in the A-double configuration. The first semi-trailer and dolly follow a trajectory closer to the inside of the turn than the tractor's trajectory. This indicates that the first semi-trailer follows a less sharp turn, as shown in Fig. 6.1. The articulation angle between the dolly and second semi-trailer reduces for less sharp trajectories. Combined, the tail swing of the rearmost semi-trailer improves for the baseline A-double compared to the tractor semi-trailer combination.

From Table 6.1 and Fig. 6.5a it follows that the tail swing performance of the 4x4 dolly A-double matches the performance achieved the tractor semi-trailer combination. This can be explained by the fact that path follower steering system on the 4x4 dolly actively steers the dolly to follow the fifth wheel trajectory of the tractor. From Fig. 6.5 it follows that the corrected articulation angle between the dolly and second semi-trailer matches the articulation angle magnitude of the tractor semi-trailer combination. This results in the same tail swing performance, as supported by Table 6.1 and Fig. 6.5a.

The best tail swing performance is achieved by the 4x2 dolly, according to Table 6.1 and Fig. 6.5a. The tail swing of the first semi-trailer causes the pin coupling trajectories of the 4x2 dolly and baseline A-doubles to exceed the entry path tangent. When initiating the turn, insufficient lateral tyre force can be generated by the non-steered, baseline dolly, which causes the front of the dolly to swing outside the entry path tangent. This causes the articulation angle to increase, until sufficient lateral tyre forces are generated by the dolly. The 4x2 dolly is able to limit this effect by means of the implemented krone steering system. This reduces the articulation angle between the 4x2 dolly and second semi-trailer as shown in Fig. 6.5b.

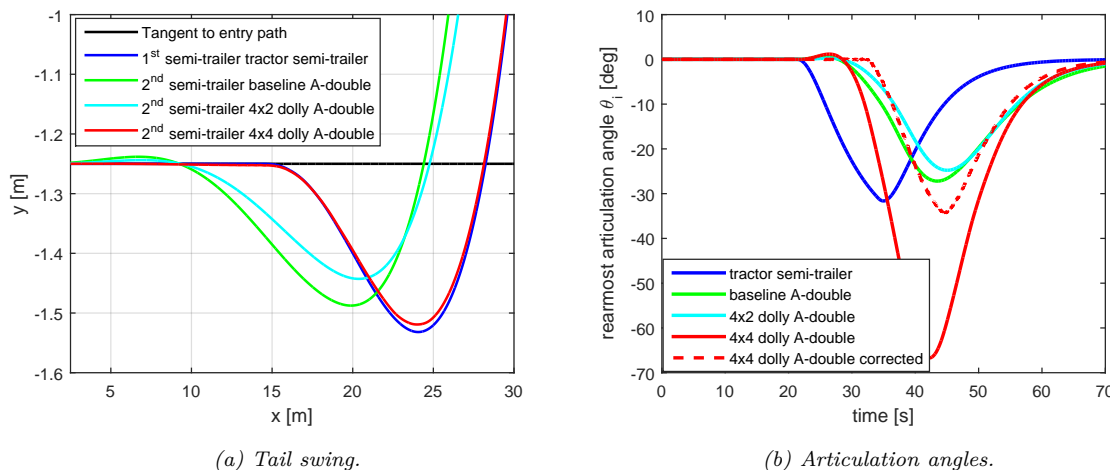(a) Tail swing. (b) Articulation angles.

Figure 6.5: Tail swing performance and rearmost semi-trailer articulation angles of the tractor semi-trailer and three A-double HCVs during the 90 degree turn manoeuvre with fully loaded semi-trailers.

The 360 degree swept paths

The 360 degree swept path performance values of the four vehicles are listed in Table 6.1. During this test, the vehicles encounter the same swept path behaviour as for the 90 degree turn. The tyres on the vehicle need to generate lateral tyre forces to initiate a turn. Coupling the dolly and second semi-trailer to the tractor semi-trailer combination, induces large coupling forces that require larger lateral tire forces. The preceding vehicles are closer to the inside of the turn, since large tyre side slip angles are required to counteract these pin coupling forces. One difference between the behaviour of the vehicles during the 360 degree turn and 90 degree turn is that the swept path during the 360 degree turn is gradually increased. This is caused by the fact that it takes some time for all tyres to generate sufficient lateral tyre force. Therefore, the swept path of the 360 degree turns is gradually increased until an equilibrium is found between the forces at the couplings and the generated tyre forces at all axles of the vehicle.

From Table 6.1 it can be concluded that the baseline A-double exceeds the Dutch HCV swept path limit with 1.63 meter. The corresponding trajectories of the innermost wheels of the first and second semi-trailer during this manoeuvre are shown in Fig. 6.6. From Fig. 6.6 it follows that the centre axle of the last semi-trailer exceeds the inner limit of 6.5 m, set by the Dutch HCV legislation. Furthermore, it can be seen that the swept path of the first semi-trailer is smaller for the tractor semi-trailer combination. This is caused by the absence of pin coupling forces in the tractor semi-trailer combination.
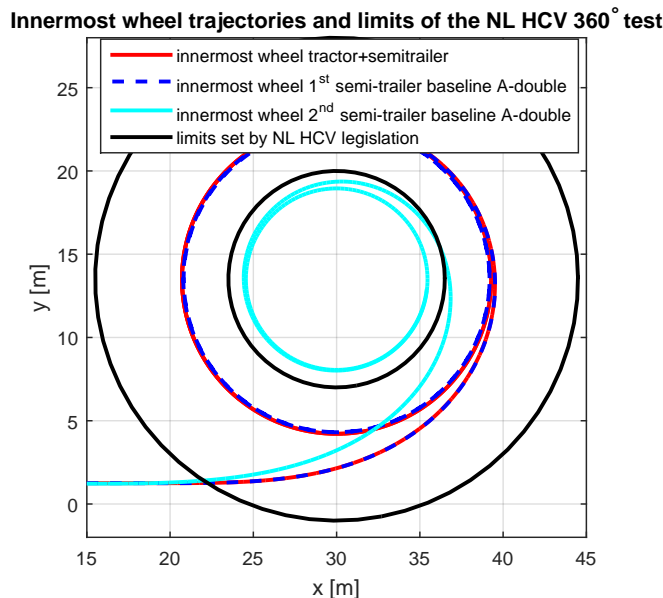

Figure 6.6: Trajectories of the inner- and outermost wheels of a tractor semi-trailer combination and baseline A-double HCV during the NL 360 degree turn.

The trajectory and orientation of the baseline A-double during the EU 360 degree turn are shown in Fig. 6.7. During the EU swept path test, large pin coupling forces in combination with a small turning radius require large tyre forces. The tyre side slip angles of the second semi-trailer need to increase, since the tyres of this semi-trailer cannot generate sufficient lateral tyre forces. The articulation angles increase, which increases the lateral component of the pin coupling force that is acting on the first semi-trailer. The increase in lateral pin coupling force decreases the distance of the first semi-trailer to the centre of the turn, which decreases the swept path performance even more. From Fig. 6.7 it follows that the A-double HCV is unable to complete the 360 degree turn manoeuvre, without jackknifing. This behaviour occurs due to the large articulation angles and tyre side slip angles which can reach values up to 90 degree, as shown in Fig. 6.8.

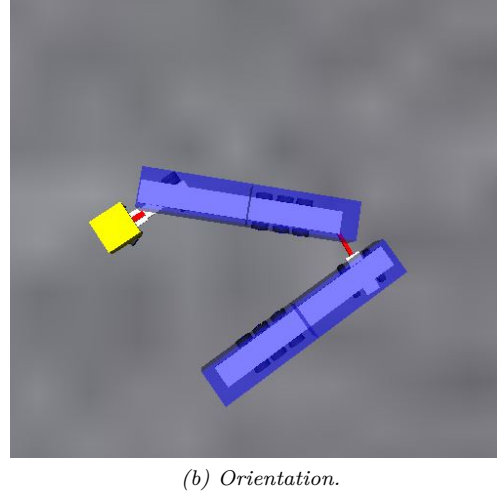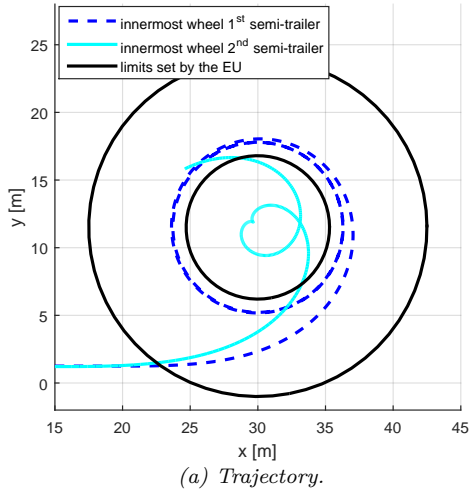*(a) Trajectory.*

(b) Orientation.

Figure 6.7: Trajectory of the innermost wheel and orientation of the baseline A-double during the EU 360 degree turn test.

(a) Baseline A-double.
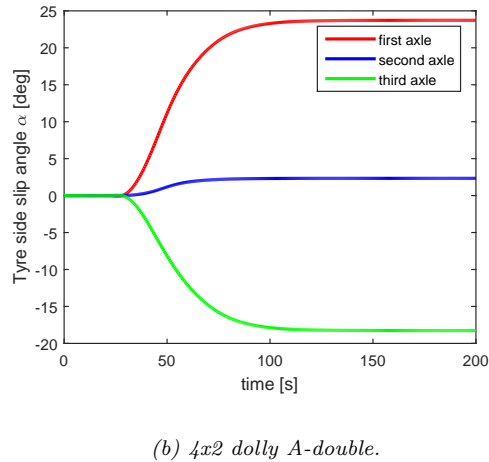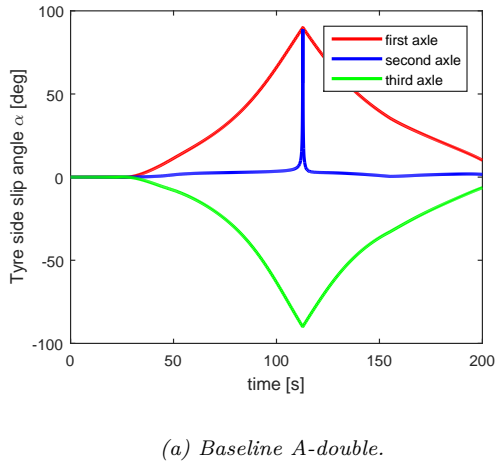

(b) 4x2 dolly A-double.

Figure 6.8: Tyre side slip angles on the rear semi-trailer of the baseline A-double and 4x2 dolly A-double during the EU 360 degree PBS test.

From Table 6.1 it follows that the A-double HCV equipped with 4x2 dolly reaches swept path values of 9.96 m and 8.03 m for the EU and Dutch 360 degree turn, respectively. Although the EU swept path limit is still not met by the 4x2 dolly A-double, the vehicle is able to complete this manoeuvre without jackknifing, as can be seen in Fig. 6.8b and Fig. 6.9a. The circular swept path limit of the Swedish HCV legislation equals 10.5 m, for an outer radius of 12.5 meter. The A-double equipped with 4x2 dolly meets the Swedish legislation with a swept path value of 9.96 m. Furthermore, this A-double also meets the swept path limit of the Dutch HCV legislation.

As mentioned in Chapter 4, steering the 4x4 dolly towards the lead point trajectory of the tractor's fifth wheel, should result in the same manoeuvrability performance as achieved by the tractor semi-trailer combination. This can indeed be obtained from Table 6.1 and Fig. 6.9b. However, a small difference of 8 cm is obtained for the EU 360 degree turn performance, because of the presence of a large lateral pin coupling force. As explained in the low speed swept path test, this lateral pin coupling force needs to be counteracted by the tyre forces on the preceding vehicles. This implies that larger side slip angles are required and the first semi-trailer and tractor are oriented more to the inside of the turn in comparison with the tractor semi-trailer combination. The swept path differences between the tractor semi-trailer combination and the 4x4 dolly A-double are reduced when this pin coupling force can be cancelled completely. As shown in Fig. 6.9b, the 4x4 dolly A-double is able to complete the EU 360 degree turn

manoeuvre, without exceeding the limits. Furthermore, in comparison with the baseline A-double, the 4x4 dolly A-double is able to reduce the swept paths of the 90 degree turn and Dutch HCV roundabout tests with 25% and 39%, respectively.
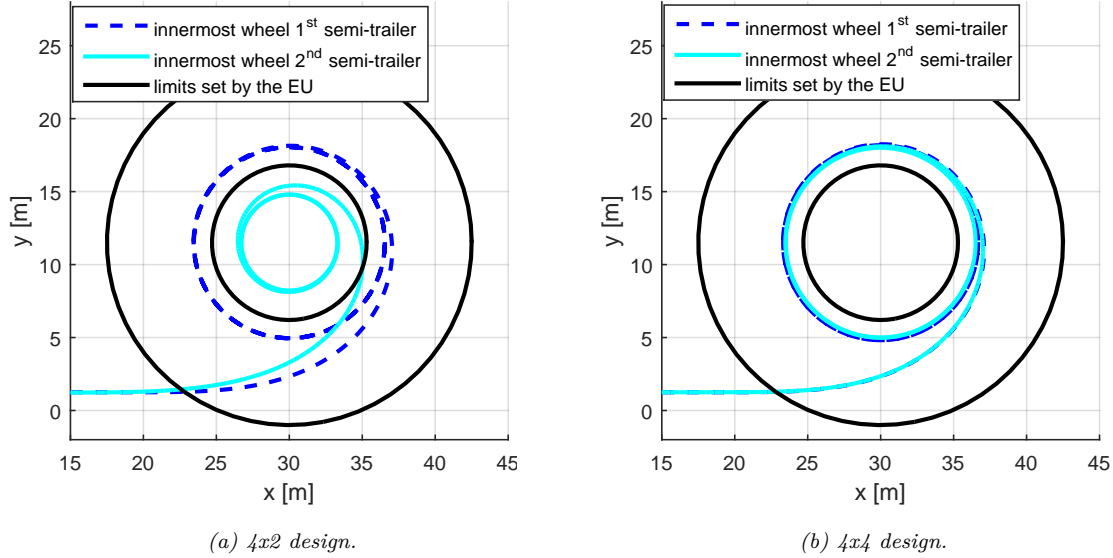

(a) 4x2 design.　　　　*(b) 4x4 design.*

Figure 6.9: Trajectories of the innermost paths of the smart dolly A-doubles during the EU 360 degree turn test.

6.3　High speed PBS comparison

The high speed PBS performance of the different vehicles are evaluated in this section. At high velocities the damping of the yawrate and articulation angles plays an important role in the stability of the vehicle. Therefore, the effect of the dolly design parameters on the yawrate and articulation angle damping is evaluated first, by means of two basic single track models. These single track models describe the yaw dynamics of the hauling unit and trailing units.

The dynamics of multi-articulated vehicles are represented by high order equations of motion [31]. To reduce the complexity, it is chosen to decouple the dolly and trailing semi-trailer from the A-double configuration and investigate the yaw behaviour separately. It is further assumed that the articulation angles, steer angles and tyre side slip angles are small, such that (4.2) holds. Furthermore, body roll and aerodynamic forces are neglected and a constant longitudinal velocity is assumed. The free body diagrams of the dolly and semi-trailer are shown in Fig. 6.10. The steer angles δ_i are determined by the 4x4 dolly path follower steering system or by (4.11) for the 4x2 dolly. Note, the steer angle of the rear axle δ_2 equals zero for the 4x2 dolly design. The semi-trailer in Fig. 6.10a is connected to a hauling vehicle that is moving in longitudinal direction. For simplicity reasons it is assumed that forces transmitted to the coupling are not influencing the movement of the hauling unit. These two models are used to evaluate the damping of the articulation angles and yawrate of the dolly and semi-trailer.

From Fig. 6.10b it can be obtained that the equations of motion for the dolly are:

$$m_d(\dot{v} + ur) = F_{y1} + F_{y2} - F_{c3y} \tag{6.1}$$

$$I_{zz}\dot{r} = aF_{y1} + (b-c)F_{c3y} - bF_{y2} \tag{6.2}$$

The lateral tyre forces are represented by F_{yi}. The mass of the dolly is represented by m_d, the inertia of the dolly with respect to the vertical axis by I_{zz} and the distances from the front and rear axle to the CoG by a and b, respectively. The lateral acceleration of the dolly is a function of the lateral velocity of the CoG v, yawrate r and longitudinal velocity u. The fifth wheel coupling force acting on the chassis of the dolly is represented by F_{c3y}. The distance $b-c$ equals zero for the 4x4 dolly design. However, for

70

the 4x2 dolly $b - c > 0$, which induces a moment around the CoG of the dolly as shown in (6.2). This already implies that the yaw damping coefficient of the 4x2 dolly is influenced more by the fifth wheel force than the 4x4 dolly.

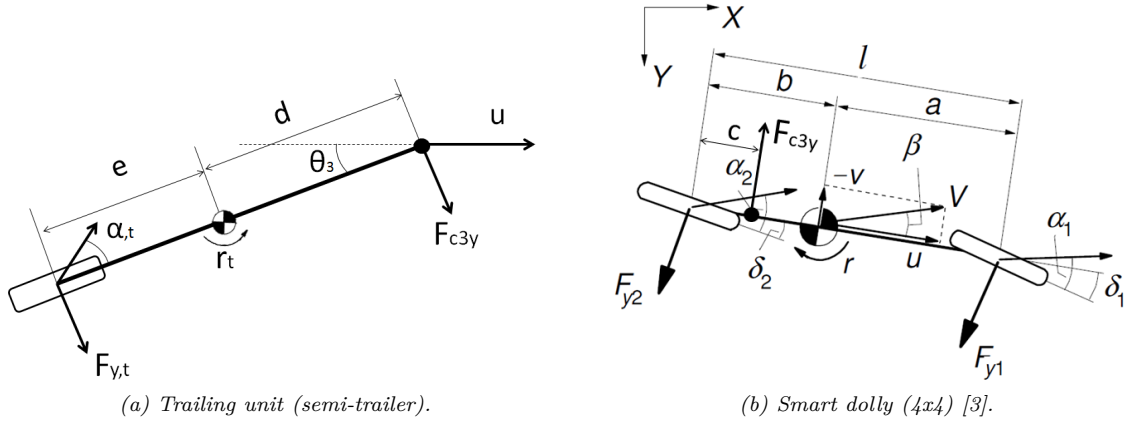(a) Trailing unit (semi-trailer).

(b) Smart dolly (4x4) [3].

Figure 6.10: Free body diagrams of a trailing unit attached to a longitudinal moving hauling unit and free body diagram of the 4x4 smart dolly.

The equations of motion of the 4x4 dolly are derived with F_{c3y} equal to zero. Physically, this can be interpreted as the driving without a second semi-trailer attached to the dolly. By combining (4.2), with (6.1) and (6.2) and using $F_{c3y} = 0$, the following equations of motion are obtained:

$$m\dot{v} + \frac{1}{u}2C_{f\alpha}v + \left(mu + \frac{1}{u}(a-b)C_{f\alpha}\right)r = C_{f\alpha}(\delta_1 + \delta_2) \tag{6.3}$$

$$I_{zz}\dot{r} + \frac{1}{u}(a^2 + b^2)C_{f\alpha}r + \frac{1}{u}(a-b)C_{f\alpha}v = C_{f\alpha}(a\delta_1 - b\delta_2) \tag{6.4}$$

The cornering stiffness is represented by $C_{f\alpha}$ and is assumed to be equal for all tyres. These two single order differential equations in (6.3) and (6.4) are combined via the elimination method to evaluate the yaw damping of the dolly. The detailed derivation is shown in Appendix E. Eventually, the yaw dynamics of this dolly are described by:

$$muI_{zz}\ddot{r} + \left((a^2 + b^2)mC_{f\alpha} + 2C_{f\alpha}I_{zz}\right)\dot{r} + \frac{1}{u}\left(C_{f\alpha}^2 l^2 - mu^2 C_{f\alpha}(a-b)\right)r = \dots$$
$$muC_{f\alpha}(a\dot{\delta}_1 - b\dot{\delta}_2) + lC_{f\alpha}^2(\delta_1 - \delta_2) \tag{6.5}$$

The parameter l is defined as the wheelbase of the dolly, which equals the sum of a and b. From the second order differential equation shown in (6.5) it follows that the yawrate damping of the dolly equals:

$$D_{yaw} = \frac{(a^2 + b^2)mC_{f\alpha} + 2C_{f\alpha}I_{zz}}{muI_{zz}} \tag{6.6}$$

From (6.6) it follows that increasing the distances a and b, increases the yaw damping of the dolly. Oscillations in the yawrate are better damped by the smart dollies, since both smart dolly designs have a larger wheelbase compared to the standard non-steered dolly. Furthermore, it can be concluded from (6.6) that the yaw damping of the dolly decreases for increasing longitudinal velocities.

A basic single track trailer model is used to evaluate the damping of the articulation angles [23]. For this approach it is assumed that the semi-trailer is attached to a hauling vehicle in front, that drives in longitudinal direction. The only state variable in this model is the articulation angle between the semi-trailer and fifth wheel coupling, represented by θ_3. It is assumed that the movement of the trailing unit does not affect the movement of the preceding vehicle. The free body diagram of this system is shown in Fig. 6.10a and the equations of motion are:

$$m_t\ddot{\theta}_3 = F_{y,t} + F_{c3y} \tag{6.7}$$

$$I_{zz,t}\ddot{\theta}_3 = eF_{y,t} - dF_{c3y} \tag{6.8}$$

71

In which the lateral fifth wheel coupling force at the semi-trailer is represented by F_{c3y} and the lateral tyre force of the semi-trailer by $F_{y,t}$. The mass of the trailer is represented by m_t and the inertia of the trailer by $I_{zz,t}$. The distance from the coupling point to the CoG of the semi-trailer is represented by the parameter d, whereas the distance between the axle and CoG is represented by the parameter e. Substituting (4.2) in (6.7) and rearanging yields:

$$F_{3cy} = m_t \ddot{\theta}_3 + C_{f\alpha}\left(\frac{(e+d)}{u}\dot{\theta}3 + \theta_3\right) \tag{6.9}$$

Substituting (6.9) in (6.8) yields:

$$\left(I_{zz,t} + m_t d^2\right)\ddot{\theta}_3 + \left(\frac{1}{u}l_t^2 C_{f\alpha}\right)\dot{\theta}_3 + \left(l_t C_{f\alpha}\right)\theta_3 = 0 \tag{6.10}$$

The distance l_t represents the wheelbase of the trailer, which is defined as the sum of d and e. From the second order differential equation in (6.10), it follows that the articulation angle damping equals:

$$D_\theta = \frac{l_t^2 C_{f\alpha}}{u(I_{zz,t} + m_t d^2)} \tag{6.11}$$

From (6.11) it follows that articulations angles are better damped for trailing vehicles with greater distances between the articulation points and the axle groups. Furthermore, it can be concluded that increasing the velocity or mass of the trailing unit decreases the damping of the articulation angle.

Static roll-over threshold

It is expected that the static roll-over threshold of the baseline A-double equals the one of tractor semi-trailer combination, since the dolly drawbar can roll with respect to the pin coupling. However, from Table. 6.1 it follows that the static roll-over performance of the baseline A-double decreases compared to the performance achieved by the tractor semi-trailer combination. This can be explained by the lateral axle accelerations of each vehicle in the A-double configuration. The lateral axle accelerations of all four vehicles in the baseline A-double HCV are shown in Fig. 6.11a.

For the static roll-over test, the velocity of the vehicle is gradually increased with 0.396 m/s^2. This causes the path follower controller of the tractor to constantly adapt the steer angle of the tractor's steer axle. As a result the steer axle acceleration signal oscillates, as shown in Fig. 6.11a. At higher velocities, these oscillations are amplified more towards the rear of the vehicle. The rear semi-trailer, therefore, encounters higher lateral accelerations, which increases the overturning moment at this semi-trailer. Therefore, roll-over of the rearmost semi-trailer in the baseline A-double configuration occurs at lower lateral acceleration than the first semi-trailer in a tractor semi-trailer combination.

In [18] it is claimed that the A-double performs better in terms of the static roll-over threshold, since it can reach a roll-over threshold level of 0.43 g. However, the mass of the load transported by the A-double in [18] is lower, which results in a lower CoG height and mass of the vehicle. Reducing the mass and CoG height is beneficial for the overturning moment during the static roll-over test, see in Chapter 2.

(a) Lateral accelerations.
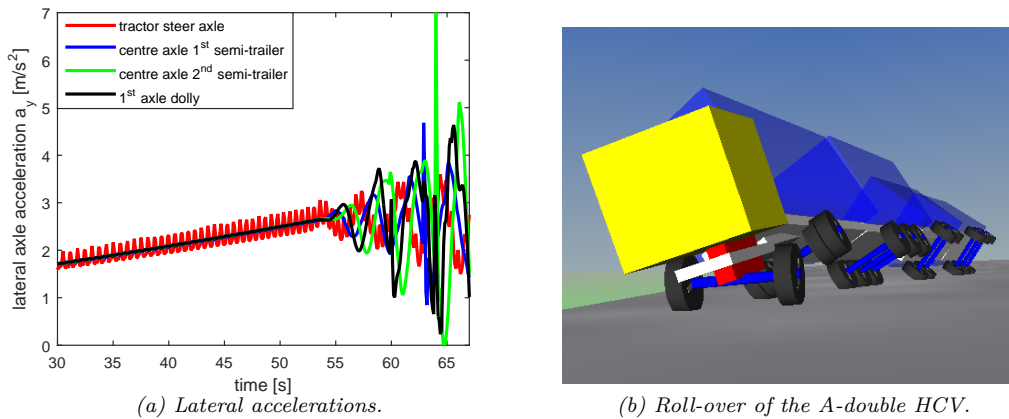

(b) Roll-over of the A-double HCV.

Figure 6.11: Lateral acceleration and vehicle orientation of the baseline A-double HCV with fully loaded semi-trailers during the static roll-over test.

The static roll-over threshold of the smart A-doubles in Table 6.1 compared to the baseline A-double. This is caused by the increased wheelbase of the smart dollies and the increased dolly mass. The articulation angles and yawrate are better damped by the smart dollies, due to the larger wheelbase of the smart dollies and greater distance between the coupling and rearmost axle, see (6.11) and (6.6). The oscillating lateral acceleration of the tractor's steer axle is amplified less, such that a higher roll-over threshold is obtained. Furthermore, both smart dolly designs are 1.5 t heavier than a standard dolly. When an articulation angle is present between the dolly and second semi-trailer, the roll-over tendency of the semi-trailer is counteracted by the pitch limitation of the dolly. A pitch movement of the dolly is induced when the second semi-trailer starts to roll. This pitch movement is limited by the pin coupling of the first semi-trailer. Increasing the dolly mass further reduces this pitch movement, such that the roll-over tendency of the dolly semi-trailer combination decreases.

The worst case loading condition for the static roll-over test is operation with fully loaded containers. For fully loaded containers, the GVW and centre of gravity height of the vehicles increase, which increases the resulting overturning moment, see Chapter 2. The vehicle rolls over when the returning moment of the vertical load transfer is too small to counteract this overturning moment. More information is provided in Appendix A.

Yaw damping

During the single sine manoeuvre, lateral tyre forces are generated by the tractor as a results of the single sine steer input. Accordingly, the trailing units need to generate lateral tyre forces to follow the single sine input trajectory and to counteract the lateral forces originating from the couplings. Yaw moments at trailing vehicle are induced, since it takes some time to generate these lateral tyre forces.

From Table 6.1 it can be concluded that the yaw damping coefficient decreases for the baseline A-double in comparison with the tractor semi-trailer combination. The finite yawrate/articulation angle damping of trailing vehicles amplifies the yawrate of the rearmost vehicles. The poor yaw damping performance of the baseline A-double can be explained by the relatively small distance between the pin coupling and rearmost axle of the dolly. From (6.11) it can be concluded that a small distance between the coupling and rearmost axle results in a less good damping of the yawrate and articulation angles. Combining the small wheelbase of the dolly with the finite yawrate/articulation angle damping of the first semi-trailer, results amplified yawrates on the dolly and second semi-trailer.

The yawrates of the tractor (red), first and second semi-trailer (blue and green) and dolly (black) of the baseline A-double during the single sine manoeuvre are shown in Fig. 6.12a. The first peaks in the yawrate signals in the interval 5-10 s are used to describe the damping performance of the total vehicle. In Fig. 6.12a it can be seen that the dolly yawrate reaches higher amplitudes than the yawrate of the first semi-trailer. This is caused by the small wheelbase and small distance between the pin coupling and dolly axles in comparison with the semi-trailers, see (6.6) and (6.11). Note, the amplifications in yawrate between the tractor/semi-trailer 1 and dolly/semi-trailer 2 are smaller, because of the larger wheelbases of the semi-trailers, which result in better damping.

The worst case loading conditions for the single sine PBS criteria are fully loaded semi-trailers. Increasing semi-trailer mass decreases the yaw damping performance, as shown in (6.11). Using the increased yawrate of the baseline A-double in (4.39), results in larger lateral accelerations at the trailing vehicles. These lateral acceleration introduce a roll moment at the dolly and second semi-trailer. Simulations of the baseline A-double and 4x2 dolly equipped A-double show that the wheels at the rearmost semi-trailer actually loose contact with the ground during the single sine manoeuvre, see Fig. 6.12b and Fig. 6.14b.

From Table 6.1 it follows that both A-doubles are unable to meet the yaw damping performance of the tractor semi-trailer combination. Regardless of the steering system and fifth wheel position, the relatively small distance between the pin coupling and dolly axles results in a worse yaw damping coefficient. In comparison with the baseline A-double, the 4x2 dolly equipped A-double deteriorates the yaw damping coefficient, whereas the 4x4 dolly equipped A-double improves the yaw damping coefficient.
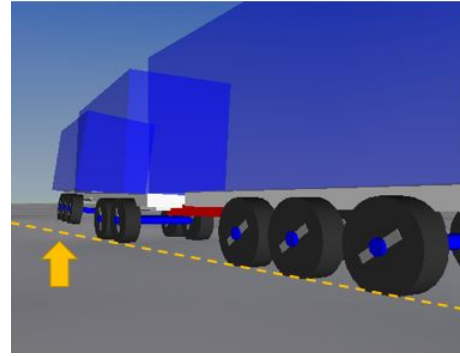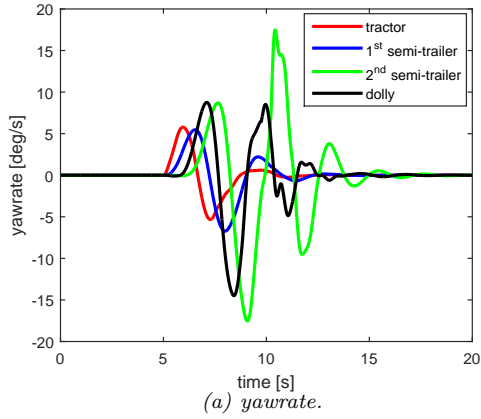
(a) yawrate.

(b) Rearmost tri-axles lift-off.

Figure 6.12: yawrate and orientation of the baseline A-double during the single sine manoeuvre with fully loaded semi-trailers.

Although the 4x2 dolly in the A-double HCV has a larger dolly wheelbase, it has worse yaw damping performance compared to the baseline A-double. This can be explained by the offset $b - c$ between the CoG of the dolly and the fifth wheel coupling, see Fig. 6.10b. The offset $b - c$ introduces additional yaw moments at the 4x2 dolly, which needs to be counteracted by the lateral tyre forces of the dolly and second semi-trailer, see (6.2). The yawrates of all four vehicles in the 4x2 dolly equipped A-double are shown in Fig. 6.13a. From Fig. 6.13a if follows that the dolly amplifies the yawrate towards the second semi-trailer. The yawrate of the baseline dolly and 4x2 dolly A-double are shown in Fig. 6.14a. Remark from Chapter 2 that the yaw damping coefficient is defined as the required time to cancel any sway oscillation in the yawrate signal. From Fig. 6.14a it follows that the yawrate signal of the 4x2 dolly takes longer to decay, but the maximum absolute yawrate decreases for the 4x2 dolly.

The 4x4 dolly equipped A-double improves the yaw damping coefficient in comparsion with the baseline A-double. This is caused by the active steering of the dolly wheels and the increased distance between the pin coupling and rearmost axle of the dolly. As explained in Chapter 4.4, steering the dolly towards the high speed lead point trajectory, counteracts the high yawrates of a non-steered dolly. Since the steer angles are actively controlled on the 4x4 dolly, lateral tyre forces can be generated by the dolly earlier, such that the yaw amplification between the first semi-trailer and dolly improves in comparison with a non-steered dolly. The improvement of the 4x4 dolly equipped A-double can be obtained from Fig. 6.13b. From this figure it can be obtained that the yawrates of the 4x4 dolly and first semi-trailer increase less than for the 4x2 dolly equipped A-double.
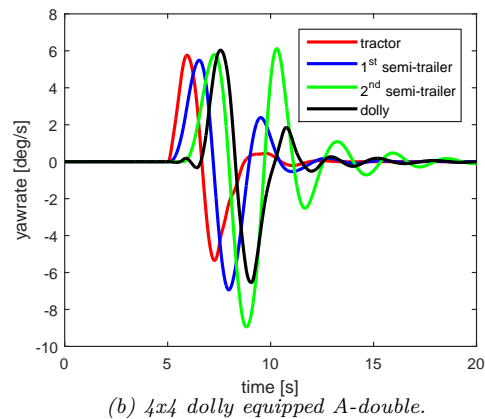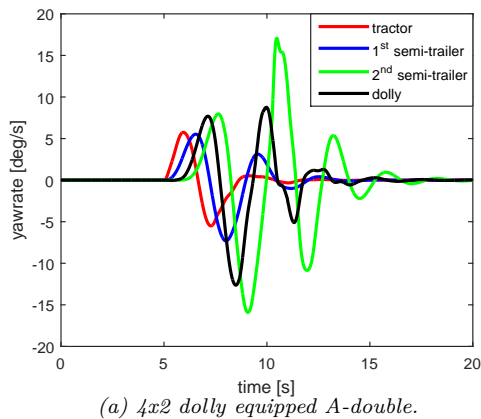

(a) 4x2 dolly equipped A-double.

(b) 4x4 dolly equipped A-double.

Figure 6.13: Yawrates of the smart dolly equipped A-doubles with fully loaded semi-trailers during the single sine manoeuvre.

(a) Yawrate of the 4x2 and baseline dolly.   *(b) DLTR of the 2nd semi-trailer.*
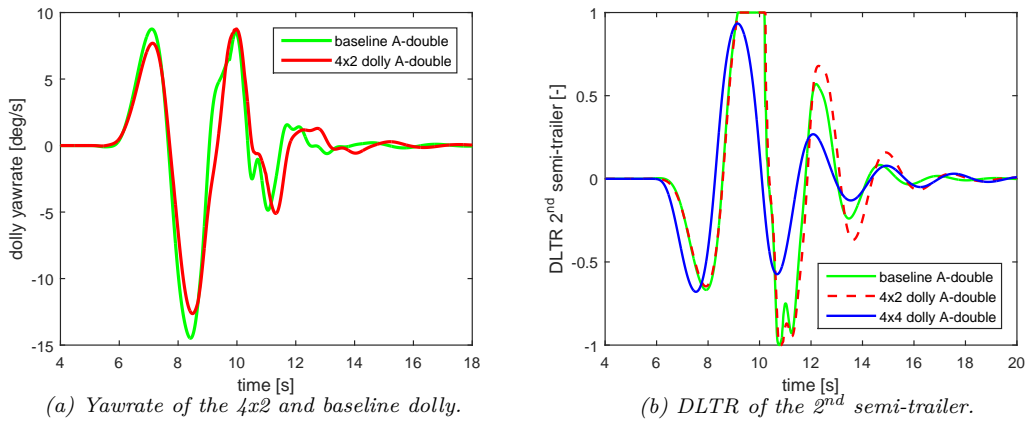
Figure 6.14: Yawrate of the baseline dolly and 4x2 dolly and DLTR of the second semi-trailers in the fully loaded A-double HCV configurations during the singe sine manoeuvre.

Rearward amplification and high speed off-tracking

From Table 6.1 it follows that the rearward amplification and high speed off-tracking performance of the baseline A-double are worse than the performance achieved by the tractor semi-trailer combination. The decreased rearward amplification and high speed-off tracking performance of the A-double can be explained by the poor yaw damping performance of the baseline A-double. The rearward amplification increases, since the oscillations of the yawrate and articulation angles are less damped by the baseline dolly. In combination with (4.39) this results in higher lateral accelerations on the rearmost semi-trailer. Higher lateral accelerations imply that larger tyre forces are required to counteract the yaw movements of the dolly and second semi-trailer. This causes the dolly and second semi-trailer to swing more to the outside as shown in Fig. 6.15b. The high speed off-tracking of the baseline A-double HCV is increased with 1.11 m in comparison with the tractor semi-trailer combination.

From Table 6.1 it can be concluded that both smart dollies improve the rearward amplification and high speed off-tracking of the A-double HCV. The lateral acceleration acting on the CoG of the dollies in the three different A-double configuration are shown in Fig. 6.15a. From Fig. 6.15a it follows that both smart dolly design are able to reduce the lateral accelerations of the dolly in comparison with the baseline A-double.

The yawrates of the 4x2 dolly and baseline dolly are shown in Fig. 6.14a. From Fig. 6.14a it follows that the maxima of the dolly yawrate are smaller for the 4x2 dolly than the baseline dolly. This reduction in yawrate reduces the lateral acceleration of the 4x2 dolly and second semi-trailer in the A-double configuration. Although the reduction in lateral acceleration is small, the rearward amplification and high speed off-tracking are improved for the 4x2 dolly equipped A-double. The improved yaw damping performance and active steering of the 4x4 dolly improve the rearward amplification and high speed off-tracking significantly in comparison with the baseline and 4x2 dolly A-doubles. The 4x4 path follower steering system actively steers the dolly towards the high speed lead point trajectory, which reduces the swing out of the dolly as shown in Fig. 6.15b.

When the high speed stability performance of the 4x2 dolly and 4x4 dolly A-doubles from Table 6.1 are compared, it can be concluded that the 4x4 dolly achieves the best performance. Compared to baseline A-double, the 4x4 dolly can reduce the high speed off-tracking and rearward amplification with 51 % and 34%. Furthermore, the 4x4 dolly steering system steers the wheels on the dolly such that the high speed lead point trajectory is followed, whereas the front wheels of the 4x2 dolly are locked at high velocities. From Fig. 6.14b it follows that the wheels at the rearmost semi-trailer actually loose contact with the ground for the 4x2 A-double and baseline A-double configuration. Slight increases in lateral accelerations during the single sine manoeuvre may lead to roll-over of the rearmost semi-trailers. It can, therefore, be concluded that the baseline A-double and A-double equipped with 4x2 dolly are unstable during the single sine manoeuvres.

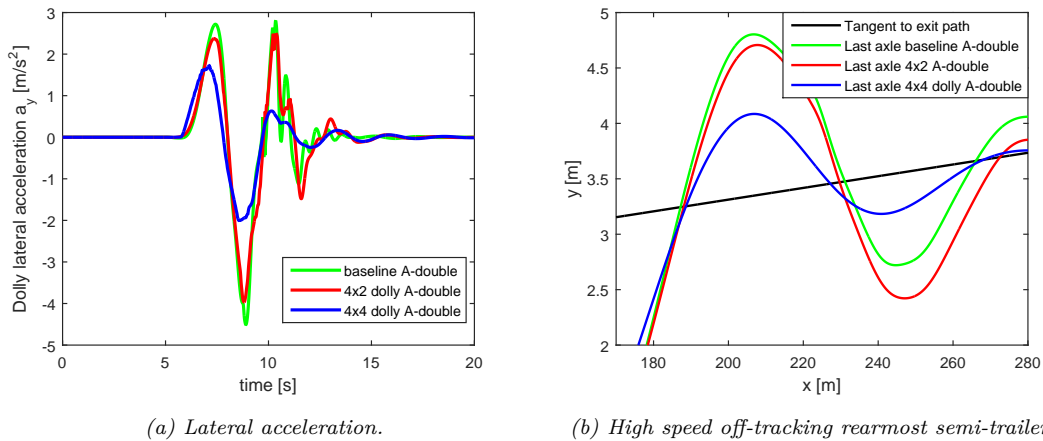*(a) Lateral acceleration.*   *(b) High speed off-tracking rearmost semi-trailers.*

Figure 6.15: High speed off-tracking of the last axle of the baseline, 4x2 and 4x4 dolly equipped A-doubles and lateral accelerations of the baseline, 4x2 and 4x4 dolly during the single sine manoeuvre with fully loaded semi-trailers.

6.4   Selection of the best smart dolly design based on PBS performance

From Table 6.1 it follows that, in terms of absolute performance, the baseline A-double performs significantly worse than a tractor semi-trailer combination for both the stability and manoeuvrability PBS. The frontal swing and tail swing performance of the baseline A-double are the only two PBS criteria that can meet the PBS performance of the tractor semi-trailer combination. The swept path and high speed stability performance of the baseline A-double HCV decreases significantly in comparison with the tractor semi-trailer combination. Based on these observations, it can be concluded that it is unsafe to use the A-double equipped with a non-steered, non-driven dolly on the public roads.

From Table 6.1 it can be concluded that both smart dollies improve the high speed stability and manoeuvrability of the A-double HCV compared to the baseline A-double HCV. The PBS differences in terms of percentage between the A-doubles equipped with smart dollies and tractor semi-trailer combination are listed in Table 6.2. From Table 6.2 it follows that the swept path performance of the 4x4 dolly A-double HCV matches the performance achieved by the tractor semi-trailer combination. From Table 6.2 it can be concluded that, compared to the tractor semi-trailer combination, the manoeuvrability of the 4x4 dolly A-double decreases less than that of the 4x2 dolly A-double. The tail swing, DoM and MoD improve for both smart dolly A-doubles compared to the tractor semi-trailer combination.

From Table. 6.2 it follows that the yaw damping coefficient, high speed off-tracking and rearward amplification of both smart dolly A-doubles show a significant decrease in performance. Disregarding the static roll-over threshold, it can be concluded that the high speed stability PBS of the 4x4 dolly A-double matches better with the tractor semi-trailer performance. However, future research is recommended to improve the high speed stability further. Concluding from the above, the 4x4 dolly A-double matches the high speed stability and manoeuvrability performance of the tractor semi-trailer better than the 4x2 dolly A-double. Therefore, the 4x4 dolly design is the most promising design to continue with in future research.

Table 6.2: PBS performance difference in terms of percentage between the 4x2 smart dolly A-double/4x4 smart dolly A-double and the tractor semi-trailer combination.

| PBS	4x2 dolly A-double	4x4 dolly A-double
Low speed sept path	+21.2	0.0
Frontal swing, MoD*	−2.6	−5.3
Frontal swing, DoM*	−10.0	−20.0
Frontal swing, max width	0.0	0.0
Tail swing	−32.1	−7.1
EU 360 degree swept path	+48.7	+1.2
NL 360 degree swept path	+36.6	+0.3
Static roll-over threshold	+5.7	−5.7
Yaw damping coefficient	−51.9	−22.2
High speed off-tracking	+291.4	+102.9
Rearward amplification	+131.7	+52.4

* Calculated between the tractor and first semi-trailer.

6.5   Final design

This section summarizes the design choices that are made in the previous chapters. The dolly designs below are found to be the best designs regarding: vertical axle forces, low speed manoeuvrability and high speed stability in the context of an A-double HCV. The 3D representations of both dollies are shown at the end of this section.

The 4x2 dolly design has axles offsets to the CoG of 1.40 m and the fifth wheel coupling is mounted 0.97 m in front of the rear axle. This dolly is propelled by a single electric motor that drives both wheels via a driveshaft. If needed, a gearbox can be mounted between the wheels and the motors to amplify the output torque of the motor. To meet the performance of the tractor and first semi-trailer this dolly should have a total motor output power of 307 kW for a driveline efficiency of 95%. The maximum required torque per driven wheel equals 25.2 kNm. The 4x2 dolly steering system is similar to the Krone dolly steering system. With a gain between the drawbar angle and steering wheels of 0.37, the low speed manoeuvrability can be improved with respect to the baseline A-double. A basic 3D sketch of this dolly is shown in Fig. 6.16a. The space available between both axles at the side of the chassis is larger than for the 4x4 dolly design, since the rear wheels cannot be steered in the 4x2 dolly design.

The 4x4 dolly design has equal values for the axle positions to the CoG and has the fifth wheel exactly mounted at the centre. The chosen values for a, b and c, therefore, equal 1.39 m. Due to this geometry, the dolly is able to achieve 50-50 load distribution among its axles. Furthermore, since all four wheels can be steered, a path following steering system is implemented. To ensure that the 4x4 dolly and second semi-trailer should not limit the performance of the leading tractor and semi-trailer, the sum of the electric motors needs to be at least 307 kW. Four wheels are driven in the 4x4 dolly design, so the requested maximum torque at each wheel equals 12.6 kNm. The 3D sketch of this dolly design is shown in Fig. 6.16b. Since the this dolly is driven by in-wheel motors more space below the dolly chassis is available in comparison with the 4x2 design.
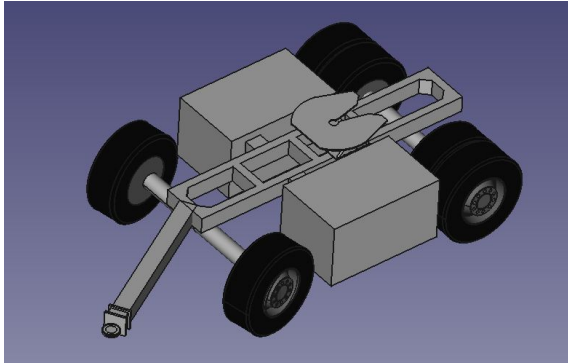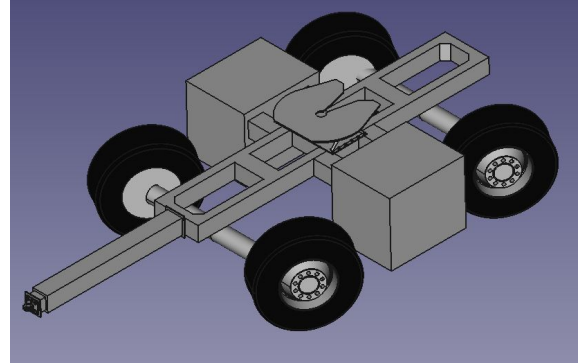
<div style="text-align: center;">(a) 4x2　　　　　　　　　　　　　(b) 4x4</div>

Figure 6.16: Basic 3D sketches of the 4x2 smart dolly and 4x4 smart dolly designs to be used in an A-double HCV configuration.

6.6 Summary

In this chapter the PBS manoeuvrability and high speed stability performances have been compared between the four different vehicles. It is concluded that the baseline A-double, which uses a non-steered, non-driven dolly, performs much worse in terms of the PBS criteria compared with a tractor semi-trailer combination. Both smart dolly designs are able to improve the low speed manoeuvrability performance of the vehicle in comparison with the baseline A-double.

In terms of manoeuvrability, the 4x2 dolly is able to meet the swept path limits of the Dutch and Swedish HCV 360 degree legislation, but exceeds the swept path limit of the EU 360 degree turn. The high speed stability of the vehicle was found to be almost the same as for the baseline A-double. However, the yaw damping coefficient of the 4x2 dolly is found to be worse than the yaw damping of the baseline A-double, due to the offset of the fifth wheel to the CoG of the dolly.

Based on the PBS results, the 4x4 dolly seems to be the most promising design. In comparison with the baseline A-double, this dolly reduces the swept paths of the A-double HCV during the 90 degree turn and Dutch HCV roundabout tests with 25% and 39%, respectively. Also the high speed stability of this dolly is better than the 4x2 design, since it is able to reduce the high speed off-tracking and rearward amplification with 51 % and 34% compared to the baseline A-double. Both smart dolly equipped A-doubles are, however, unable to meet the high speed stability performance levels of the tractor semi-trailer combination.

Chapter 7
Conclusions and recommendations

7.1 Conclusions

HCVs show some significant improvements in terms of efficiency and emissions in comparison with standard commercial vehicles. However, special tractors, trucks and/or trailers are required, which increases the investment cost and decreases the transport efficiency of the vehicle when driving on non-HCV roads. Therefore, a more beneficial HCV is derived that couples a second semi-trailer via a dolly to a tractor semi-trailer combination. This HCV configuration is known as an A-double HCV. Since the manoeuvrability, stability and acceleration performance decrease for the A-double HCV in comparison with the tractor semi-trailer combination, the dolly needs to be equipped with a powertrain and steering system. Doing so results in a HCV in which the dolly is the only smart component in the configuration and all the other modules can be kept standard. In this report a preliminary design has been derived for a smart, steered and propelled dolly that can be used in an A-double HCV

Two designs of such a dolly are proposed, which are the 4x2 smart dolly and 4x4 smart dolly designs. The 4x2 dolly has a less complex design and uses a single electric motor to propel the wheels via a driveshaft and differential. The presence of the driveshaft and differential makes it unable to steer the rear wheels of the 4x2 dolly. Two steering systems have been evaluated for this design. It is found that the Krone steering system achieves the best performance for the 4x2 dolly. In such a steering system, the drawbar can rotate both around the pin coupling and the dolly's chassis. This steering system uses a constant gain between the steering angle and drawbar angle. In comparison with an A-double equipped with non-steered dolly, the 4x2 steering system reduces the swept path of a 90 degree turn and Dutch HCV 360 degree turn with 9 % and 16%, respectively. The high speed stability of this 4x2 driven dolly is less good due to additional articulation possibility of the drawbar. Locking the steering system in the 4x2 dolly at high speeds, improves the high speed stability of the 4x2 dolly.

The 4x4 dolly reduces the swept paths of the 90 degree turn and Dutch HCV 360 degree turn with 25% and 39%, respectively. Furthermore, this dolly design is the only dolly that is able to pass the EU 360 degree swept path test without exceeding the limits. The 4x4 dolly is driven by four in-wheel motors and has four-wheel-steering. With a path follower steering system, a lead point located at the fifth wheel of the tractor is tracked and followed by the dolly. This report shows that with the path follower control methodology and inter- and extrapolation of the velocity vectors, it is possible to calculate the required steer angles for both axles individually. Since the fifth wheel of the dolly follows the fifth wheel trajectory of the tractor, the low-speed manoeuvrability was found to be the same as for the tractor semi-trailer combination. However, the rearward amplification and yaw damping of the 4x4 dolly design are worse than the performance achieved by the tractor semi-trailer combination. In comparison with the A-double equipped with non-steered dolly, the 4x4 dolly can reduce the high speed off-tracking and rearward amplification with 51 % and 34%, respectively.

The forces transferred through the drawbar should be minimized in the A-double HCV to ensure that the performance of the tractor with first semi-trailer is unaffected. The implemented powertrain controller is able to control the longitudinal pin coupling force to zero. However, the control of the lateral force at the pin coupling requires more research. To ensure that the acceleration capability of the tractor and first semi-trailer is not influenced, the sum of the required output power of the electric motor(s) equals 307 kW. The required output torque at each driven wheel equals 25.9 and 12.62 kNm for the 4x2 dolly and 4x4 dolly, respectively.

The 4x4 driven dolly design with path following steering is the best design to continue with in future research. This dolly meets the weight and dimension limits, set by the EU and Dutch government. The 4x4 dolly has a 50-50 load distribution among its axles and has almost equal performance in the manoeuvrability compared to a tractor semi-trailer combination. The 4x2 dolly design is able to meet most of the Dutch and Swedish legislations, but it has significantly worse performance than the 4x4 dolly design. The high speed stability performance of the A-doubles equipped with smart dollies is still significantly less than the performance achieved by the tractor semi-trailer combination. Future research is needed to further improve the high speed stability of the A-double HCV.

7.2   Recommendations

In Chapter 5.1, it is assumed that the total required dolly tractive force for startability on an inclined road is equally distributed among the four wheels of the 4x4 dolly. However, due to the presence of the dynamic load transfer and the road inclination angle, the vertical force on the rear axle is larger compared to the vertical force on the front axle. This implies that the rear tyres can transfer more force to the road than the front tyres. A control approach has to be derived that divides the total requested torque over the wheels, based on the vertical tyre force distribution. This control approach should ensure that the front wheels do not slip during startability tests.

The smart dollies improve the manoeuvrability of the A-double HCV compared to a non-steered dolly. However, the smart dolly equipped A-doubles are not able to meet the high speed stability performance of the tractor semi-trailer combination. It is recommended to do more research on the steering system design and/or active roll suspension design, to improve the roll behaviour and stability of the smart dolly A-doubles. Next, it is recommended to perform a detailed high speed stability assessment on the A-double HCV. One possible approach is to use stability criterion like e.g. the Hurwitz criterion. For this approach the equations of motions are required, which need to be derived first.

The driveline controller of the 4x4 design is not able to control the lateral force at the pin coupling to zero. More research needs to be done on control strategies like e.g. torque vectoring to reduce the lateral pin coupling force. In this research a basic driveline controller is derived and implemented in the simulation model. Startability simulations have not been performed, so the driveline controller is not tested for the longitudinal driving scenarios. It is recommended to extend the simulation models with a detailed driveline model for the dolly. Furthermore a brake system needs to be implemented too. By doing so, longitudinal driving scenarios like e.g. startability and braking stability can be evaluated too.

For the final driveline design of the dollies it is recommended to perform a detailed component sizing. This should include the selection of e.g. the correct motors, batteries and inverters. A typical commercial vehicle drive cycle can be used in this calculation to determine the required battery pack size. Accordingly, the regulations concerning hybrid drivetrains on commercial vehicles need to be consulted. After the driverain component selection, the driveline control strategy can be extended to enable propulsion during longitudinal dynamics like e.g. hill-assist. A second controller is required that controls the charging of the batteries.

The autonomous operation of the dolly needs to be researched to evaluate if the dolly can be used for auto-docking applications. Calculations on the cost, strength, and transport efficiency of the smart dolly designs should be made too. The design of the smart dolly can be considered infeasible, when the increase in costs are not covered by the increase in transport efficiency.

Bibliography

[1] Aurell, J., Wadman, T., Nordiska, *Vehicle combinations based on the modular concept, Background and analysis*, Volvo Trucks, 2007, Sweden

[2] Australasian Legal Information Institute, *National Transport Commision Road Transport Legislation – Heavy Vehicle Standards Regulations, Regulations 2006 - schedule 1*, 2006, [viewed 17 February], available from: http://www5.austlii.edu.au/au/legis/cth/num_reg/ntctlhvsrr2006n25o20061154/sch1.html

[3] Besselink, I. J. M., *Vehicle Dynamics 4l150, lecture notes 2014*, Eindhoven University of Technology, 2014

[4] Besselink, I. J. M., *Tractor semi-trailer optimal brake force distribution, Course 4J570 "Advanced Vehicle Dynamics" Third exercise (16/03/2009)*, Eindhoven University of Technology, 2009

[5] BOS Trailer service, *Bos Matrix trailer, VAN HOOL schuifzeiloplegger*, [viewed 17 February 2016], available from: www.bostrailer.nl/matrix.php

[6] Cancade Company Ltd., *Converter Dollies*, [viewed 24 February 2016], available from: http://www.cancade.com/detailed.asp?id=343&tab=trailers&cat=converter%20dollies&section=converter%20dollie&sid=tts

[7] European Commission, *Directive 96/53/EC*, 2015

[8] European Commission, *Directive 97/27/EC*, 1997

[9] European Commission, *70/221/EEC*, 2006

[10] European Commission, European Commission's White Paper on Transport, *European transport policy for 2010: time to decide*, 2001, [viewed 17 February 2016], available from: http://ec.europa.eu/transport/themes/strategies/2001_white_paper_en.htm

[11] Eurostat, *Modal split of freight transport*, [viewed 24 August 2016], available from: http://ec.europa.eu/eurostat/tgm/refreshTableAction.do;jsessionid=UBq8OJawjmblCtfRVnB8GJOUBFcfy_EQMLm4rG4IVL4NNZZJW6lG!-125362223?tab=table&plugin=1&pcode=tsdtr220&language=en

[12] Fahrzeugwerk Bernard Krone GmbH, *Data sheets*, [viewed 17 February 2016], available from: www.krone-trailer.com/english/download/data-sheets/

[13] Fahrzeugwerk Bernard Krone GmbH, *Loads of Length - The Long HGV, The commercial vehicle combination of the future*, [viewed 17 February 2016], available from: http://int.krone-trailer.com/fileadmin/contentmedia/pdf/prospekte/lang_lkw_en.pdf

[14] Fahrzeugwerk Bernard Krone GmbH, *we deliver the future Curtain siders*, [viewed 17 February 2016], available from: http://www.krone-trailer.com/fileadmin/contentmedia/pdf/prospekte/pritschensattelauflieger_en.pdf

[15] Fliegl fahrzeugbau GmbH, *Gardinensattelauflieger und Courtainsider von Fliegl Trailer*, [viewed 17 February 2016], available from: http://www.fliegl-fahrzeugbau.de/gardinensattelauflieger-und-courtainsider-von-fliegl-trailer/150/1417/504,

[16] Guzzella, L., Sciarretta, A. *Vehicle Propulsion Systems: Introduction to Modeling and Optimization*, Third edition, Springer berline Heidelberg, 2013, ISBN: 978-3-642-35912-5

[17] Hatzidimitris, P., *Active Trailer steering Control for Longer Heavie Vehicles*, Eindhoven University of Technology, Dynamics and Control Group, 2015

[18] HTAS EMS project consortium, *Greening and Safety Assurance of Future Modular Road Vehicles, book of requirements*, 2014

[19] Isiklar, G., *Simulation of complex articulated commercial vehicles for different driving manoeuvres*, Eindhoven University of Technology, Dynamics and Control Group, 2007

[20] Jong de, T., Iepieleaks, *Scania tests LHV consisting of two semi trailer*, 2014 [viewed 17 February 2016], available from:http://iepieleaks.nl/scania-tests-lhv-consisting-two-semi-trailers/

[21] Jong de, T., Iepieleaks, *Giant Finnish roadtrain on the move...*, 2015 [viewed 17 February 2016], available from:http://iepieleaks.nl/giant-finnish-roadtrain-on-the-move/

[22] Kabos, T., *Auto Docking - Design and Implementation for a Semi-trailer Tuck*, DAF trucks NV, 2015, [confidential]

[23] Karnopp, D. *Vehicle Dynamics, Stability, and Control*, Second edition, CRC Press Boca Raton, Florida, 2013, ISBN: 9781466560857

[24] Kässbohrer, *K.SHG S Enduring Performance by Kässbohrer*, [viewed 17 February 2016], available from: www.kaessbohrer.com/product/kshg-s/72/

[25] Kässbohrer, *K.SCS X+ Engineering in Action by Kässbohrer*, [viewed 17 February], available from: www.kaessbohrer.com/product/kscs-x%E2%81%BA-maxima/4/

[26] Krone, B., Evers, H., *Dolly axle*, Fahrzeugwerk Bernard Krone GmbH,Patent, 2009, [viewed 24 August 2016], available from: https://www.google.com/patents/EP1900618B1?cl=fr

[27] Kural, K., et al. *Assesment of Dutch longer and heavier vehicles with a performance based approach and its applicability to Europe*, Han university of Applied Sciences, Arnhem, Eindhoven University of Technology, 2012

[28] Kural, K., Prati, A., Besselink, I., Pauwelussen, J. et al., "Validation of Longer and Heavier Vehicle Combination Simulation Models," SAE Int. J. Commer. Veh. 6(2):2013, doi:10.4271/2013-01-2369.

[29] Larsson, S., *Weight and dimensions of heavy commercial vehicles as established by Directive 96/53/EC and the European Modular System (EMS)*, European Commision, Brussels, 2009 [viewed 17 February 2016], available from: http://ec.europa.eu/transport/modes/road/events/doc/2009_06_24/2009_gigaliners_workshop_acea.pdf

[30] LeciTrailer, *Curtainsiders and Semicurtainsiders, Fixed curtainsiders*, [viewed 17 February 2016], available from: www.lecitrailer.com/documentos/fichas-tecnicas/curtainsider-fisso_ita.pdf

[31] Luijten, M.F.J., " Lateral Dynamic Behaviour of Articulated Commercial Vehicles", Eindhoven University of Technology, Dynamics and Control Group, 2010

[32] MAN Truck & Bus UK Bodybuilder, *spec sheets/TGX 4x2 Tractor*, 2011, [viewed 24 August 2016], available from: http://www.man-bodybuilder.co.uk/specs/pdf/tgx/TGX%204x2%20Tractor.pdf

[33] MANTED, *Guidelines to fitting bodies*, 2011, [viewed 6 September August 2016], available from: https://www.manted.de/manted/aufbaurichtlinien/_pdf/tgs_tgx_e2016_v1_en.pdf

[34] Manjurul Islam, *Long truck combination with Active Dolly Steering demonstration*, [viewed 24 August 2016], available from: https://www.youtube.com/watch?v=gYVnp9x6UCk, contact info: https://www.chalmers.se/en/staff/Pages/manjurul-islam.aspx

[35] NTC Australia, *Performance-Based Standards Scheme - the Standards and Vehicle Assesment Rules*, Australia, 2008

[36] Odhams, A.M.C., Roebuck, R.L., Jujnovich, B.A., Cebon, D., '*Active Steering of a Tractor Semi-trailer*', Proceedings of the Institution of Mechanical Engineers, Part D: Journal of Automobile Engineering July 2011, 225(7): 847âĂŞ869

[37] OECD, *Moving Freight with Better Trucks: Improving Safety, Productivity and Sustainability*, OECD Publishing, 2011

[38] Overheid.nl, *Instellingsbesluit Ambtelijke adviescommisie LZV*, 2015, [viewed 17 February 2016], available from: http://wetten.overheid.nl/BWBR0016098/geldigheidsdatum_11-01-2016

[39] Powertech Engines Inc., *Iveco data, CURSOR C13 ENT*, [viewed 6 September 2016], available from: http://www.powertechengines.com/IvecoData/C13ENT-DS-P2G04C003U.pdf

[40] Rijkswaterstaat Ministry of Transport, Public Works and Water Management, *Longer and Heavier Vehicles in the Netherlands, Facts, figures and experiences in the period 1995-2010*, 2010

[41] Schmitz Cargobull, *S.KO Express Box Semitrailer, The Benchmark for Courier, Express and Package Delivery*, [viewed 17 February 2016], available from: www.cargobull.com/en/Semitrailers-S.KO-Express-Box_25_209.html

[42] Schmitz Cargobull, *Curtainsider/Platform Trailers, Curtainsiders from Schmitz Cargobull*, [viewed 17 February 2016], available from: www.cargobull.com/en/Curtainsider-Platform-Trailers_7_592.html

[43] Schramm Arthur G., Steerable dolly, United States Patent,'US310574 A', 1963-10-1, available from: http://www.google.com/patents/US3105704

[44] Schwarzmüller Gruppe, *3-axle sliding tarpaulin platform semitrailer*, [viewed 17 February 2016], available from: http://schwarzmueller.com/en/vehicles/3-axle-sliding-tarpaulin-platform-semitrailer/

[45] Schwarzmüller Gruppe, *3-axle container semitrailer chassis*, [viewed 17 February 2016], available from: http://schwarzmueller.com/en/vehicles/3-axle-container-semitrailer-chassis/

[46] Schwarzmüller Gruppe, *3-axle container semitrailer chassis - offset*, [viewed 17 February 2016], available from: http://schwarzmueller.com/en/vehicles/3-axle-container-semitrailer-chassis-offset/

[47] Seacom AG, *Drawbar trailer type 10*, [viewed 6 September 2016], available from: http://www.seacom-trailer.com/industry/heavy-duty-drawbar-trailers/trailer-type-10/?L=1

[48] Sommer, *Pritschensattelauflieger SP24-120-CU*, [viewed 17 February 2016], available from: www.sommer-online.de/fileadmin/user_upload/Dokumente/Prospekte_und_Datenblaetter/SOMMER_Datenblatt_SP_web.pdf

[49] Sorniotti, A., D'Alfio, N., *Vehicle Dynamics Simulation to Develop an Active Roll Control System*, SAE Technical Paper 2007-01-0828, 2007, doi:10.4271/2007-01-0828.

[50] Syed, U., Vigliani, A., *Vehicle Side Slip and Roll Angle Estimation*, SAE Technical Paper 2016-01-1654, 2016, doi:10.4271/2016-01-1654.

[51] Trackaxle Ltd., *Products, Dollies*, [viewed 24 August 2016], available from: http://www.trackaxle.com.au/dollies.html

[52] TrailerTotaal, *Krone*, [viewed 24 February 2016], available from: http://trailertotaal.nl/merken/item/krone

[53] TrailerTotaal, *Spaanse LZV proef van start*, 2016, [viewed 24 August 2016], available from: http://trailertotaal.nl/nieuwsarchief/item/spaanse-lzv-proef-van-start

[54] TrailerTotaal, *Tij keert voor LZV in Duitsland*, 2016,[viewed 24 August 2016], available from: http://trailertotaal.nl/nieuwsarchief/item/tij-keert-voor-lzv-in-duitsland

[55] Transformers, *Results, Hybrid-on-demand driveline*, [viewed 17 February 2016], available from: http://www.transformers-project.eu/articles/results/#.VsMK6PnhBpg

[56] TrucksPlanet.com, *5440 multi-tier 2nd version*, 2012, [viewed 17 February 2016], available from: http://www.trucksplanet.com/ru/catalog/model.php?id=1838

[57] Truck & Trailer Groep Nederland, *Kässbohrer oplegger schuifzeilopbouw*, [viewed 17 February 2016], available from: http://trailergroep.nl/afbeeldingen/pdf/NLBENSTD90%20SCHUIFZEIL.pdf

[58] TTM.nl, Eisma Industriemedia, *Foto's: Lichtgewicht gestuurde dolly van Fliegl*, 2013, [viewed 8 September 2016], available from: https://www.ttm.nl/nieuws/fotos-lichtgewicht-gestuurde-dolly-van-fliegl/59200/

[59] United Nations Economic Commision for Europe, *European agrement on main international traffic arteries (AGR)*, 2007, [viewed 8 September 2016], available from: http://www.unece.org/fileadmin/DAM/trans/conventn/ECE-TRANS-SC1-384e.pdf

[60] vanHool, *Curtainsider semi-trailer Standard*, [viewed 17 February 2016], available from: www.vanhool.be/ENG/industriele%20voertuigen/schuifzeiloplegger/standaardschuifz.html

[61] Wamprecht, P.A.M., *Scaled test track: Investigation of active steering for large heavy truck combinations and implementation of a demonstrator in 1:14 scale*, Chalmers University of Technology, Sweden, 2014

[62] Woodroofe, J. et all, OECD, *Safety, Productivity, Infrastructure Wear, Fuel Use and Emissions Assessment of the International Truck Fleet, A Comparative Analysis*, OECD, August 2010, [viewed 8 September 2016], available from: http://efficientandresponsible.org/wp-content/uploads/2014/12/Woodroofe-study.pdf

[63] ZF Friedrichshafen AG, *ZF technology for buses, Axle systems* , [viewed 7 September 2016], available from: http://www.zf.com/corporate/en_de/products/product_range/buses/buses_axles_ave130.shtml#tabs1-1

Appendix A
Roll behaviour of a commercial vehicle

Roll dynamics are relevant when a vehicle is cornering and are caused by the lateral acceleration of the truck's CoG. Too high lateral accelerations may result in roll-over of the vehicle. In this chapter the roll-over behaviour of a commercial vehicle is explained.

A.1   Roll moments

The free body diagram of a truck while cornering is shown in Fig. A.1. From Fig. A.1 it follows that three moments influence the roll movement of the vehicle [19]. These moments can be categorized in overturning and returning moments. An overturning moment is destabilizing the vehicle and a returning moment is stabilizing the vehicle.
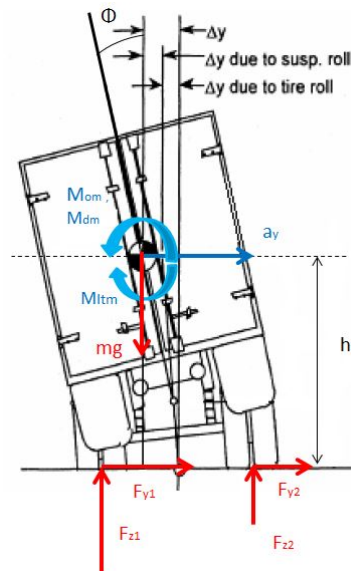

Figure A.1: Free body diagram of truck while cornering [19].

During cornering, the tyres generate lateral forces that result in a lateral acceleration a_y towards the turning centre of the corner, as shown in Fig. A.1. This results in the following equation:

$$m_v a_y = F_{y1} + F_{y2} \tag{A.1}$$

In this equation the vehicle mass is represented by m_v, the lateral acceleration is represented by a_y and F_{y1} and F_{y2} represent the lateral tyre forces at the left and right side of the vehicle, respectively. From (A.1) it follows that an increased lateral tyre forces result in higher lateral accelerations. This lateral acceleration induces a moment around the CoG of the truck which is defined as the primary overturning moment. The primary overturning moment M_{om} is given by:

$$M_{om} = m_v a_y h_t \tag{A.2}$$

In this equation the CoG height of the vehicle, measured from the ground, is represented by h_t. Since this moment results in the undesired roll of the vehicle, it needs to be as small as possible. From (A.2) it follows that the overturning moment can be decreased by reducing the mass of the vehicle and/or the CoG height of the vehicle, for a given lateral acceleration.

The second moment that is acting on the truck's CoG is known as the displacement moment and originates from the lateral shift of the CoG. This CoG shift is caused by the compression of the suspension on the outer side of the vehicle and extension of the suspension on the inner side. The shift of the CoG in lateral direction Δy can be calculated with:

$$\Delta_y = h_t sin(\Phi) \tag{A.3}$$

The suspension roll angle is represented by Φ and the CoG height of the trailer is represented by h_t. The resulting displacement moment M_{dm} is calculated with:

$$M_{dm} = m_v g \Delta y \tag{A.4}$$

During cornering, the vertical forces at the outer tyres increase and generate a moment against the roll movement of the vehicle. This restoring moment can be calculated with the following equation:

$$M_{ltm} = (F_{z2} - F_{z1})s_t/2 \tag{A.5}$$

In (A.5), F_{zi} represents the vertical tyre forces at the left and right side of the vehicle and s_t represents the track width of the vehicle. This moment is defined as the load transfer moment or M_{ltm}.

By using the three roll moments above, the following moment equilibrium is obtained:

$$m_v a_y h_t + m_v g h_t sin(\Phi) = (F_{z2} - F_{z1})s_t/2 \tag{A.6}$$

To ensure that the vehicle does not roll-over for increasing lateral accelerations, the returning moment needs to be greater than the overturning moment. To improve the roll-over tendency of the vehicle, either the overturning moments must be decreased or the returning moment must be increased. The overturning moment can be decreased by lowering the CoG height or using active roll suspension, which limits the lateral displacement moment. lowering the CoG height, however, is hard to achieve, since this mainly depends on the cargo to be transported. To increase the returning moment, active roll suspension can be implemented and/or the track width of the vehicle can be increased. Increasing the track width is however limited by the EU legislations, since it states that the vehicle width should not exceed 2.55 m [8].

The roll angle Φ of a vehicle can be estimated by e.g. using the vertical axle forces on a vehicle or using the lateral accelerations of the sprung mass [50] [49]. When the suspension properties like the roll centre height, roll stiffens and roll damping are known, the roll angles can be estimated. For more information on the roll angle estimation of a vehicle, [50] and [49] can be consulted.

A.2 Roll-over of a vehicle

The roll stability of a vehicle is often evaluated with the static roll-over threshold. This value describes the lateral acceleration, divided by the gravitational constant, at which vehicle roll-over occurs. Roll-over is defined as the point where the lateral acceleration of the vehicle decreases for increasing roll angle. This means that "the point of roll instability is achieved when the vertical forces on all the tyres along one side of the vehicle are equal to zero, excluding the tyres on the lightly loaded side of a steer axle with soft springs" [35]. To understand the behaviour of the vehicle during this roll instability, the moments derived in (A.2), (A.4) and (A.5) are plotted in Fig. A.2 for increasing roll angle Φ and lateral acceleration a_y. For this figure all axles of the vehicle are lumped into a single equivalent axle and small roll angles are assumed, such that $sin(\Phi) = \Phi$.

From Fig. A.2 it follows that the load transfer moment increases linearly with the roll angle, until the maximum load transfer is achieved. At this point, the tyres at one side of the vehicle loose contact with the ground and the load transfer can no longer increase. The maximum value of the load transfer moment equals:

$$max(M_{ltm}) = m_v g s_t/2 \tag{A.7}$$

At this point, the total vehicle weight rests on the tyres at one side of the vehicle, whereas the vertical force on the tyres of the other side equals zero. The displacement moment, which is a function of the vertical tyre force difference, decreases linearly with the roll angle. The vehicle reaction moment is defined as the sum of the load transfer moment and displacement moment and acts as the vehicle's reaction to the overturning moment. After the maximum load transfer moment is reached at point A, the slope of the vehicle reaction moment becomes negative. At this point the vehicle will roll-over. The primary overturning moment, however, increases linearly for increasing acceleration. One remark is that in reality the sprung mass of the vehicle rotates around the suspension roll centre, instead of a point on the ground. This roll centre is determined by the suspension geometry. Changing the suspension design may result in higher roll-over thresholds. The unsprung mass, however, still rotates around a point at the ground. The unsprung mass of the vehicle is defined as the sum of the axle mass and mass of all wheels.
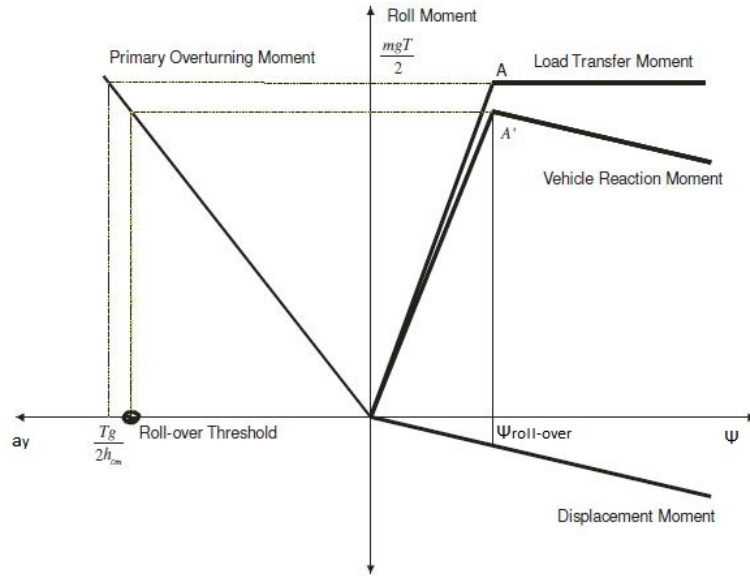

Figure A.2: Roll moments of a single axle vehicle versus lateral acceleration and roll angle [19].

The roll-over behaviour of a vehicle with multiple axles is evaluated next. The three load transfer moments of the steer axle, drive axle and the centre axle of the semi-trailer are shown in Fig. A.3. The trailer axles have the highest roll stiffness and the steer axle of the tractor the lowest, in a normal tractor semi-trailer combination [19]. This also follows from the slopes of the load transfer moments of the vehicle in Fig. A.3. During cornering at high lateral accelerations, the vertical tyre forces of the semi-trailer axle are transferred to one side of the vehicle first, due to the high roll stiffness of this axle. The maximum load transfer moment for the trailer axle occurs at point B. At this point the semi-trailer wheels at the inner side loose contact with the ground. After point B, the stiffness of the total vehicle reaction moment decreases, since the semi-trailer can no longer generate a load transfer moment. The decreasing stiffness corresponds to the slope decrease of the vehicle reaction moment till point A". At point A", the wheels at the inner side of the tractor's drive axle loose contact with the ground. From Fig. A.3 it follows that the slope of the load transfer moment of the steer axles is smaller than the slope of the displacement moment, due to the low stiffness of the steer axle. Therefore, insufficient vehicle reaction moment can be generated to counteract the primary overturning moment after point A". Accordingly, the slope of the vehicle reaction moment decreases and the entire vehicle will roll-over.
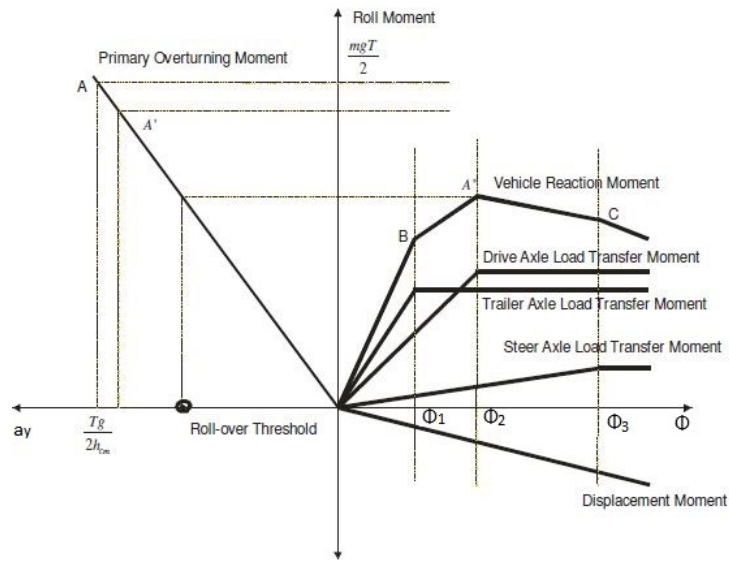
Figure A.3: Roll moments of a tractor semi-trailer combination versus lateral acceleration and roll angle [19].

Appendix B
Semi-trailer dimensions

Table B.1: Container semi-trailer dimensions.

Manufacturer	Kässbohrer	Krone	Krone	Krone	Schwarzmuller	Schwarzmuller
Type	K.SHG S	SDC 27 eL40	SDC 27 eL45	SDC 27 eLT3	3-axle container semi-trailer chassis	3-axle container semi-trailer chassis offset
Kind	gooseneck	flat	flat	gooseneck	flat	gooseneck
45 ft. container possible	no	no	yes	no	optionally	optionally
Total length ($l_{tot,t}$) [mm]	12730	12435	13285	12561	12575	12680
Front overhang of trailer (l_{fo}) [mm]	-	1160	1999	1147	1180	1530
King pin - rear of trailer ($l_{rear,t}$) [mm]	-	11275	11275	11414	10595	11150
King pin - support legs (l_{sl}) [mm]	-	2450	2475	2615	-	-
Chassis thickness rear (h_{chass}) [mm]	-	-	400	370	-	-
King pin height (h_{kp}) [mm]	1100	1150	1050	1100	1130	1160
Total height ($h_{tot,t}$) [mm]	3995	–	-	-	-	-
Wheelbase (l_t) [mm]	7580	8115	7480	7480	6665	7400
Rear overhang (l_{ro}) [mm]	-	1279	1925	2053	2049	2055
Total width (w_t) [mm]	2550	-	-	2548	-	-
Tare weight [kg]	4820	4900	5000	4950	4800	-
Permissible payload [kg]	-	38100	36000	36050	31000	31000
Source	[24]	[12]	[12]	[12]	[45]	[46]

Manufacturer	Kässbohrer	Krone	Fliegl	Schmitz cargobull	Schmitz cargobull	vanHool	Schwarzmuller	LeciTrailer	Sommer
Type	K.SCS X+	Profiliner	300 SDS 350 Gardine Standard	S.KO Express	S.CS Universal	curtainsider standard	3-axle sliding tarpaulin platform semi-trailer	curtainsider Fisso	SP24-120-CU
Kind	curtain	curtain	curtain	box body	curtain	curtain	curtain	curtain	curtain
Total length ($l_{tot,t}$) [mm]	13680	13620	13650	13685	13620	13620	13675	13620	13620
Front overhang of trailer (l_{fo}) [mm]	-	-	-	1685	-	-	1675	1650	-
King pin - rear of trailer ($l_{rear,t}$) [mm]	-	-	-	-	-	-	12000	11970	-
King pin - support legs (l_{sl}) [mm]	-	-	-	-	2320	-	-	-	-
King pin Height (h_{kp}) [mm]	1150	1170	1150	1141	1150	1130	1190	1150	1120
Total height ($h_{tot,t}$) [mm]	4020	4000	4000	3993	3935	4000	4000	4000	4000
Wheelbase (l_t) [mm]	7700	-	-	7700	7700	7450	7620	7820	-
Rear overhang (l_{ro}) [mm]	-	-	-	2419	2419	-	2499	-	-
Total width (w_t) [mm]	2550	2550	2550	2550	2550	2550	2550	-	2550
Tare weight [kg]	6450	6160	6400	6982	6330	-	6000	-	6280
Permissible payload [kg]	33430	32350	28600	32018	29670	-	27000	-	27000
Source	[25], [57],	[12]	[15]	[41]	[42]	[60], [5]	[44]	[30]	[48]

Table B.2: Closed semi-trailer dimensions.

Appendix C
Vertical tyre forces derivations

C.1 Vertical tyre forces on an inclined road

In Fig. C.1 the free body diagrams of a dolly and semi-trailer on an inclined road are shown. The dolly and second semi-trailer are decoupled from the A-double HCV, since it is assumed that there are no forces transferred via the drawbar. Furthermore, for the derivations it is assumed that the lateral acceleration equals zero, such that roll movements can be neglected. Lastly, the three semi-trailer axles are lumped into one equivalent axle.
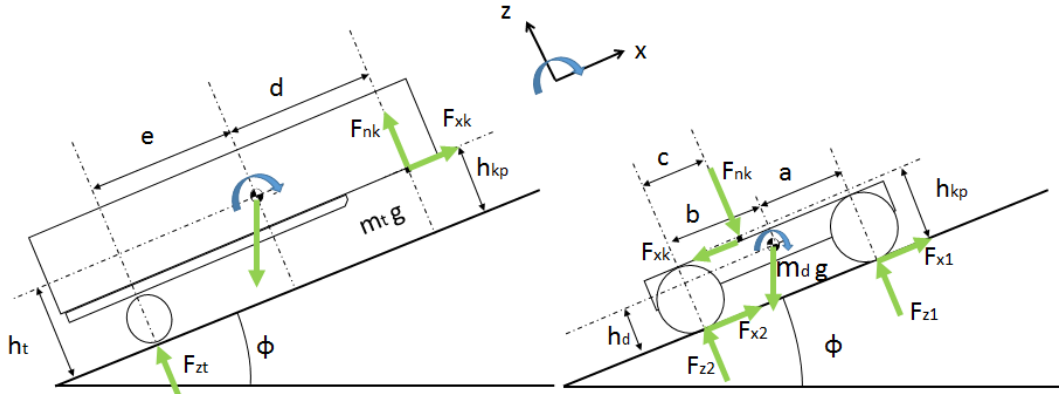

Figure C.1: Free body diagram of dolly semi-trailer combination.

With Newton's second law of motion the following equations can be derived:

$$\sum F_x = m \cdot a_x \tag{C.1}$$

$$\sum F_z = 0 \tag{C.2}$$

$$\sum M_y = 0 \tag{C.3}$$

Furthermore, the wheelbase of the dolly and trailer are defined by:

$$l_d = a + b \tag{C.4}$$

$$l_t = d + e \tag{C.5}$$

When the combination is split into two bodies, six equations can be derived which are listed below. Using Newton's second law for the dolly, yields:

$$m_d \cdot a_x = F_{x2} + F_{x1} - F_{xk} - m_d g sin(\phi) \tag{C.6}$$

$$F_{z2} + F_{z1} - F_{nk} - m_d g cos(\phi) = 0 \tag{C.7}$$

$$F_{z2} \cdot b - F_{z1} \cdot a - F_{nk}(b-c) - F_{xk}(h_{kp} - h_d) - (F_{x1} + F_{x2})h_d = 0 \tag{C.8}$$

The following equations are derived for the semi-trailer:

$$m_t \cdot a_x = F_{xk} - m_t g sin(\phi) \tag{C.9}$$

$$F_{zt} + F_{nk} - m_t g cos(\phi) = 0 \tag{C.10}$$

$$F_{zt} \cdot e - F_{nk} \cdot d - F_{xk}(h_t - h_{kp}) = 0 \tag{C.11}$$

Rearranging of (C.9) results in:

$$F_{xk} = m_t g sin(\phi) + m_t \cdot a_x \tag{C.12}$$

Next, substitution of (C.12) in (C.6) results in:

$$F_{x2} + F_{x1} = (m_d + m_t)(a_x + gsin(\phi)) \tag{C.13}$$

From (C.10):

$$F_{zt} = m_t gcos(\phi) - F_{nk} \tag{C.14}$$

Rearranging (C.11):

$$F_{nk}d = F_{zt}e - F_{xk}(h_t - h_{kp}) \tag{C.15}$$

Substitution of (C.13) and (C.14) in (C.15) yields:

$$F_{nk}d = (m_t gcos(\phi) - F_{nk})e - (m_t gsin(\phi) + m_t \cdot a_x)(h_t - h_{kp})$$
$$F_{nk} = \frac{m_t}{l_t}(egcos(\phi) - (a_x + gsin(\phi))(h_t - h_{kp}) \tag{C.16}$$

On a similar way, the vertical axle force on the trailer equals:

$$F_{zt} = m_t gcos(\phi) - \frac{m_t}{l_t}(egcos(\phi) - (a_x + gsin(\phi))(h_t - h_{kp})$$
$$F_{zt} = \frac{m_t}{l_t}(dgcos(\phi) + (a_x + gsin(\phi))(h_t - h_{kp}) \tag{C.17}$$

Rearranging (C.7) and (C.8), yields:

$$F_{z1} = m_d gcos(\phi) + F_{nk} - F_{z2} \tag{C.18}$$

$$F_{z2}b = F_{z1}a + F_{nk}(b - c) + F_{xk}(h_{kp} - h_d) + (F_{x1} + F_{x2})h_d \tag{C.19}$$

Rearranging and using the equations derived earlier:

$$F_{z2} = \frac{1}{l_d}\left(gcos(\phi)\left(am_d + \frac{m_t e}{l_t}(l_d - c)\right)\right) +$$
$$\frac{1}{l_d}\left((a_x + gsin(\phi))\left(\frac{m_t}{l_t}(h_{kp} - h_t)(l_d - c) + h_{kp}m_t + h_d m_d\right)\right) \tag{C.20}$$

Using (C.18) in combination with (C.16) and (C.20), the last equation for the front vertical axle force can be derived, resulting in:

$$F_{z1} = \frac{1}{l_d}\left(gcos(\phi)\left(m_d b + \frac{m_t e}{l_t}c\right)\right) +$$
$$\frac{1}{l_d}\left((a_x + gsin(\phi))\left(\frac{m_t}{l_t}(h_{kp} - h_t)c - h_{kp}m_t - h_d m_d\right)\right) \tag{C.21}$$

C.2 Vertical tyre forces during severe braking

The equations and free body diagrams above need to be adapted to evaluate the vertical axle forces during braking. The adapted free body diagrams are shown in Fig. C.2. First of all, the trailer axle can now also generate a longitudinal tyre force while braking. Secondly, some parameters are introduced to evaluate the braking performance. Assuming that each axle brakes its own load, the following equation holds:

$$\frac{F_{xt}}{F_{zt}} = \frac{F_{x1}}{F_{z1}} = \frac{F_{x2}}{F_{z2}} = k \tag{C.22}$$

Note that in this equation k corresponds to the required road friction coefficient [4], which equals μ. Ideally, if all required road frictions coefficients of the tyres are equal, the following relation holds:

$$\frac{F_{xt} + F_{x1} + F_{x2}}{F_{zt} + F_{z1} + F_{z2}} = \frac{m_{tot}a_x}{m_{tot}g} = z \tag{C.23}$$

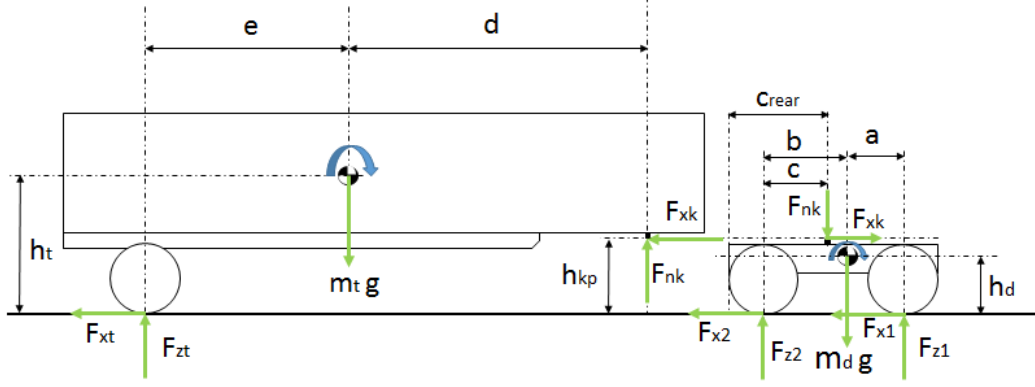The parameter z in this equation, is the dimensionless deceleration.

Figure C.2: Free body diagram of a dolly semi-trailer combination on flat road while braking.

By again using Newton's second law, the following set of equations can be derived; for the dolly:

$$m_d \cdot a_x = -F_{x2} - F_{x1} + F_{xk} \tag{C.24}$$

$$F_{z2} + F_{z1} - F_{nk} - m_d g = 0 \tag{C.25}$$

$$F_{z2} \cdot b - F_{z1} \cdot a - F_{nk}(b-c) + F_{xk}(h_{kp} - h_d) + (F_{x1} + F_{x2})h_d = 0 \tag{C.26}$$

and for the trailer:

$$m_t \cdot a_x = -F_{xk} - F_{xt} \tag{C.27}$$

$$F_{zt} + F_{nk} - m_t g = 0 \tag{C.28}$$

$$F_{zt} \cdot e - F_{nk} \cdot d + F_{xt} \cdot h_t + F_{xk}(h_t - h_{kp}) = 0 \tag{C.29}$$

From (C.27) and (C.28) it directly follows that the following two relations hold:

$$F_{xk} = -m_t \cdot a_x - F_{xt} \tag{C.30}$$

$$F_{nk} = m_t g - F_{zt} \tag{C.31}$$

Substituting these in (C.24), (C.25), (C.26) and (C.29) results in the following equations:

$$-F_{x2} - F_{x1} - F_{xt} = (m_t + m_d) \cdot a_x \tag{C.32}$$

$$F_{z2} + F_{z1} + F_{zt} = (m_t + m_d) \cdot g \tag{C.33}$$

$$F_{z2} \cdot b - F_{z1} \cdot a - (m_t g - F_{zt})(b-c) + (m_t \cdot a_x + F_{xt})(h_d - h_{kp}) + (F_{x1} + F_{x2})h_d = 0 \tag{C.34}$$

$$F_{zt} \cdot e - (m_t g - F_{zt}) \cdot d + F_{xt} \cdot h_t + (-m_t \cdot a_x - F_{xt})(h_t - h_{kp}) = 0 \tag{C.35}$$

The most ideal brake force distribution is when $z = k$ in (C.22) and (C.23). If this holds, the following relation is obtained:

$$F_{xi} = -a_x/g F_{zi} = k F_{zi} \tag{C.36}$$

Substituting (C.36) in (C.32)-(C.35), results in:

$$F_{z2} + F_{z1} + F_{zt} = (m_t + m_d) \cdot a_x \frac{g}{ax} \tag{C.37}$$

$$F_{z2} + F_{z1} + F_{zt} = (m_t + m_d) \cdot g \tag{C.38}$$

$$F_{z2} \cdot b - F_{z1} \cdot a - (m_t g - F_{zt})(b-c) + (F_{zt}k - m_t g k)(h_d - h_{kp}) - \frac{a_x}{g}(F_{z1} + F_{z2})h_d = 0 \tag{C.39}$$

$$F_{zt} \cdot e - (m_t g - F_{zt}) \cdot d - \frac{a_x}{g}F_{zt} \cdot h_t + \left(\frac{a_x}{g}F_{zt} - m_t \cdot a_x\right)(h_t - h_{kp}) = 0 \tag{C.40}$$

Solving this last set of equations for F_{z1}, F_{z2} and F_{zt} results in the set of equations listed below. Rearranging (C.40) yields:

$$F_{zt} = m_t g \frac{d - k(h_t - h_{kp})}{l_t + k h_{kp}} \tag{C.41}$$

Substituting (C.41) in (C.31) results in:

$$F_{nk} = m_t g \frac{e + k h_t}{l_t + k h_{kp}} \tag{C.42}$$

92

By combining (C.38) and (C.39) yields:

$$F_{z2}l_d = F_{z}t(c - l_d + kh_{kp}) + m_tg(l_d - c - kh_{kp}) + m_dg(a - kh_d)$$

$$F_{z2} = \frac{1}{l_d}\left(m_dg(a - kh_d) + (l_d - c - kh_{kp})m_tg\frac{e + kh_t}{l_t + kh_{kp}}\right) \tag{C.43}$$

Substituting this last equation in (C.38) results in the vertical force on the front axle of the dolly during braking manoeuvres, represented by:

$$F_{z1} = \frac{1}{l_d}\left(m_dg(b + kh_d) + (c + kh_{kp})m_tg\frac{e + kh_t}{l_t + kh_{kp}}\right) \tag{C.44}$$

Appendix D
Lateral powertrain controller

From the 4x4 dolly equipped A-double HCV simulations in Chapter 5.5b it is obtained that large pin coupling forces are present during the low speed 360 degree turn manoeuvres. Although the longitudinal pin coupling force is controlled to zero with the controller derived in Chapter 5.2, the lateral force cannot actively be controlled to zero yet. Therefore, a large lateral force component of 10 kN is still present at the pin coupling. The presence of this lateral pin coupling force causes the first semi-trailer to deliver a reaction force. As a result of this, larger tyre side slip angles are generated on the first semi-trailer. This indicates that the first semi-trailer is closer to the instantaneous centre of the turn than in a tractor semi-trailer combination. In comparison with the tractor semi-trailer combination, the critical radius of the first semi-trailer $r_{crit,1}$ is reduced with 8 cm in the A-double HCV configuration.

The lateral pin coupling force of the 4x2 dolly in the A-double HCV configuration is much smaller than the coupling force of the 4x4 dolly. This can be explained by the additional rotating point of the drawbar at the dolly chassis. Lateral forces or moments introduced at this joint, are counteracted by a rotation of the drawbar with respect to the dolly chassis. A lateral powertrain controller has to be derived to reduce the lateral pin coupling force in the 4x4 dolly simulations. Two solutions to reduce this lateral pin coupling force are: changing the steer angle of the wheels and introducing a yaw rotation around the dolly's CoG by means of torque vectoring.

Torque vectoring is a control strategy that controls the torque of the individual wheels. Via braking or propulsion of the wheel, a positive- or negative torque is sent to the individual wheels. This difference in torque results in a yaw rotation of the vehicle around it's CoG. The principle of torque vectoring can be explained by using Fig. 5.1 and the equations derived in Chapter 5.2. The moment equilibrium of the free body diagram shown in Fig. 5.1 is defined as:

$$
\begin{aligned}
I_{zz,d}\dot{r}_d = &\frac{w_d}{2}\big(F_{x2,chas} + F_{x4,chas} - F_{x1,chas} - F_{x3,chas}\big) + ... \\
&a(F_{y2,chas} + F_{y1,chas}) + l_{fw}(F_{c2y}) - b\big(F_{y3,chas} + F_{y4,chas}\big)
\end{aligned}
\tag{D.1}
$$

Substitution of (5.22) and (5.23) in (D.1) yields:

$$
\begin{aligned}
I_{zzd}\dot{r}_d = &a\Big(cos(\delta_1)(F_{y1} + F_{y2}) - sin(\delta_1)(F_{x1} + F_{y2})\Big)... \\
&-b\Big(cos(\delta_2)(F_{y3} + F_{y4}) - sin(\delta_2)(F_{x3} + F_{y4,3})\Big)... \\
&+w_d/2\Big(F_{x2}cos(\delta_1) + F_{y2}sin(\delta_1) + F_{x4}cos(\delta_2) + F_{y4}sin(\delta_2)\Big)... \\
&-w_d/2\Big(F_{x1}cos(\delta_1) + F_{y1}sin(\delta_1) + F_{x3}cos(\delta_1) + F_{y3}sin(\delta_1)\Big)... \\
&+l_{fw}(F_{c2y})
\end{aligned}
\tag{D.2}
$$

In this equation, the longitudinal tractive force at each of the four wheels is represented by F_{xn}, the lateral tyre force at the wheel is represented by F_{yn} and the steer angles at the front and rear axle by δ_1 and δ_2. The width of the dolly is represented by w_d and the offset of the axle positions with reference to the CoG are defined as a and b. The distance between the pin coupling and fifth wheel coupling at the dolly is defined as l_{fw}.

Increasing the tractive force (F_{xn}) at for example the left side of the dolly, introduces a yaw acceleration $\dot{r}_d$ around the CoG, see (D.2). A lateral force at the pin coupling is induced, due to this yaw rotation of the dolly. This lateral force counteracts the lateral pin coupling force. However, simply adding an additional tractive force for the wheels at the left side of the vehicle may result in a violation of (5.26). Violating (5.26) implies that the total sum of the longitudinal wheel forces is not equal to $F_{x,pin}$ any more. To ensure that the longitudinal force at the pin coupling remains zero, an equal amount of tractive force is subtracted from the tractive force at the other side of the dolly. The required tractive force at each wheel should, therefore, satisfy:

$$F_{xn} = \begin{cases} \frac{1}{4}\frac{1}{cos(\delta_1)}F_{xpin,measured}(1+\sigma_{tv}) & n = 1 \\ \frac{1}{4}\frac{1}{cos(\delta_1)}F_{xpin,measured}(1-\sigma_{tv}) & n = 2 \\ \frac{1}{4}\frac{1}{cos(\delta_2)}F_{xpin,measured}(1+\sigma_{tv}) & n = 3 \\ \frac{1}{4}\frac{1}{cos(\delta_2)}F_{xpin,measured}(1-\sigma_{tv}) & n = 4 \end{cases} \tag{D.3}$$

The parameter σ_{tv} represents the additional tractive force send to the left or right wheels. An equal amount of tractive force is subtracted from the wheels at the other side of the vehicle. By satisfying D.3, it is ensured that (5.25) holds and the longitudinal force transmitted through the drawbar remains equal to 0 kN. A controller should be used to calculate the desired torque vectoring factor σ_{tv} to control the lateral pin coupling force to zero.

The other approach, that reduces the lateral pin coupling force via an additional steer angle, can also be explained with (D.2). When the steer angle increases, the lateral components of the tractive forces F_{xn} at each wheel increases too. These additional lateral tyre forces counteract the lateral pin coupling force F_{c2y}. However, changing the steer angles results in a less good tracking of the path following steer controller, as derived in Chapter 4. Furthermore, the geometry of the dolly limits the maximum achievable steer angle of the wheels. When too large steer angles are required, the performance that can be achieved by this approach is limited by the maximum achievable steer angle.

Appendix E
Yaw dynamics of the decoupled 4x4 dolly

In this chapter the yaw plane equations of motion are derived for the 4x4 dolly. Remark that this dolly is decoupled from the first semi-trailer and second semi-trailer for simplicity reasons. The free body diagram of this dolly is shown in Fig. E.1.
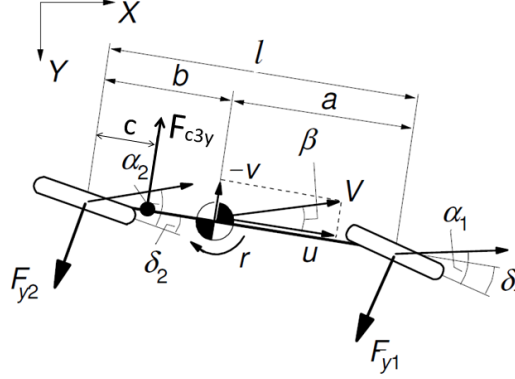

Figure E.1: Free body diagram of the (4x4) dolly in the yaw plane of motion [3].

Using Newton's second law of motion and neglecting the fifth wheel coupling force F_{c3y}, yields:

$$m_d(\dot{v} + u_r) = F_{y1} + F_{y2} \tag{E.1}$$

$$I_{zz}\dot{r} = aF_{y1} - bF_{y2} \tag{E.2}$$

The lateral tyre forces are represented by F_{yi}. The mass of the dolly is represented by m_d, the inertia of the dolly by I_{zz}. The distances from the front and rear axle to the CoG are represented by a and b, respectively. The lateral acceleration of the dolly is a function of the lateral acceleration of the CoG v, yawrate r and longitudinal dolly velocity u.

The lateral tyre force of the dolly can be approximated with:

$$F_{yi} = C_{f\alpha}\alpha_i \tag{E.3}$$

In this equation, the tyre side slip angle is represented by α_i and the cornering stiffness of the tyre by $C_{f\alpha}$. The tyre side slip angles at the front and rear axles are calculated with:

$$\alpha_1 = \delta_1 - \frac{1}{u}(v + ar) \tag{E.4}$$

and

$$\alpha_2 = \delta_2 - \frac{1}{u}(v - br) \tag{E.5}$$

Combining the equations above results in the following equations of motion:

$$m\dot{v} + \frac{1}{u}2C_{f\alpha}v + \left(mu + \frac{1}{u}(a-b)C_{f\alpha}\right)r = C_{f\alpha}(\delta_1 + \delta_2) \tag{E.6}$$

$$I_{zz}\dot{r} + \frac{1}{u}(a^2 + b^2)C_{f\alpha}r + \frac{1}{u}(a-b)C_{f\alpha}v = C_{f\alpha}(a\delta_1 - b\delta_2) \tag{E.7}$$

The two linear first order differential equations in (E.6) and (E.7) can be rewritten via the elimination method to a second order differential equation. Rearranging (E.7) results in:

$$v = \frac{1}{(a-b)C_{f\alpha}}\left(uC_{f\alpha}(a\delta_1 - b\delta_2) - uI_{zz}\dot{r} - (a^2 + b^2)C_{f\alpha}r\right) \tag{E.8}$$

Substituting (E.8) in (E.6) results in:

$$\frac{m}{(a-b)C_{f\alpha}}\left(uC_{f\alpha}(a\dot{\delta}_1 - b\dot{\delta}_2) - uI_{zz}\ddot{r} - (a^2+b^2)C_{f\alpha}\dot{r}\right) + \left(mu + \frac{1}{u}(a-b)C_{f\alpha}\right)r + ...$$
$$\frac{1}{u}\frac{2C_{f\alpha}}{(a-b)C_{f\alpha}}\left(uC_{f\alpha}(a\delta_1 - b\delta_2) - uI_{zz}\dot{r} - (a^2+b^2)C_{f\alpha}r\right) = C_{f\alpha}(\delta_1 + \delta_2)$$

$$muI_{zz}\ddot{r} + \left((a^2+b^2)mC_{f\alpha} + 2C_{f\alpha}I_{zz}\right)\dot{r} - \frac{1}{u}\left(-2C_{f\alpha}^2(a^2+b^2) + mu^2C_{f\alpha}(a-b) + C_{f\alpha}^2(a-b)^2\right)r = ...$$
$$muC_{f\alpha}(a\dot{\delta}_1 - b\dot{\delta}_2) + 2C_{f\alpha}^2(a\delta_1 - b\delta_2) - C_{f\alpha}^2(\delta_1 + \delta_2)(a-b)$$

$$muI_{zz}\ddot{r} + \left((a^2+b^2)mC_{f\alpha} + 2C_{f\alpha}I_{zz}\right)\dot{r} + \frac{1}{u}\left(C_{f\alpha}^2l^2 - mu^2C_{f\alpha}(a-b)\right)r = ...$$
$$muC_{f\alpha}(a\dot{\delta}_1 - b\dot{\delta}_2) + lC_{f\alpha}^2(\delta_1 - \delta_2) \tag{E.9}$$

The parameter l is defined as the wheelbase of the dolly, which equals the sum of a and b.